AOWFL

Resolving Key Uncertainties of Seabird Flight and Avoidance Behaviours at Offshore Wind Farms

Final Report for the study period 2020-2021

20 February 2023

Prepared for Vattenfall

The expert in WATER ENVIRONMENTS

AOWFL

Resolving Key Uncertainties of Seabird Flight and Avoidance Behaviours at Offshore Wind Farms

Final Report for the study period 2020-2021

Report
Project No Customer's ref.

Prepared for: Vattenfall
Represented by Robin Cox, Jesper Kyed Larsen

Contact person:	Mike Armitage
Project Manager:	Henrik Skov
Quality Supervisor:	Flemming Schlütter
Authors:	Rune Skjold Tjørnløv, Henrik Skov, Mike Armitage, Mike Barker, Jacob B. Jørgensen, Lars O. Mortensen, Katy Thomas, Thomas Uhrenholdt
Project No.:	11820296 RPS: ECO00516
Approved by:	Michael Hass
Approval date:	20th of February 2023
Revision:	Final
Classification:	**Confidential:** This document is only accessible to the project team members and sharing it outside the project team is subject to the client's prior approval.
File name:	AOWFL_Aberdeen_Seabird_Study_final_report_20_February_2023

DHI A/S • Agern Allé 5 • • DK-2970 Hørsholm • Denmark
Telephone: +45 4516 9200 • dhi@dhigroup.com • www.dhigroup.com • Company Reg. No.: 36466871

CONTENTS

FIGURES

TABLES

0 Executive summary

The main aim of the EOWDC Bird Collision Avoidance Study has been to improve our understanding of seabird flight behaviour inside an offshore wind farm. This should be achieved through collection of as detailed seabird flight data as possible rather than through estimation of avoidance rates for collision risk modelling *per se*. The focus is on seabird flight behaviour during the breeding period and post-breeding period when densities are highest in the Aberdeen area. The technical improvements of the monitoring equipment employed in the Aberdeen Offshore Wind Farm made it possible to track seabirds inside the array and measure meso-avoidance more confidently than before. It has been possible to match video camera recordings of seabird movements to a sample of their radar tracks. A total of 1,753 coupled tracks were recorded during 2020 and 1,370 tracks during 2021, which was beyond expectations and formed the basis for robust assessments of flight behaviours of target species in different parts of the wind farm array. The target sample size for species-specific meso-avoidance of 250 was reached for all key species, and the target for micro-avoidance of 100 was reached for herring gull (*Larus argentatus*) and black-legged kittiwake (*Rissa tridactyla*, hereafter referred to as kittiwake). The level of meso-avoidance recorded was 0.5 for kittiwakes, 0.7 for herring gulls and 0.5 for Northern gannets (*Morus bassanus*, hereafter referred to as gannet) and great black-backed gulls (*Larus marinus*). Together with the recorded high levels of micro-avoidance in all target species (> 0.96) it is now evident that seabirds will be exposed to very low risks of collision in offshore wind farms during daylight hours. This was also substantiated by the fact that no collisions or even narrow escapes were recorded in over 10,000 bird videos during the two years of monitoring covering the April – October period.

Detailed statistical analyses of the seabird flight data were enabled both by the large sample sizes and by the high temporal resolution in the combined radar track and video camera data (2.5 seconds). The flight data were analysed in relation to the local wind and turbulence (wake) conditions using multivariate Random Forest models. The most accurate video data were collected during 2021 when the video tracker on both cameras was upgraded to a new version which uses deep learning algorithms to separate flying seabirds from other flying objects and has the capability to keep the tracked bird in the centre of the field of view and record the tracks for longer periods. The target species displayed horizontal meso-avoidance within 100-120 m distance from the rotors. Herring gulls showed maximum meso-avoidance of 0.7 close to the blades, and kittiwakes showed avoidance of 0.5. As expected, they also displayed attraction to the areas in between the turbine rows. Gannets and great black-backed gulls only displayed avoidance at distances closer than 40 m and 50 m, respectively from the tip of the rotor blades. Both species displayed an avoidance level of 0.5.

For comparison with the ORJIP BCA study meso avoidance rates were estimated in the EOWDC study using the same algorithm and the results showed comparable rates with ORJIP for unidentified large gulls and gannet, while slightly lower rates were estimated for herring gulls and great black-backed gulls, and much lower rates were calculated for kittiwakes.

The results from the EOWDC study strongly indicate that the within wind farm avoidance response of the studied species of seabirds towards turbines mainly takes place within 100-120 m distance from rotors and that the response intensifies as the seabirds approach the rotor blades. In proximity to the rotors the recorded meso-avoidance response behaviour for all four species was manifested as a complex 3-dimensional pattern. Commuting gannets appeared to reduce flight altitude, whereas herring gulls and kittiwakes displayed a slight increase in mean flight height as they approached the rotor blades. When assessing the recorded flight orientation of the birds relative to the rotors commuting gannets and kittiwakes appeared to deflect around 80 m distance from the rotors and herring gulls at 50 m. The flight models revealed that turbulence and wind speed had the strongest effect on the profiles of flight behaviour of all target species. The pattern of responsive flight behaviour seemed to break down during situations with strong turbulence, while wind speed mainly affected the distance at which the increase in flight height took place. The trends resolved by the flight models were apparent irrespective of whether the birds were recorded as feeding or commuting.

The tendency to deflect and fly parallel to the rotor means that although meso-avoidance seems to be lower than anticipated prior to this study, micro-avoidance is very strong as seabirds are rarely recorded crossing the spinning rotors without adjustments as captured by the analyses of micro-avoidance. Large gulls (herring gull, lesser black-backed gull (*Larus fuscus*) and great black-backed gull) adjusted their flight behaviour to cross the rotor either obliquely or perpendicularly more frequently than gannets and kittiwakes. The recorded micro-avoidance rates (> 0.96) are similar to the micro-avoidance rate (0.957 ± 0.115 SD) which was estimated for large gulls in the ORJIP project using the same methods as in this project (Skov et al. 2018). These flight characteristics translate into very low risk of collision.

Despite the evidence of the low risk of collision by seabirds in the EOWDC, the Random Forest flight models revealed that the mean avoidance response pattern may break down during specific weather conditions. The model results indicate that all four target species show different flight profiles towards the rotor.

1 Introduction

1.1 Aims and Objectives

Accurately predicting the impact of offshore wind farms (OWFs) on seabirds continues to pose a significant consenting risk for their development in the UK and Europe, due to a lack of sufficient knowledge of seabird interactions with offshore wind turbines. In turn this prevents an accurate assessment of ornithological impacts, leading to precautionary and conservative assessments which are likely to overstate the effects of OWFs on seabird populations.

The overarching aim of this project is to enhance the understanding of the flight behaviour of seabirds within OWFs with respect to meso and micro-avoidance. A number of key objectives were set out during the tendering of the project and the project team comprising RPS and DHI responded positively by proposing a system capable of collecting data to meet the objectives.

The field investigations were undertaken at Vattenfall's European Offshore Wind Deployment Centre (EOWDC) using an integrated radar-camera system to collect fine-scale data about seabird movements. Significant derivatives of this are the quantification of avoidance rates in the meso and micro zones and determining the factors that influence flight behaviour within a wind farm.

Table 1-1 Overview of Project Objectives

Objective No.	Objective	Factors to Consider
1	Produce a dataset to enable significant gaps in knowledge and certainty of seabird avoidance behaviour in operational offshore wind farms to be filled.	Gaps in knowledge include seabird meso and micro-avoidance behaviour in close proximity to offshore wind turbines and seabird activity in different meteorological conditions and at different times of day.
2	Provide a high confidence dataset capable of assisting the reduction of OWF consent risk due to seabird collision.	In order to generate sufficient confidence, the dataset must be suitably large and collected using known levels of accuracy. Either the system in question must be proven, or sufficient testing is required. A radar-camera system has been identified as the ideal solution based on the ORJIP (Skov et al. 2018) and Block Island projects.
3	Provide accurate information on seabird flight heights in OWFs.	The use of triangulation of tracked seabirds between radar and camera has been tested and confirmed to be an ideal solution.
4	Deliver information on whether seabird behaviour in OWFs, including flight height, intensity, and avoidance, is affected by environmental factors.	Key environmental parameters have been identified as wind speed and direction relative to the bird as well as poor weather and visibility or darkness. The system should be capable of collecting data in variable conditions.
5	Apply rigorous, justifiable, and proven analysis techniques to provide avoidance rates suitable for informing collision risk prediction techniques.	The project team has prior experience of developing and applying robust methods for determining seabird avoidance rates in the ORJIP project and will utilise these methods to produce justifiable and robust outputs.

The aims of this Project are therefore to collect evidence on seabird flight patterns and behavioural responses to offshore wind turbines, with the ultimate objective of informing and refining predictive models for collision risk assessments.

The focus is on seabird flight behaviour during the breeding period and post-breeding period, i.e. during the period when seabirds are commuting from their breeding colonies to their offshore feeding areas, and in particular for the target species: gannet (hereafter 'gannet'), kittiwake (hereafter 'kittiwake') and large gulls (herring gull, lesser black-backed gull and great black-backed gull).

The main objectives were to collect species-specific data on three-dimensional (3-D) flight behaviour to document:

- Micro-avoidance behaviour – flight behaviour within and in the immediate vicinity of individual wind turbine rotor swept areas, including flight speeds and flight heights, and collision events; and
- Meso-avoidance behaviour – flight behaviour within and in the immediate vicinity of the wind farm, including flight speeds and flight heights.
- Effects of wind conditions on seabird flight behaviour – the influence of wind speed and wind direction on specific flight parameters, e.g. flight height and flight speed.

This final report includes data collected during the study period April 2020 – October 2021.

1.2 Report Structure

The final report is based on data collected between April to October in 2020 and 2021, summarising the main findings relating to the objectives above:

Section 1 includes a brief introduction and background to the study;

Section 2 provides a list of definitions which have been used throughout the report;

Section 3 provides details on the equipment and systems implemented as part of the study and its deployment offshore.

Section 4 summarises the weather conditions recorded by EOWFD

Section 5 presents an overview of the methods applied for video analyses and processing of radar data as well as a description of the statistical methods applied for modelling seabird flight behaviour

Section 6 gives an overview of the performance of the radar and camera equipment, including sample sizes obtained

Section 7 summarises the densities of target species of seabirds recorded by the radar

Section 8 presents species composition and seabird temporal dynamics analysed from video recordings;

Section 9 summarises the video recordings on feeding activity inside the Aberdeen Offshore Wind Farm

Section 10 presents meso-avoidance analyses of changes in track density and flight direction of target species in relation to distance (100 m +) to turbines;

Section 11 presents micro-avoidance analyses and observed flight behaviour in the vicinity of the rotor swept zone;

Section 12 provides analyses of changes in flight height of target species in relation to distance (100 m +) to turbines and bird behaviour;

Section 13 provides analyses of flight speeds of target species in relation to distance (100 m +) to turbines and bird behaviour.

Section 14 provides analyses of flight directions of target species in relation to distance (100 m +) from the rotors and rotor orientation.

Section 15 discusses the results in terms of equipment performance, 3-D avoidance behaviour of seabirds and implications of the study for refining empirical collision risk models.

1.3 Study Area and Project Design

The study site is the EOWDC, situated 3 - 4.9 km off the coast of Aberdeen in north-eastern Scotland. The site was considered suitable for the study based on its location with nearby breeding colonies and offshore feeding grounds of gannet, kittiwake and large gulls revealed by previous surveys in the area.

To fulfil the Project aims and objectives, an integrated radar-camera monitoring unit was deployed on the EOWDC which was capable of generating 3-dimensional (3-D) flight tracks, supported by video footage for species identification and behavioural classification as they moved through the wind farm. This is discussed further in Section 3.

The Project is focused on diurnal flight activity during the breeding season and post-breeding dispersal period (i.e., April to October) in 2020 and 2021. The monitored areas represent the micro and meso zones of the wind farm.

2 Definitions

Table 2-1 provides a glossary of terms and definitions which are used throughout this report.

Table 2-1 Glossary of terms

Term	Definition
AOWFL	**Aberdeen Offshore Wind Farm Limited**
Avoidance behaviour	Any action taken by a bird, when close to an operational wind farm, which prevents collision (SNH, 2010). Such action may be taken early enough to avoid entering into the wind farm (macro avoidance) or taken within the wind farm, avoiding the rotor swept zone (RSZ) (meso avoidance) or individual turbine rotor blades (micro avoidance)
Avoidance rate	Correction factor applied in collision risk models in order to take account of the likely degree of successful avoidance of a bird colliding with the turbine rotors
AWF06 and AWF10	Turbines 6 and 10 within the EOWDC
Collision risk	Risk of injury or death caused by an encounter or collision with turbines or rotor blades at a wind farm (Band, 2012)
Clutter	Clutter is a term used for unwanted echoes in electronic systems, particularly in reference to radars. Sea clutter refers to those echoes returned from the sea surface, which can cause serious performance issues with radar systems
Detection probability	Probability for the sensor to pick up a bird or a flock of birds, which is dependent on distance, orientation, shape, size, clutter, etc. The maximum detection is the distance where the detection probability falls below 0.5 (equal chance of detecting a bird or not)
EOWDC	European Offshore Wind Deployment Centre
Meso-avoidance	Bird behavioural response within the wind farm footprint to individual turbines (considering a 10 m buffer around the rotor swept zone (RSZ)) and resulting in a redistribution of the birds within the wind farm footprint
Micro-avoidance	Bird behavioural response within 10 m of the rotor swept zone, considered as the bird's 'last-second action' taken to avoid collision with a rotor blade
MUSE	Multi-sensor high-speed processing software which facilitates the communication between radar and camera equipment
Rotor	Part of a wind turbine that extracts kinetic energy from the air and coverts this wind into rotational energy in the drive train. The current generation of horizontal axis turbines have rotors with three blades. In the context of this analysis the 'rotor' also defines the ellipse representing the blades at a given time.
Rotor swept zone (RSZ)	Zone swept by the rotating turbine blades (the rotor) of a wind turbine. As viewed from above, while the rotor refers to the ellipse representing the blades at any given time, for the purposes of analysing empirical micro-avoidance, the RSZ refers to the circle drawn by the rotor blades.
Sensor	The radars and cameras used in this study to detect flying seabirds and collect bird behavioural information at different scales (meso-, micro-) as well as data on flight heights

Term	Definition
Track	Recorded trajectory of one or a group of several birds by the study sensors. A track is made of different recorded positions or nodes
Track density	Estimation of empirical avoidance rates based on a ratio of the density of bird tracks detected in avoidance/non-avoidance areas. This can be estimated using the number of tracks within a given area, or using the lengths of tracks within a given area

3 MUSE System

The following section provides an overview of the sensor and software settings of the MUSE system and of the methods employed during video analyses.

3.1 Overview of sensors and software settings

The radar-camera monitoring unit deployed on the EOWDC collects radar tracks and video footage enabling species identification and analysis of meso- and micro-avoidance behaviours in an operational OWF. The communication between the camera and radar is facilitated by a multi-sensor, high-speed processing software (DHI MUSE); this software allows birds discovered by the radar to be automatically targeted by the cameras and followed, using motion detection and video.

The radar (Furuno FAR-3000) is oriented horizontally and movements of birds in the wind farm area are tracked automatically. Tracking information from the radar is continuously recorded to a geo-database by the system. Samples of radar tracks that have triggered video recordings are combined with images from the camera, which are flagged with the same track identification code. Information about the height of the bird is also recorded during the period it is viewed by the camera; the target's height is calculated using the MUSE software by triangulation of the combined distance measurements from the radar and the measurements of inclination angle by the camera.

In this project, the camera setup consists of two pan-tilt cameras with strong zoom. One camera is a HD FLIR M400 combined long-range zoom daylight camera and thermal sensor. The other, a RVision MiniHP, is a rugged daylight camera. The range at which movements of medium-sized seabirds like large gulls can be tracked by motion detection is approximately 1,000 m, and the minimum distance is approximately 50 m. New camera AI-based tracking software with enhanced motion detection and tracking capabilities were installed in both cameras on the 10th of January 2021.

The radar and the FLIR M400 camera were installed on AWF10, while the RVision MiniHP was installed on AWF06. The detection and tracking ranges of the radar and cameras are illustrated on Figure 3-1 below. The installation positions of the radar and cameras have been sketched in Figure 3-2.

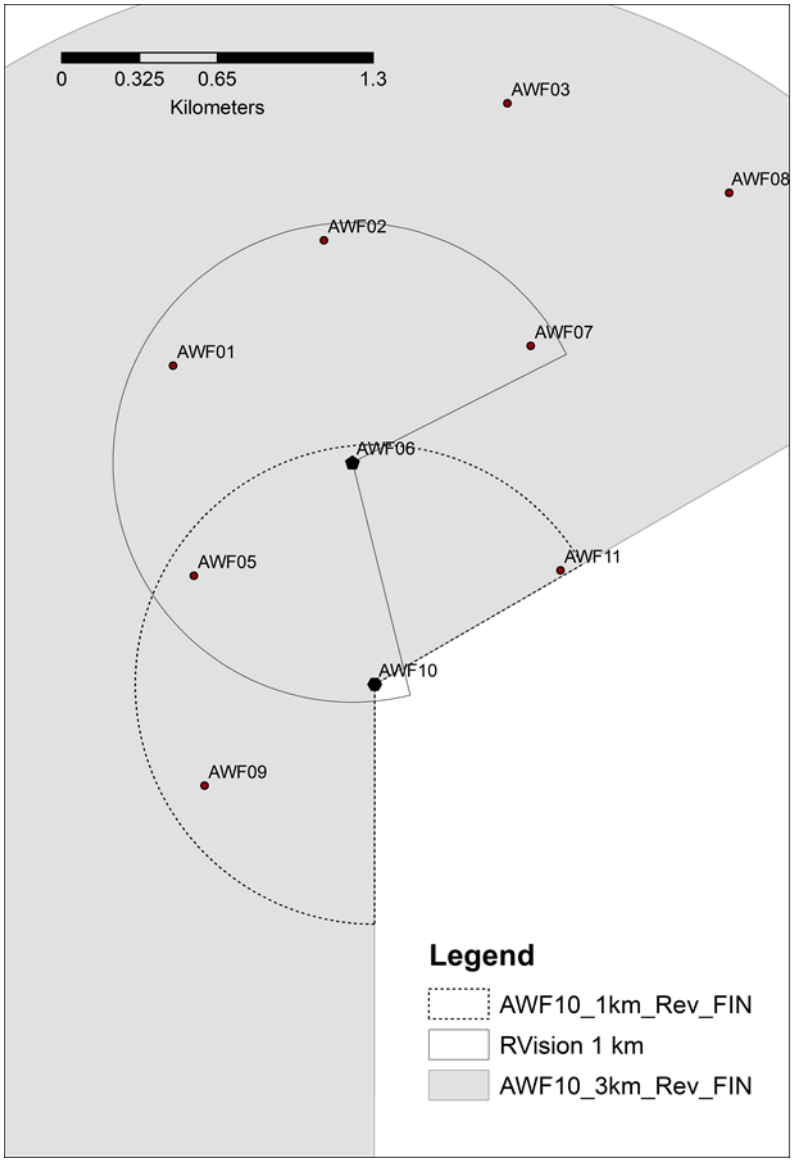

Figure 3-1 Set up and tracking ranges of the EOWDC radar and cameras

Prior to installation, field tests were undertaken at a coastal test location in Ebeltoft, Denmark.

Checks and calibration of all radar signal processing in the MUSE software were carried out in a laboratory. The database storage was tested with track data from the field; the MUSE system saves all bird tracks as geo-referenced tracks with unique ID which includes a timestamp. Parameters included and checked in the database include UTM coordinates for each node in the tracks, order of track nodes, flight direction, variation of flight direction and flight speed. The alignment of the camera with the initial target position was tested by including annotations of the angle, elevation and zoom level in the video output from the camera.

Following calibration of the radar, the cameras were calibrated remotely to optimise focus and zoom levels, motion detection controls and division of the scanned area between cameras.

In addition to empirical tests of the detection probability of the FAR-3000 radar carried out in 2016 (DHI 2017) a series of theoretical (modelled) tests of the vertical coverage and detection probability of different sizes of birds (radar cross sections) were made on the computer. The results showed good detection of passerines up to 3 km, of gulls up to 4 km, of gannets to 5 km and of large flocks of birds up to 6 km during calm sea states, with detection probability dropping at higher sea states (4+).

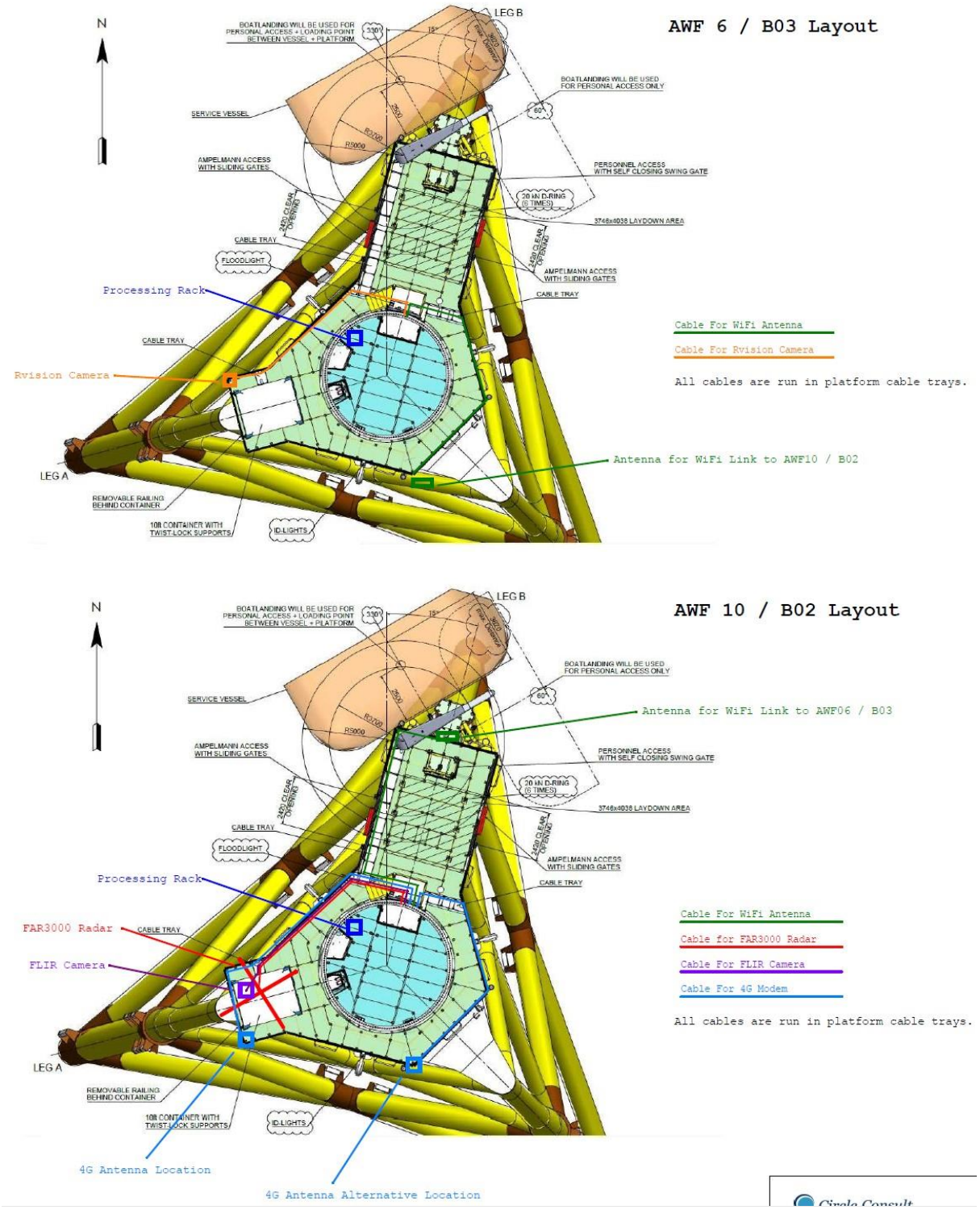

Figure 3-2 Conceptual installation drawings of the RVision camera on turbine AWF06 and the FAR-3000 Radar and FLIR camera on turbine AWF10

3.2 Radar specification, including tracking of seabirds

The FAR-3000 S-band solid state radar is used for horizontal scanning of bird movements within the wind farm. The technical and functional specifications of the FAR-3000 are included in Appendix 1. The FAR-3000 S was selected due to its good clutter suppression and bird tracking capacity in conditions with prominent sea and rain clutter. An illustrative example of the different levels of sensitivity to waves and precipitation of the FAR-3000 radar and a standard magnetron-based radar is illustrated by a situation with intensive rain and waves in Figure 3-3. Downtime is minimised using auto-alarms and remotely controlled operations.

The radar is oriented horizontally and movements of birds in the wind farm area are tracked automatically. Simulations of the vertical coverage and detection probability of different sizes of birds (radar cross sections) have been made using Carpet software (*https://www.tno.nl/en/focus-areas/defence-safety-security/roadmaps/information-sensor-systems/carpet-computer-aided-radar-performance-evaluation-tool/*). The results show good detection of passerines to 3 km, of gulls to 4 km, of gannets to 5 km and of large flocks of birds to 6 km during sea state 0. During high sea states (sea state 4+). the detection of passerines and gulls close to the radar drops. Within the distances of good detection, the vertical coverage is at least 400 m for all types of birds. In conclusion, the radar provides good detection of the target species (large gulls) within the entire 3 km range applied in the EOWDC. During higher sea states the detection of gulls close to the radar is reduced.

The installation of the radar on top of the container on turbine 10 is shown in Figure 3-4.

The MUSE software samples at 100 MHz and performs real time filtering of standardized echo sizes based on calibrated dB-values from the radar. Both static and dynamic noise is filtered by the software before initiating tracking. Each track consists of nodes with a temporal resolution of 2.5 seconds equivalent to one antenna rotation.

Additional to the generation of bird tracks the MUSE system automatically stores radar screen images every 2 seconds. These data constitute a backup facility and supplementary data.

On account of the vertical angle (12.5°) of the radar beam and the height of the radar on AWF10, low-flying (< 10 m) seabirds cannot be detected closer than 30 m from the radar.

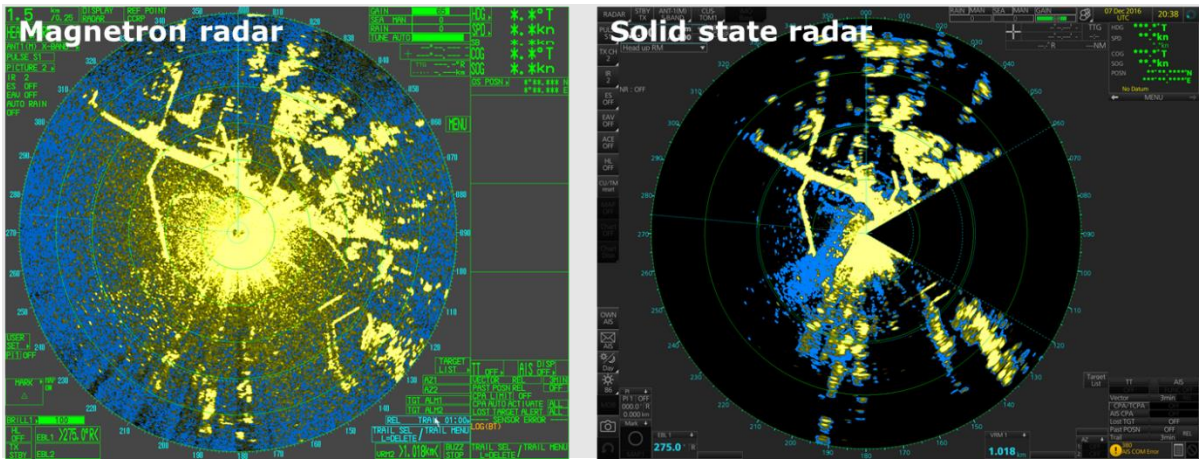

Figure 3-3 Example of contamination of magnetron-based X-band radar (FAR-2127) recordings by rain and waves as compared to recordings by FAR-3000. Left image shows echoes recorded by FAR-2127 during a situation with rain and waves (sea state 5), and right image shows echoes recorded by FAR-3000 at the same time. Rain droplets recorded by the FAR-2127 radar are seen as small or yellow dots. No birds are present in scanned area.

Figure 3-4 FAR-3000 radar installed on AWF10, EOWDC

3.3 Camera specifications, including tracking of seabirds

The FLIR M400 is a combined thermal and daylight camera (Figure 3-5, Appendix 2). This camera (FLIR M400) consists of a pan-tilt housing with 30x zoom daylight camera and a 4x zoom thermal camera. With the M400 daylight camera, bird movements can be recorded at the species level to a distance of 1,000 m for a medium-sized bird and 2,000 m for a large bird. The rugged camera system is designed for long-term deployment in offshore conditions and does not require frequent cleaning or other servicing. The pan-tilt camera's environmental housing is fully capable of sustaining the harsh environment of the salty sea conditions offshore. Additionally, the camera is sufficiently durable to withstand continuous operation in an offshore environment.

The RVision SeeHP camera is a rugged daylight camera, which consists of a pan-tilt housing with a Sony x30 daylight camera block (Figure 3-6, Appendix 2). The range at which movements of seabirds can be tracked by motion detection is approximately 1,000 m, and the minimum distance is approximately 50 m.

The video format applied in MUSE is PAL which is supported by both cameras and was used during the field tests.

The camera turn response speed on the radar signal for the initial bird detection has been tested. The speed of the M400 is 50 degrees per second, while the speed of the RVision is 20 degrees per second. Each camera scans areas of maximum 250˚ in EOWDC. Accordingly, the maximum delay related to the turn speed is 5 seconds (M400) and 12.5 seconds (RVision). As the cameras are zoomed out initially, this delay is not likely to limit the detection of the bird by the cameras to any large degree. To further reduce the delay, a decision rule was introduced in the MUSE software which in cases of multiple targets makes the camera select the target which is closest to its current position.

During the 2020 season, camera tracking was carried out using motion detection which resulted in a relatively high level of false positives. This was especially the case in situations when multiple bird targets appeared in the field of view. During the 2021 season, camera tracking was greatly improved by adopting an AI-based tracking algorithm which allowed initial zoom to 65% followed by an increasing zoom level to 95% and resulted in significantly fewer false positives, more species identifications, an increased length of recorded videos, and more height estimates as birds were in the centre of the field of view more frequently.

Figure 3-5 FLIR M400 camera, showing installation process at EOWDC

Figure 3-6 The RVision SeeHP camera in position at AWF6, EOWDC

3.3.1 Radar-camera integration and operating modes

The dynamic and fully integrated coupling between the horizontal radar and the pan-tilt cameras in MUSE allows the cameras to move in two dimensions and detect and follow birds across a large area of the wind farm. Triggered by the radar, the digital camera will detect the bird target and will zoom and focus on the bird and track and record its movements. Recordings of flight height and tracking of 3-D movements of birds were obtained by triangulation of measurements of distance from FAR-3000 and inclination angle measured by the cameras (Figure 3-7). The integrated track database included flags for horizontal tracks with associated height data, and height measurements were added for each node in the horizontal track.

The triangulation was made using the radar measurement of its distance and the angle observed with the camera, which was obtained from the fraction of the total field of view (FOV). The % accuracy was given by the sum of the % accuracy in the angle and the distance. The high accuracy of the height estimates have been validated using test undertaken in Denmark using a drone.

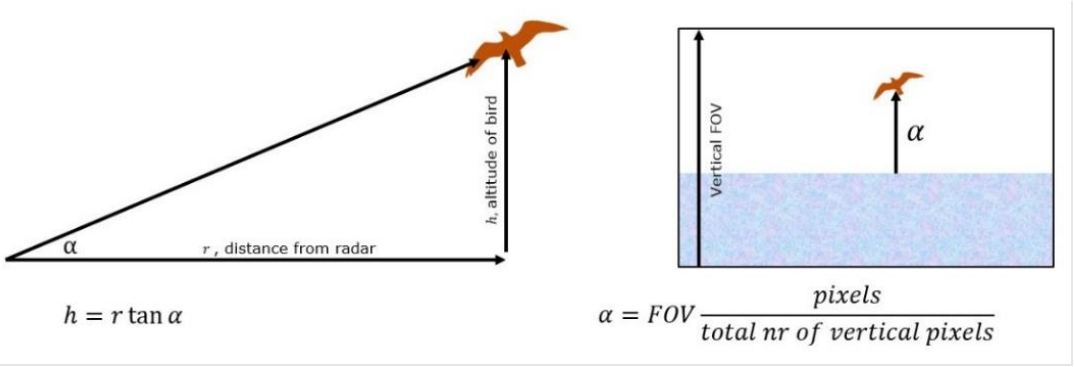

Figure 3-7 Sketch of the estimation of flight height by triangulation of radar and camera measurements

Data on meso- and micro-avoidance of seabirds were collected in two different sensor modes; dual mode and solo mode.

Sensor dual mode with integrated radar and camera tracking was the priority mode of operation during the 2020 breeding season as it allowed for 3-D tracks and estimation of flight heights through triangulation of the radar (distance) and camera (inclination angle) for any given track. In this mode the radar will always trigger the camera to record the bird movement by motion detection, and unless the camera is engaged in tracking it is available to receive information on bird targets from the radar.

The camera records the bird movement for as long as the bird can be detected by the camera's motion detection. If the camera loses the target, information on the location of the bird is transferred from the radar to the camera, in which case it can continue following the bird.

The performance of the radar is affected during strong weather conditions in which high waves cause the dynamic clutter filter in the MUSE software to generate a high level of false negative bird detections (failure to record birds), which affects the system when operating in dual mode. During such conditions, it is possible for the system to operate in solo mode, when the camera is moved to a fixed position and awaits a target to follow by motion detection. In solo mode, a bird's movement is followed and recorded if a bird is detected in the camera frame; however, no associated radar track of its position is generated. The wind speed threshold was set to 15 m/sec, and the camera mode was changed automatically by the system by reading wind speeds recorded by a weather station on AWF10 (Young 86000 Ultrasonic Anemometer). The use of solo mode was implemented to increase the sample size of videos of birds' movements but is subject to a higher degree of subjectivity in the analysis of the birds' flight behaviour and position in space.

During the 2020 breeding season, the system was only operated in dual mode with camera recordings being triggered only by radar to optimise the number of coupled radar-camera tracks collected and thereby enhancing the assessment of 3-D avoidance behaviour. In July 2021, the operational mode of the RVision camera on AWF06 was changed to a fixed solo mode, in which the camera was configured to focus on a specific turbine and picked up a target coming into the field of view by means of the camera's motion detection system. The RVision camera was configured to switch to a new turbine (either AWF01, AWF02, AWF05) after an operational time interval of one hour. Switching the RVision camera from dual mode to fixed solo mode was done with the aim of collecting more videos of micro-avoidance behaviour.

3.4 Potential sources of bias

The analytical framework for this project has been based on proportional statistics on behavioural data without assuming detection of all birds in the ranges of radar and cameras. Still, potential biases may have been introduced. The monitoring design assumes that the observed behavioural responses are representative of any weather and visibility conditions. Tests of false negatives and false positive detections by the FAR-3000 radar have documented that although false positives are

controlled efficiently by the clutter filter of the MUSE system, false negatives will appear as sea states increase above sea state 4. As track densities are only compared for the same weather scenarios the tendency for false negatives may not necessarily introduce a bias. However, during severe weather with sea states above 5 it is likely that the level of false negatives will be significant leading to small sample sizes and less robust patterns of track distributions. The tendency for false negatives during adverse weather conditions will be the same irrespective of the flight height of the birds. Hence, a bias against low-flying birds should not be expected.

Obviously, during the course of the project oceanographic and habitat variability in time and space has been taking place. Although the effect of the variability in the weather conditions on seabird flight behaviour has been quantified, the oceanographic variability has not been accounted for within this study. The oceanographic variability has most likely affected the dynamics of abundance of seabirds within the AOWFL but is unlikely to have biased recordings of avoidance behaviour to a large extent. Rather, the changes in oceanographic conditions have introduced variation in the local feeding conditions leading to variations in the overall abundance of feeding seabirds at the site.

Birds not changing flight path recorded flying below/above the RSZ have not been included in the account of vertical meso-avoidance. Thus, vertical meso avoidance measurements are judged as un-biased.

Tracking effort at all distances from the turbines is considered similar, as only radar and camera data from zones of high detection probability for seabirds have been included. The radar has been operating with an S2 pulse, which has an even detection probability for seabirds within the entire 3 km range of the radar, and hence no detection bias is likely to have been introduced.

During 2021, the cameras were tracking using an AI-based tracking algorithm trained on a large sample of video data with flying birds, including seabirds (gulls). Although the video training data contained videos with sea as a background, the majority of the training data were videos showing birds with the sky as a background. As the performance of the AI model applied in the video tracker depends on its ability to recognise flying birds in a large variety of situations and at different distances, it is likely that a limited number of training data showing birds with the sea as a background could result in a bias against detection of low-flying birds. Tests of the detection efficiency of the AI-tracker in relation to low-flying birds is ongoing.

4 Weather conditions

Data on wind speed (m/s) and wind direction was derived from weather data collected at one turbine within the EOWDC. The temporal resolution of the collected weather data was one hour.

A monthly overview of the wind conditions at the EOWDC during the study is given in Figure 4-1 and Figure 4-2. In general, the wind directions at the site were dominated by winds from the southwest. During May-June and September-October in both years, winds from this direction were particularly strong with gale force winds recorded frequently. Frequent winds from the north-north-east were recorded during April-June and August-October 2020 as well as in June 2021, while strong north-westerlies were frequent during July 2020 and April 2021. Low wind speeds were most frequent in July-August 2021.

In Figure 4-3 an overview of the sea conditions (Beaufort Sea state) as recorded by observers reviewing the videos is provided. The figure shows that due to the proximity to the Aberdeen coast, strong sea conditions at the EOWDC happen infrequently with mean sea states above 4 being recorded on less than 10 days over the two seasons. Calm conditions were particularly prevalent during August 2020 and July 2021.

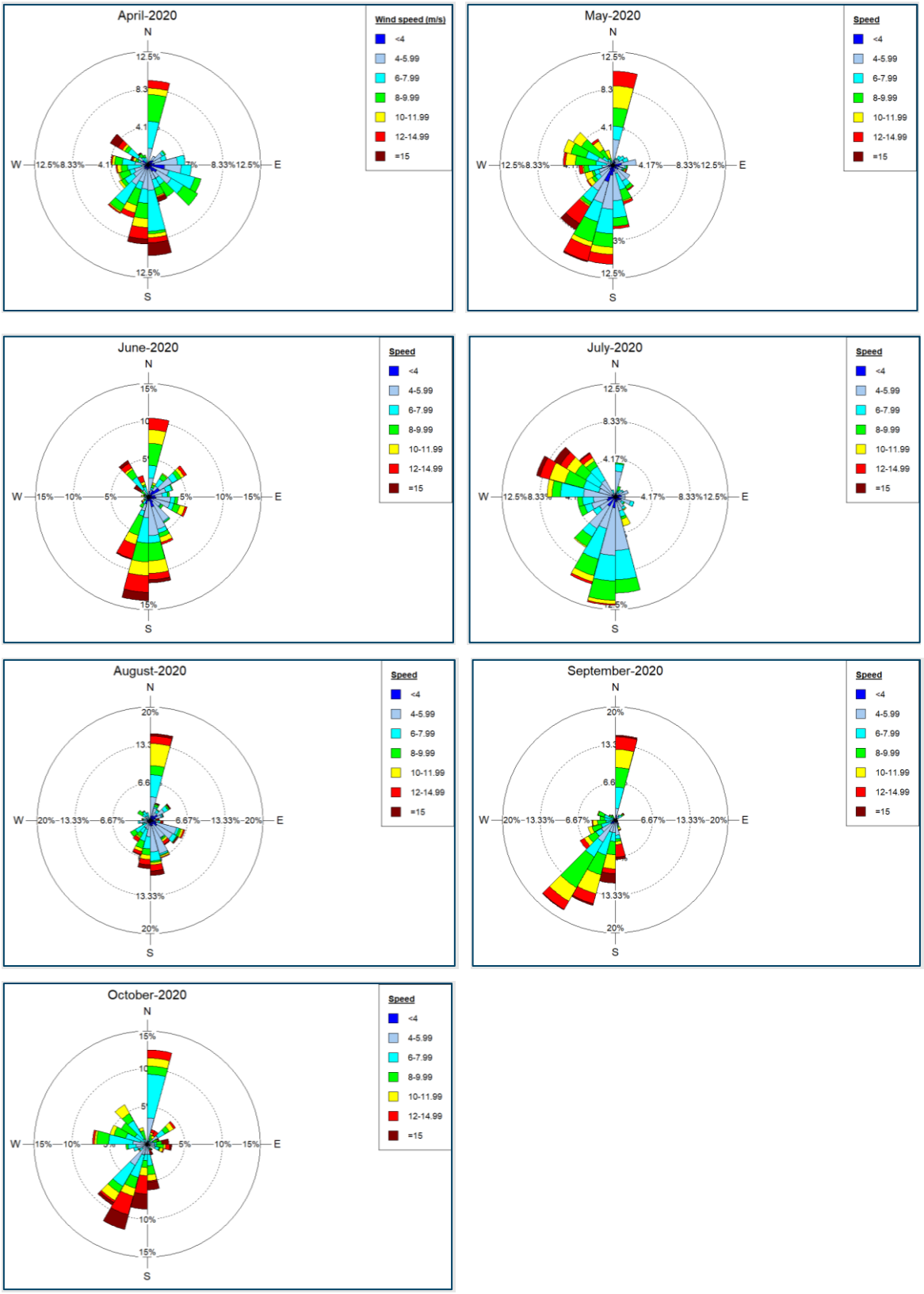

Figure 4-1 Overview of wind conditions during the monitoring campaign in 2020. Wind speed is in m/s.

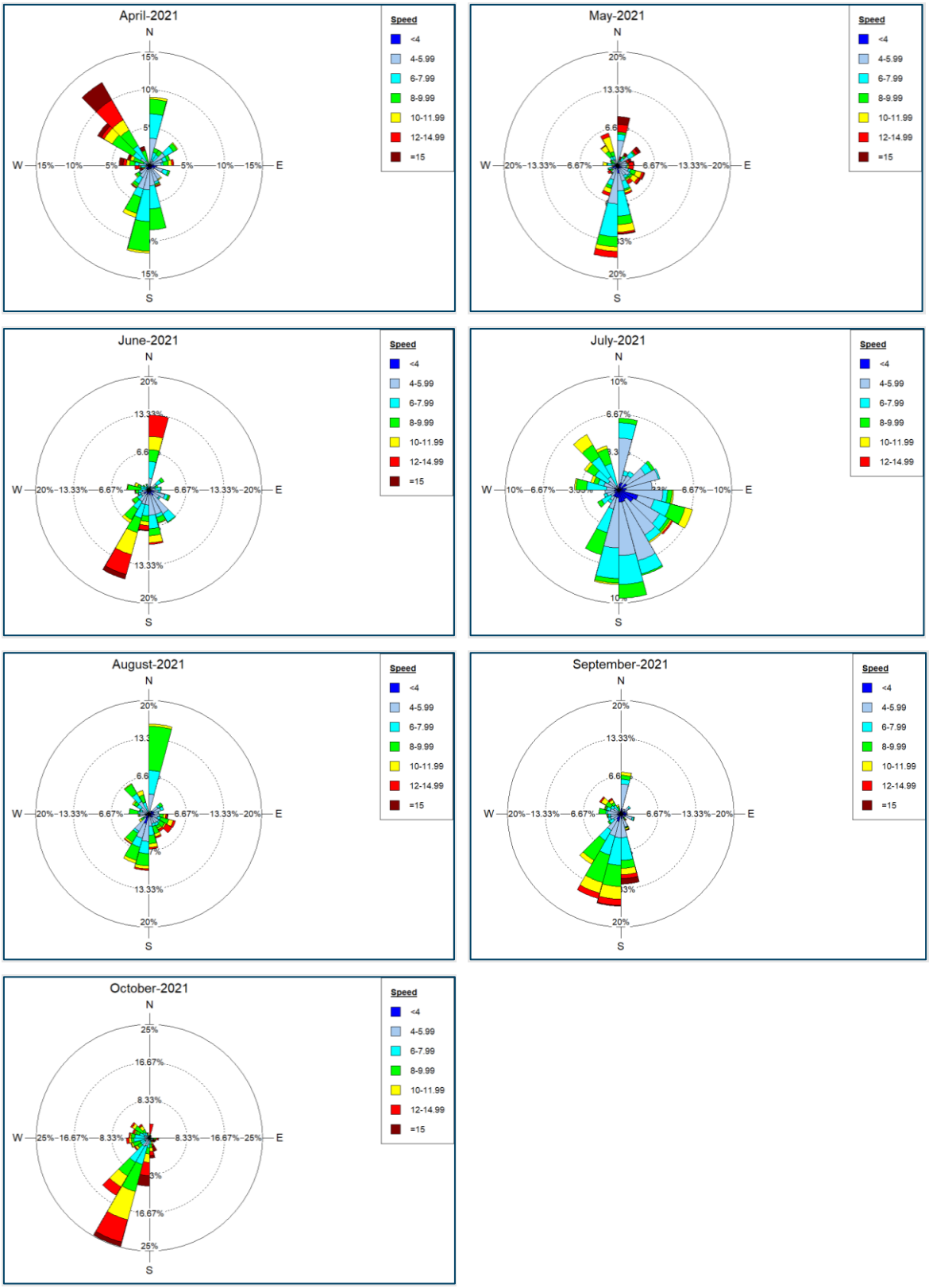

Figure 4-2 Overview of wind conditions during the monitoring campaign in 2021. Wind speed is in m/s.

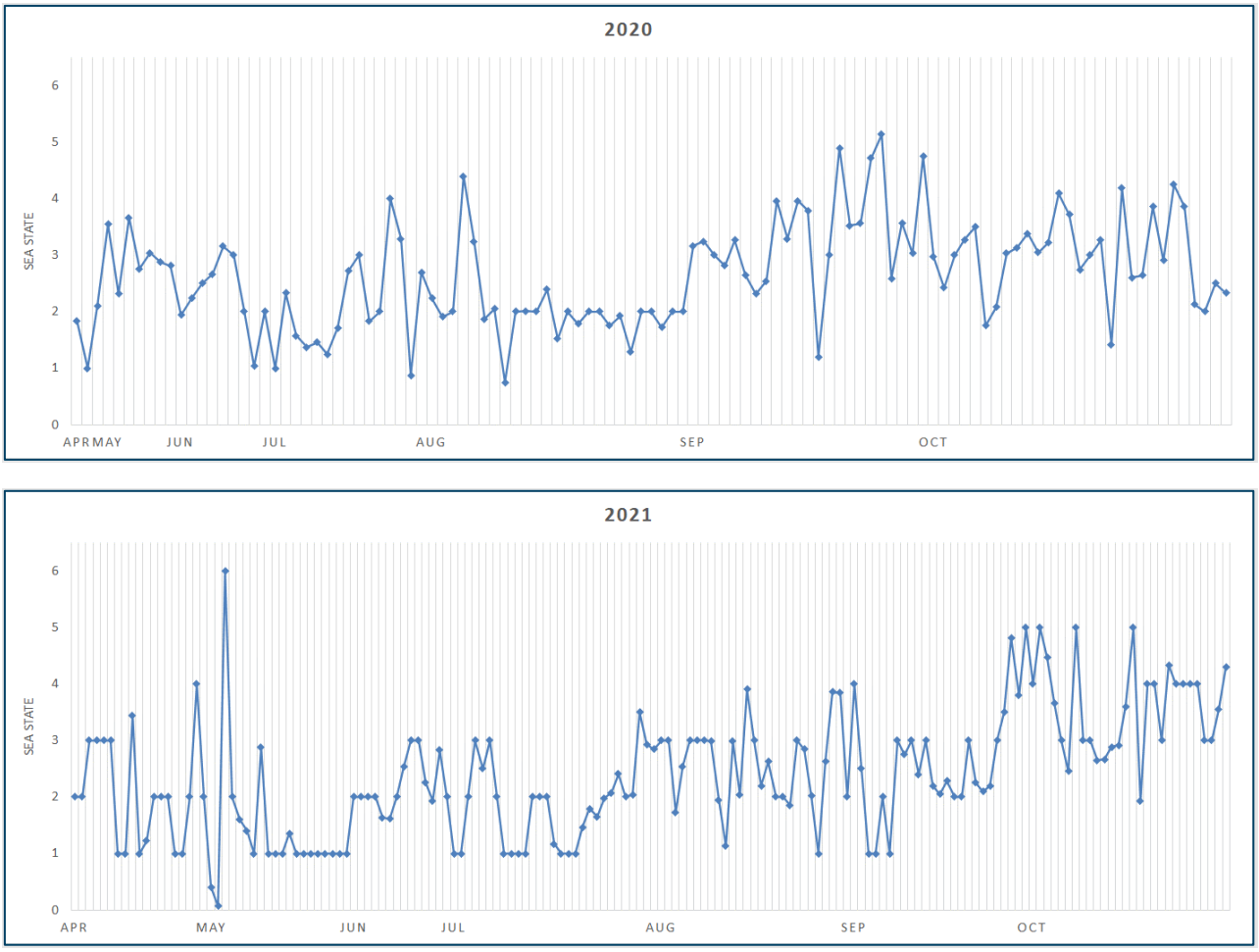

Figure 4-3 Overview of mean daily sea conditions (Beaufort Sea state) as recorded by observers on the videos

4.1 Wake conditions

The consequence of the conversion of kinetic energy from the incoming wind to electrical energy by the wind turbine is a downstream wake of reduced wind speed and enhanced turbulence. In the current project the characterisation of the size and strength of this wake and its effect on seabird flight behaviour has been addressed and quantified. The interplay of more than one turbine and hence the superposition of turbine wakes complicates the calculation, and in this study we have used an iterative method across the EOWDC in order to capture the effect.

The wind speed and direction measured simultaneously from the 11 turbines (AWF01 to AWF11) shown in **Figure 4-4** often varies more than 3 m/s and more than 20 degrees from turbine to turbine. Any wakes produced with a steady-state wake model forced with this wind would therefore show very fluctuating wake directions (but also speed) between consecutive time steps. By using the maximum wind speed over the 11 turbines in each time step (10 min averaged to 1 hour) and wind direction from the associated turbine, it is implicitly assumed that this wind speed best represents the undisturbed wind speed when no turbines are present (disregarding blocking effect as discussed later). Using this approach, we still encounter jumps in the wind direction between consecutive time steps.

A wind rose plot of the resulting time series of wind speed and wind direction is shown in Figure 4-4 the main wind direction is from the south, and this is also the direction with the strongest winds of 23-24 m/s.

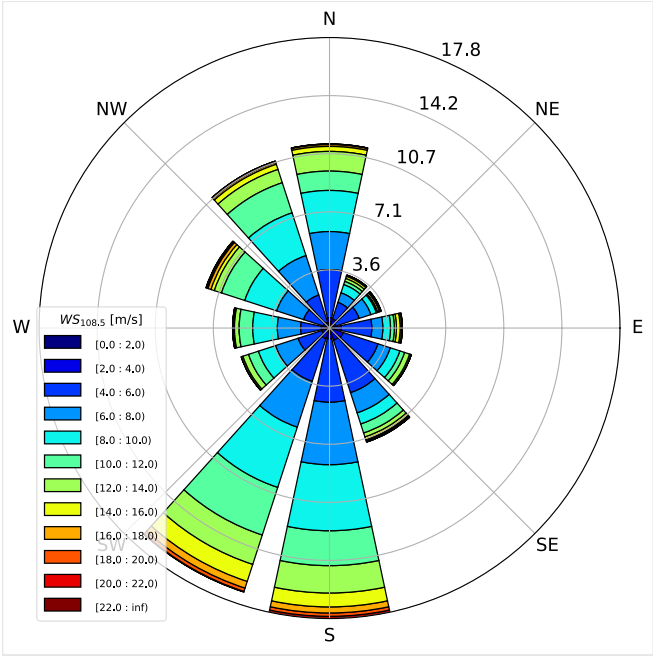

Figure 4-4 Wind rose of OWF measured wind speed and wind direction. The OWF measurement is taken as the maximum wind speed of all turbine readings in the OWF and its associated wind direction.

A scatter plot comparison with ERA5[1] wind is presented in Figure 4-5 and Figure 4-6 for wind speed and wind direction, respectively. For the wind speed the scatter index (si=0.20) and root-mean-square-error (rmse=2.18) are low and the correlation coefficient (cc=0.88) is high. There is a bias of -1.26 m/s, i.e., the values of the measurements are lower than those of ERA5. For wind direction the circular bias is small (3.59°) and the correlation coefficient is high (0.88). We have therefore decided to use a modelled wind instead of the nacelle measured wind, in this case wind from the atmospheric reanalysis model ERA5[1]. This model offers a grid resolution of ~30 km and hourly time scales, i.e., the flow is smooth which will guarantee smoothly varying wakes. Since this bias of 1.26 m/s is most pronounced for higher wind speed (above turbine rated speed ~12 m/s) the effect on the strength of the wakes is small.

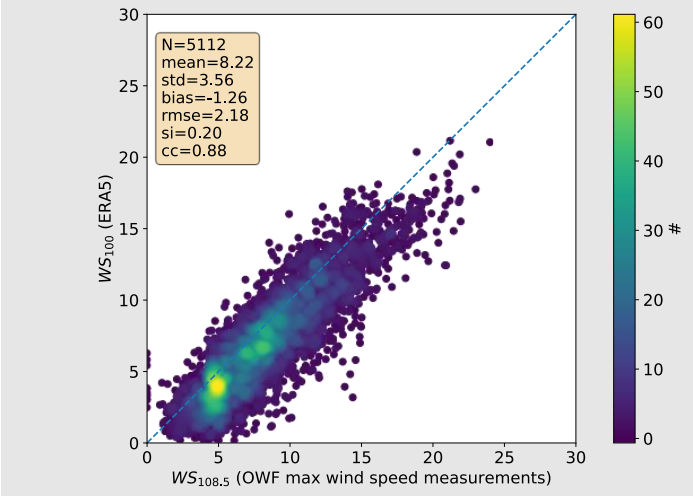

Figure 4-5 Scatter plot of 1h wind speed of OWF measurements at 108.5 mMSL and ERA5 at 100 mMSL. The OWF measurement is taken as the maximum wind speed of all

[1] Atmospheric Re-Analysis 5 (ERA5) developed by the European Centre for Medium Range Weather Forecasts (ECMWF) . ERA5 offers a grid resolution of ~30 km. https://www.ecmwf.int/en/forecasts/datasets/reanalysis-datasets/era5.

turbine readings in the OWF. Statistics added: Mean value of 1h measurements, standard deviation of 1h measurements, bias, root-mean-square-error (rmse), scatter index (si) and correlation coefficient (cc) added.

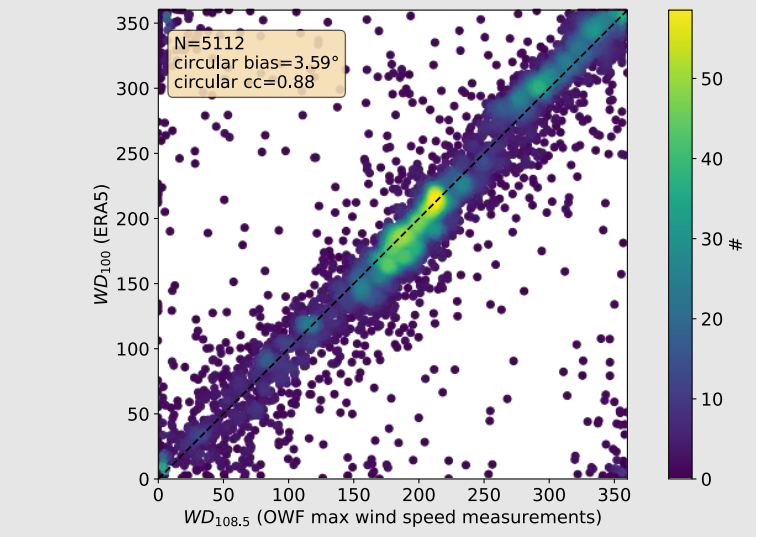

Figure 4-6 Scatter plot of 1h wind direction of OWF measurements at 108.5 mMSL and ERA5 at 100 mMSL. The OWF measurement is taken as the wind direction of the turbine with the maximum wind speed of all turbine readings in the OWF. Statistics added: Circular bias and circular corelation coefficient.

For the turbine thrust coefficient curve (ct-curve), values from the DTU 10 MW test turbine have been used (Bak et al. 2013). The rated speed is 11 m/s, i.e., the wind speed at which the thrust coefficient levels off, and the rated power of 8.6 MW is achieved. The wake model consist of several sub models: a wake deficit model to account for the reduced wind speed downstream of the rotor; a turbulence model to account for the enhanced turbulence level downstream of the rotor; a blockage deficit model to account for the reduced wind speed just in front of the rotor due to the rotor induced pressure gradient force, and speed-up along the sides of the downstream wake; and a superposition model to account for mixing with wakes from nearby turbines. The complete wake model used has been implemented using the DTU Wind Energy Open Source PyWake Package v.2.2.0 [2] using the engineering wake models listed in Table 4-1.

Table 4-1 Engineering wale models

Wake deficit model	Zong Gaussian model (Zong et al. (2020))
Turbulence model	Frandsen model (Frandsen 2007)
Superposition model	Linear sum https://topfarm.pages.windenergy.dtu.dk/PyWake/index.html
Blockage deficit model	Rathmann model https://topfarm.pages.windenergy.dtu.dk/PyWake/index.html

The majority of wake deficit models are developed with wind resource assessment studies in mind, where often accurate modelling of the far field is most relevant. In this study, however, near wake distances are equally important and hence the Zong Gaussian model is a very good candidate, and hence chosen for this study. A comparison of the chosen model with the canonical Niels Otto Jensen

[2] https://topfarm.pages.windenergy.dtu.dk/PyWake/index.html (Gögmen et al. 2016)

(NOJ) model (Jensen 1986) on the centreline is shown in Figure 4-7. The strength of the wake is defined through WS_{ratio}, which is the ratio between the local wind speed and the incoming wind speed (upstream where the wind is unaffected by turbines). In the presence of wakes $WS_{ratio}<0$. In the figure it is observed that the Zong Gaussian model used in this study has a smaller maximum deficit compared to the NOJ model, and it is located further downstream which is more realistic (Andersen et al. 2014), and of importance for this study in particular. Also, by including a blocking model the wind speed is reduced in front of the turbine. Due to the varying thrust coefficient (ct) with wind speed, the wake strength (WS_{ratio}) is also dependent on wind speed.

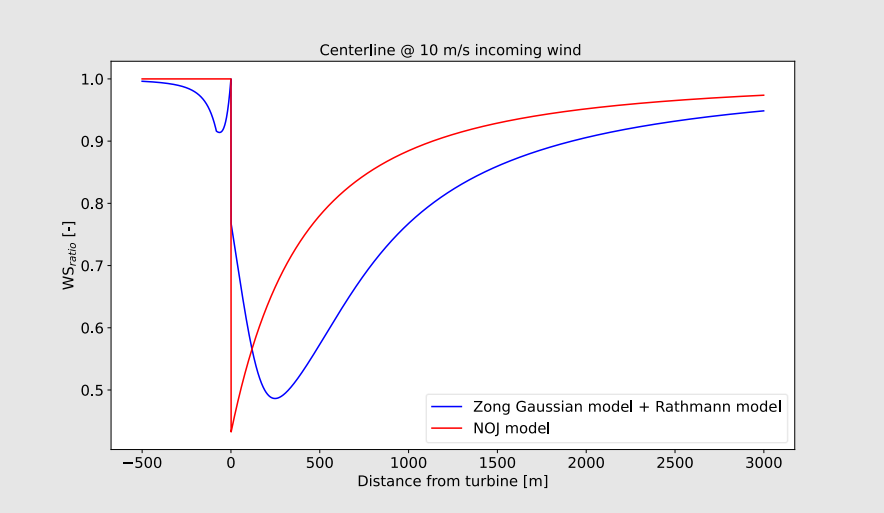

Figure 4-7 Centerline comparison between the Zong Gaussian model + Rathmann model (utilized in this study) with the canonical NOJ model. The wind speed ratio (WS_{ratio}) is plotted as function of distance from turbine (turbine at distance=0).

The time series described above based on the measurements within the park is used to force the wake combined model. The resulting flow field is obtained from an iteration procedure until convergence of the effective wind speed is obtained at all turbine positions in the OWF. An example of the resulting wind speed ratio (WS_{ratio}) across the radar scan area is shown in Figure 4-8.

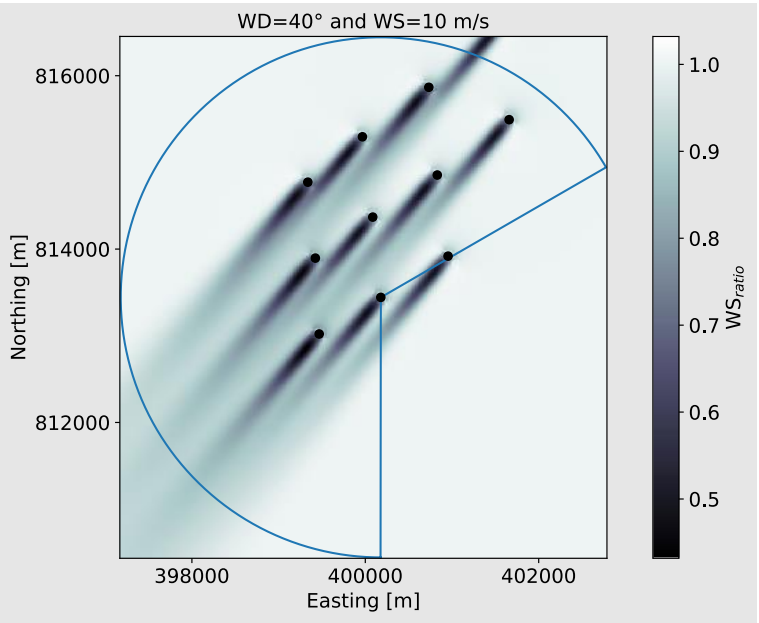

Figure 4-8 Wind speed ratio (WS_{ratio}) of EOWDC. Radar scan area shown as polygon. Wind speed is 10 m/s and wind direction is 40°. Coordinates in British National Grid.

5 Analysis of seabird flight behaviour

5.1 Analytical framework

The analytical frameworks associated with the two modes of sensor operation are shown in Figure 5-1.

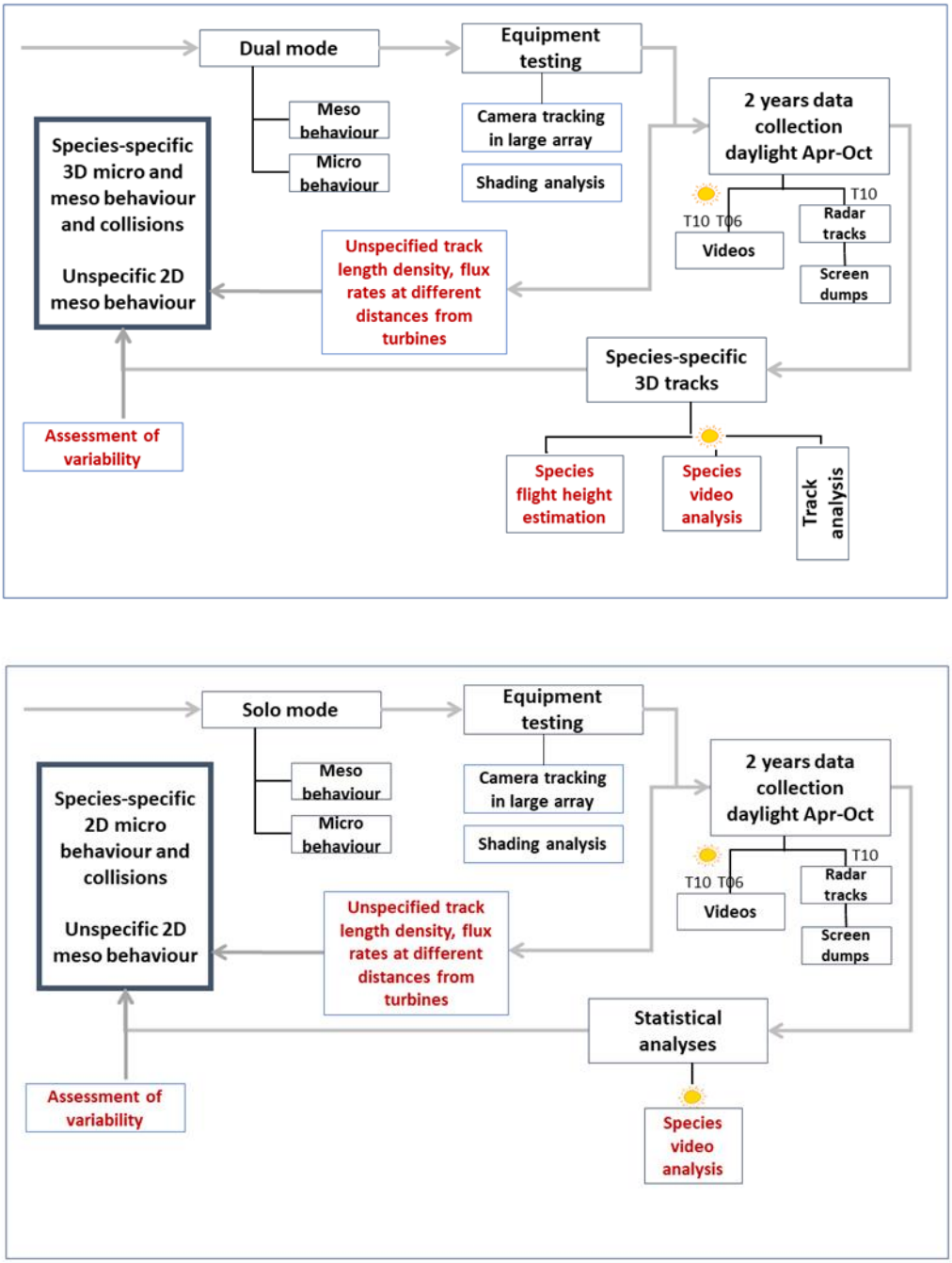

Figure 5-1 Overview of the analytical framework of the EOWDC Project

5.2 Protocols applied by video analysts

Recording of tracking information by radar and cameras

- Track-id to facilitate coupling of radar tracks and videos
- Date and time
- Bird target tracked by camera (Yes/no). For correct coupling to radar data for flight heights, speeds and directions
- Spatial assessment by radar (Yes/No). Judged by visual inspection of the associated radar track

Recording of weather conditions

- Judgement of sea state from the video recording according to the Beaufort wind force scale.

Recording of seabirds and flight behaviour

- Identification of target species to the level of species or species group
- Aging of bird targets if possible
- Recording of feeding/commuting behaviour, feeding including searching for prey
- Classification of seabird flight behaviour using standardized European Seabirds at Sea (ESAS) codes
- Behavioural confidence rating (high, medium, low)

Recording of the position of bird targets in space relative to turbines and rotors

- Categorization of the position of bird targets in macro-zone (outside wind farm array), meso-zone (inside wind farm array) and micro-zone (within +10m from rotors).
- Meso and micro-avoidance/non-avoidance behaviour of bird targets
- Collision

Recording of operational state of turbines

- Rotor speed, (stopped, very slow, operating)

5.3 QA procedures for video analyses

For validation, the data generated by the video analyses were subject to quality assurance. Because of the large sample sizes of analysed videos it was not feasible to conduct a complete quality assurance of all analysed videos. Rather quality assurance was performed partially by jack-knifing every 10th video analysis, and in addition focusing on specific parts of the video analysis that was considered particularly important:

- All recordings of micro-avoidance and collisions, including potential collisions
- All recordings of vertical meso-avoidance
- All species identification of black-backed gulls

5.4 Meso-avoidance behaviour

Meso-avoidance behaviour was assessed for the target species: Gannet, lesser black-backed gull, herring gull, great black-backed gull and kittiwake using the combined radar track and video data. Species and species groups were identified using video data, and vertical meso-avoidance was

also assessed with the video data. Although only a minor proportion of all radar tracks were associated with videos, the composition of bird species analysed from the videos were considered representative. This assumption is indeed valid as cameras were operating in dual mode for most of the time, during which their initial targets were triggered by the radar.

Spatial gradients in avoidance and attraction of target species within the array were quantified by using track length densities based on the coupled radar track and video data calculated as $1 - \frac{N_{in}}{N_{ref}}$, where N_{in} is the mean track length per unit area within 20 m wide buffer zones around the RSZ +10m and N_{ref} is the mean track length per unit area throughout the sub-area of the wind farm covered by the camera at AWF10. For the meso-avoidance analysis we only used data collected with a high and constant effort from the camera at AWF10 in 2021. The levels of meso-avoidance have been calculated at 20 m intervals from the tip of the rotor blades to approximately half distance between turbines.

The meso-avoidance behaviour was further analysed 3-dimensionally by assessing spatial gradients inside the turbine array in the following derived flight parameters which combined radar tracks and coupled dual-mode videos:

- Mean flight height;
- Mean flight speed; and
- Mean change in flight direction relative to the orientation of the rotor.

The flight statistics of the above parameters were calculated separately for feeding and commuting individuals as judged from the videos. It was also attempted to extract flight statistics separately for the different operational states of the turbines, but was not pursued due to low sample sizes for situations when the turbine was stopped.

5.5 Micro-avoidance behaviour

Assessment of micro-avoidance behaviour was primarily based on the qualitative judgements of the video analysts and quantified by calculating the proportion of birds adjusting/not adjusting their flight in the space of the rotors. The video data was screened to ensure quality data for the micro-avoidance analysis using the same process as applied in the ORJIP BCA project (Skov et al. 2018). The screening process consisted of three subsequent steps which included removing irrelevant material of movements other than birds, low quality video material and re-assessing previously coded behaviour.

The micro-avoidance analysis considered the behavioural reaction of the bird(s) to the orientation of the rotor and the presence of blades when entering the rotor swept zone (RSZ) and a 10 m buffer around it, unlike the meso-avoidance analysis, where only the position of the collected data was considered. The micro-avoidance behaviours were coded into one of the following five categories:

- Adjusting by returning before crossing the spinning rotor;
- Adjusting by stopping before crossing the spinning rotor;
- Adjusting flight path relative to rotor orientation when crossing the RSZ, sub-divided into different types of paths, i.e. perpendicular, oblique, along, etc;
- Non-adjusting flight path and crossing the RSZ; or
- Collision.

The Figure 5-2below illustrates the assessment scheme for micro-avoidance behaviour within the RSZ (blue circle) and 10 m buffer (red circle). Black arrows represent bird movement in relation to the rotor (dark blue ellipse + 10 m). The light blue arrow represents the wind direction.

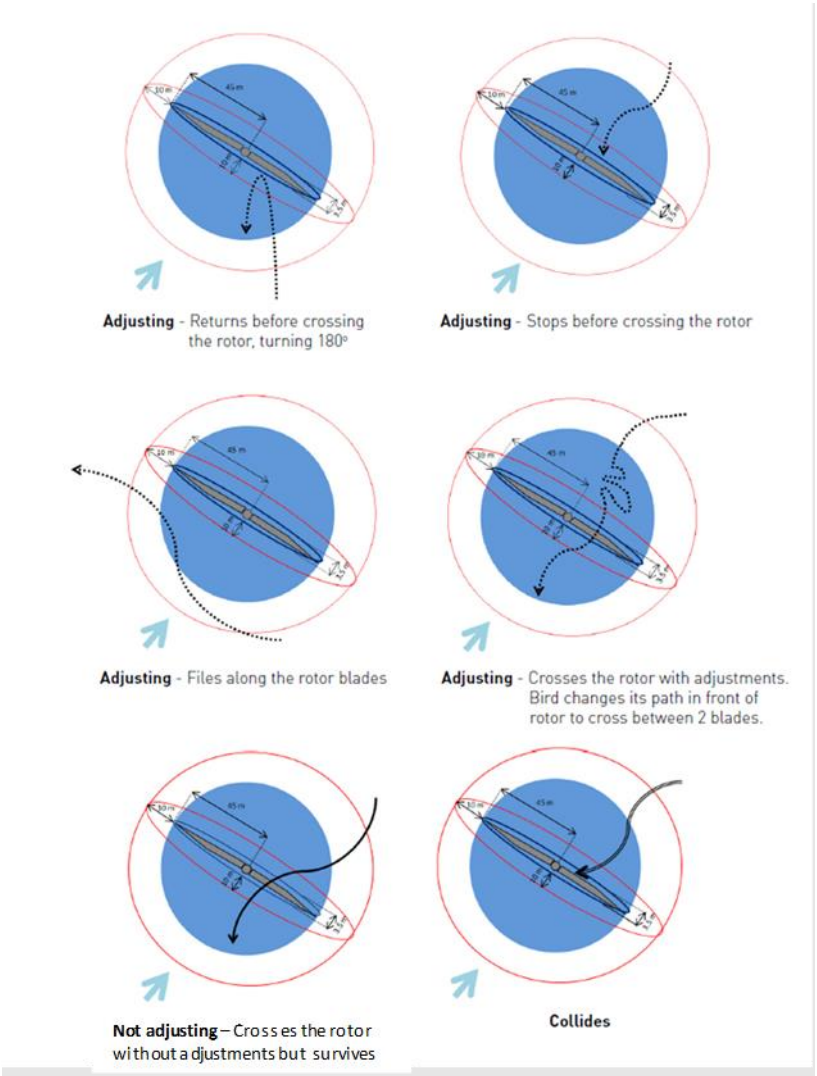

Figure 5-2 Assessment scheme for micro-avoidance behaviour (source: altered from the ORJIP BCA study (Skov et al. 2018))

Mean micro-avoidance rates for species or species groups with sufficient sample size were calculated as:

$$\frac{N_{birds\ adjusting\ flight}}{(N_{birds\ adjusting}+N_{birds\ not\ adjusting}+N_{birds\ colliding}}.$$

5.6 Collisions

No collisions have been recorded in the videos in the 2020-2021 survey periods.

5.7 Flight altitude, flight speed and flight direction

Flight height was estimated by triangulating the radar and video recordings of the same individual in close to real time for selected species. The estimated flight height was added to the video track data based on the track-id. The resolution of the 3-D tracks was similar to the 2-D tracks (approximately 30 m between track nodes) which was sufficient to generate detailed statistics on flight heights in relation to distance from rotors.

Seabird flight speeds in the wind farm were estimated from the radar tracks as the mean speed per segment of a track (every 2.5 sec) rather than the mean speed measured over the whole track.

Flight directions were assessed from the radar tracks by calculating the direction of a bird relative to the orientation of the rotors at that time. The orientation of the rotor was taken as perpendicular to the wind direction measured in the wind farm by Vattenfall at hourly intervals.

5.8 Classification of feeding/commuting birds

The analysis of bird behaviour assessed from the video recordings was undertaken by a team of trained specialists, highly skilled in species identification and good knowledge of flight behaviour. The video analysts were specifically instructed to distinguish between feeding and commuting behaviour of the identified species. The video analysts first recorded if the behaviour of a bird could be assigned to either feeding or commuting based on the flight path (tortuosity or unidirectional flight) or flight behaviour (flight speed or changes herein) as well as apparent interest (or lack thereof) in local conditions. Upon the primary classification, the type of flight behaviour was further classified using standardized codes (ESAS) for seabird flight behaviour (Camphuysen & Garthe 2004). Behaviour that could not be clearly assigned to either feeding or commuting, were assigned as ‘not determined’ and thus not included in the analysis regarding differences in flight behaviour of feeding and commuting birds. A track of a bird involved in feeding during part of or during the whole video was only classified as ‘feeding’.

5.9 Flight behaviour model

Local measurements of wind speed and wind direction were then temporally assigned to the radar bird tracks based on their time stamps. Flight altitude, speed and relative orientation in relation to wind turbine rotor were used as key parameters describing the 3-D flight and avoidance behaviour of birds in the near field of the wind turbine rotor. These three behaviours were coupled to the local wind and turbulence conditions to assess the seabird avoidance behaviour within the EOWDC. The behaviours were investigated using a machine learning (ML) random forest (RF) classifier. Recently, machine learning algorithms such as RF have been shown to outperform the traditional regression-based classifiers in studies of complex interactions between species behaviour/distribution and environmental variables (Breiman 2001, Zhang et al. 2019). The traditional regression modelling approaches are strictly assumption based (e.g., normality, data independency, and additivity) and the predictor variables need to be pre specified. These model assumptions are seldom true in an ecological context. In case of a large number of explanatory variables, the traditional regression-based approaches have a tendency of overfitting the data unless some information criteria such as Akaiki Information Criterion (AIC) are employed to reduce the number of parameters.

Here the avoidance-related flight behaviours of target species were coupled to the wind and turbulence conditions at the time of observation with a precision of 1 hour. Predictor variables were wind speed (m/s), turbulence-index (0 = high turbulence, 1 = no turbulence), activity (feeding /

commuting) and wind class (headwind, tailwind, sidewind). Distance to the tip of rotor blades of the nearest turbine was also included as a predictor as evidence from this study indicates that seabirds change their meso-avoidance behaviour as a function of distance to the turbines (Tjørnløv et al. 2021).

The relationship between flight patterns and wind conditions are likely to be non-linear, as avoidance is erratic by nature. Additionally, the bird movements inferred from the radar track nodes were spatially autocorrelated, as the position of a bird in a specific time is highly dependent on the previous position of the bird. Thus, the RF classifier was selected as appropriate, as it allows for fitting of non-linear relationships, while also being less sensitive to temporal and spatial auto-correlation than other non-linear methods like generalized additive models (Skov & Heinänen 2013).

5.9.1 Fitting of seabird flight model

The avoidance behaviour model was fitted as a multivariate random forest classifier, using the r-package RandomForestSRC. Rather than fitting each behavioural response in a univariate model, the multivariate setup allows for using the other models as covariates, when modelling each behaviour (Segal & Xiao 2011).

An individual model was fitted for each species, based on a subset of data, only using observations of the target species. Subsequently, all three behaviours were fitted as dependent variables and climatic variables as independent using the training data set. The number of trees grown and number of variables tested per split were optimized for each species using the tune function (package RandomForestSRC).

Model residuals from each behaviour were calculated and residual autocorrelation was estimated. Additionally, model coefficients and variable importance were extracted. Model precision was estimated OOB (out-of-bag) error rate, along with a prediction on the training data and a subsequent comparison between observed and predicted values from the training data set, using Spearman's and Pearson's correlation coefficients.

5.9.2 Predicting flight behaviour around rotors

The flight behaviour around the turbine rotors was predicted using static deployment data, where only one predictor would vary, keeping all other predictors steady. As the key interest was to see how birds changed their behaviour when closing in on rotors, distance to rotor was selected as the varying predictor. Next, four different climatic scenarios were created, with high/low wind speeds and high/low turbulence. Here, high wind speeds were defined as 11m/s wind, and low wind speeds was defined as 1 m/s. The turbulence coefficient was set to either 1 (no turbulence) or 0 (turbulence). This resulted in scenarios with low wind speed/low turbulence, low wind speed/high turbulence, high wind speed/low turbulence and high wind speed and high turbulence. Lastly, each scenario was predicted with head wind, tail wind and side wind, resulting in a total of 12 predictions per species.

The results of the flight models are presented in the chapters covering each of the flight parameters.

The validation of the models can be found in Appendix 5.

6 Equipment Performance Statistics

6.1 Performance

During the period of April to October in 2020 and 2021, the MUSE system has collected a large sample of radar tracks. During the early phase of the project in spring 2020 equipment coverage was lower compared to the rest of the study period. In 2021, except for a few relatively short offline periods and a single prolonged period of power outage in June 2021, coverage of the MUSE system was high up until mid-October 2021. The summary of the performance indicators of the radar and camera equipment deployed on AWF06 and AWF10 is shown in Table 6-2 below

Table 6-1 Timeline of operational performance of the MUSE system

2020

April	1	2	3	4	5	6	7	8	9	10	11	12	13	14	15	16	17	18	19	20	21	22	23	24	25	26	27	28	29	30	
May	1	2	3	4	5	6	7	8	9	10	11	12	13	14	15	16	17	18	19	20	21	22	23	24	25	26	27	28	29	30	31
June	1	2	3	4	5	6	7	8	9	10	11	12	13	14	15	16	17	18	19	20	21	22	23	24	25	26	27	28	29	30	
July	1	2	3	4	5	6	7	8	9	10	11	12	13	14	15	16	17	18	19	20	21	22	23	24	25	26	27	28	29	30	31
August	1	2	3	4	5	6	7	8	9	10	11	12	13	14	15	16	17	18	19	20	21	22	23	24	25	26	27	28	29	30	31
September	1	2	3	4	5	6	7	8	9	10	11	12	13	14	15	16	17	18	19	20	21	22	23	24	25	26	27	28	29	30	
October	1	2	3	4	5	6	7	8	9	10	11	12	13	14	15	16	17	18	19	20	21	22	23	24	25	26	27	28	29	30	31

2021

April	1	2	3	4	5	6	7	8	9	10	11	12	13	14	15	16	17	18	19	20	21	22	23	24	25	26	27	28	29	30	
May	1	2	3	4	5	6	7	8	9	10	11	12	13	14	15	16	17	18	19	20	21	22	23	24	25	26	27	28	29	30	31
June	1	2	3	4	5	6	7	8	9	10	11	12	13	14	15	16	17	18	19	20	21	22	23	24	25	26	27	28	29	30	
July	1	2	3	4	5	6	7	8	9	10	11	12	13	14	15	16	17	18	19	20	21	22	23	24	25	26	27	28	29	30	31
August	1	2	3	4	5	6	7	8	9	10	11	12	13	14	15	16	17	18	19	20	21	22	23	24	25	26	27	28	29	30	31
September	1	2	3	4	5	6	7	8	9	10	11	12	13	14	15	16	17	18	19	20	21	22	23	24	25	26	27	28	29	30	
October	1	2	3	4	5	6	7	8	9	10	11	12	13	14	15	16	17	18	19	20	21	22	23	24	25	26	27	28	29	30	31

MUSE system operational
MUSE system partially operational
Power outage (planned or unplanned)
MUSE system offline

Highest coverage of 100% across cameras, track and image data was found in July 2021, whilst the lowest overall coverage of 47% across all months was found in June 2021. Overall, the coverage across platforms has increased during 2021 averaging around 76% versus an average coverage of 59% in 2020. Moreover, coverage in the previous season in 2020 started out low in the beginning (April-June), then steadily increasing from July onward. Whereas in 2021, the coverage was high throughout the season, with only 2 months dipping below 60% coverage in June and October with an average coverage of 47% and 58% respectively.

Table 6-2 Coverage of radar track data, camera AWF06, AWF10 and radar screen images

Month	Radar track data coverage (%)	Camera AWF06 coverage (%)	Camera AWF10 coverage (%)	Radar screen images (%)
Apr-20	27	10	10	27
May-20	26	26	26	26
Jun-20	33	33	33	47
Jul-20	61	52	52	77
Aug-20	87	87	87	90
Sep-20	94	78	94	81
Oct-20	98	97	97	98
Apr-21	77	77	77	100
May-21	81	71	71	100
Jun-21	47	47	47	47
Jul-21	100	100	100	100
Aug-21	74	90	74	48
Sep-21	97	97	77	100
Oct-21	58	58	58	58
Average	76	77	72	79

6.2 Sample Sizes

A summary of the number of radar tracks and videos collected in 2020 and 2021 is shown in Figure 6-1 and Figure 6-2. The number of tracks recorded was higher in 2021 than 2020 with an average of 147,130. The new tracker installed on the 10th of January 2021, has had an effect on the sample sizes in 2021 by considerably reducing the number of videos collected and increased the frequency of flight height estimates along each track. The total number of recorded coupled radar and video tracks was 3,123. The seasonal average of number of radar tracks/hour was reduced substantially from 357 in 2020 to 268 in 2021. The number of videos was also reduced in 2021 compared to 2020, with an average of 3 videos/hour in 2021, versus 20 videos/hour in 2020. Whereas the reduction in the number of radar tracks during 2021 is considered to be a result of lower abundance of feeding seabirds compared to 2020, the significantly lower number of videos recorded during 2021 is due to the application of the AI-based camera tracker and the resulting lower level of false positive recordings as compared to 2020.

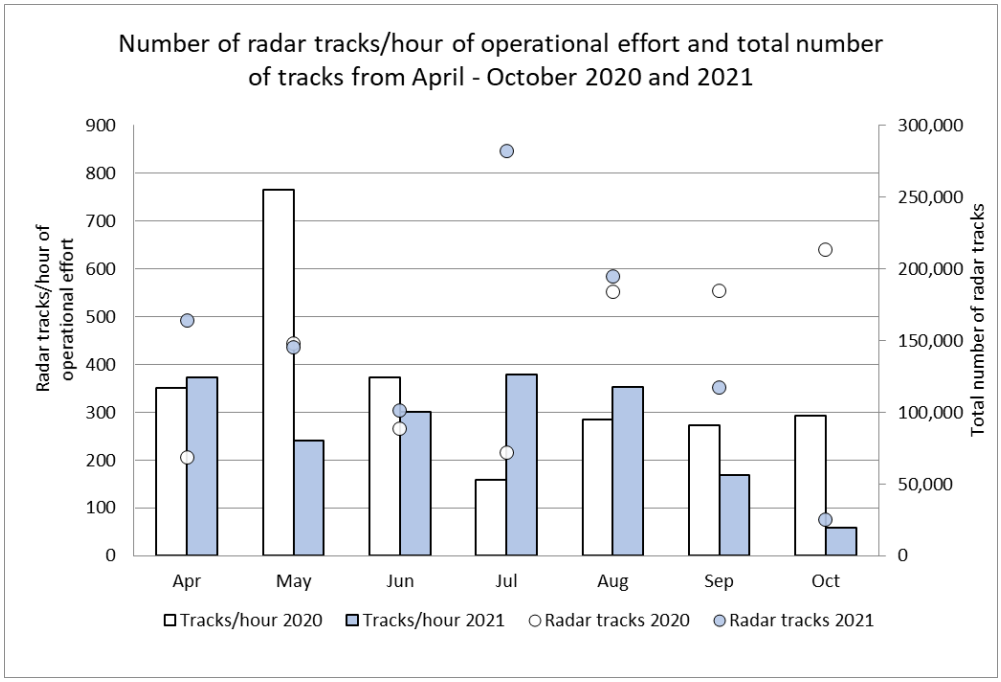

Figure 6-1 Number of radar tracks/hour of operational effort and total number of tracks from April-October 2020 (= white bars) and 2021 (= blue bars). Total number of radar tracks are depicted with a circle corresponding to the secondary axis (white circle = total radar tracks in 2020, blue circle = total radar tracks in 2021).

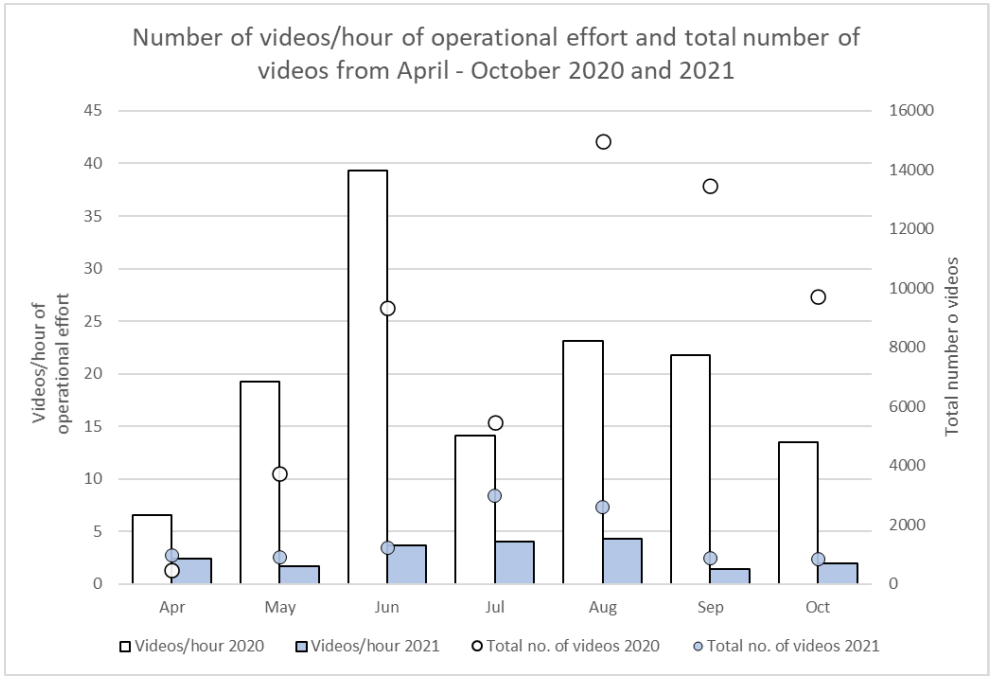

Figure 6-2 Number of videos/hour of operational effort and total number of video´s from April-October 2020 (= white bars) and 2021 (= blue bars). Total number of videos is depicted with a circle corresponding to the secondary access (white circle = total number of videos in 2020, blue circle = total number of videos in 2021). Note: there was a change in operational mode for camera AWF06 from June onward; regardless of this change, the videos/hour were similar for both cameras, so the average of both is still depicted.

7 Radar track densities

Radar bird tracks consist of track nodes collected with a temporal resolution of approximately 2.5 seconds corresponding to the rotation time of the radar antenna. When consecutive node positions in a track are connected by a line representing bird flight paths, the total length of all lines can be summarized within grids of a given size in order to generate track length densities across the entire radar detection zone. Compared to a simple count of track nodes in a grid, track length densities are insensitive to the size of the area over which densities are calculated. As track length densities are computed and plotted across the entire detection zone of the radar the resulting plots illustrate diurnal bird activity patterns both inside and outside the windfarm area. Individual rotor areas appear as white circles in the plot as these areas were not included in the processing and analysis of track length densities. Moreover, trace areas of low detection appear behind the rotor zones as a result of 'shading' from the rotors. Monthly mean track length densities during daylight hours are presented month-wise, side-by-side for both study years (Figure 7-1).

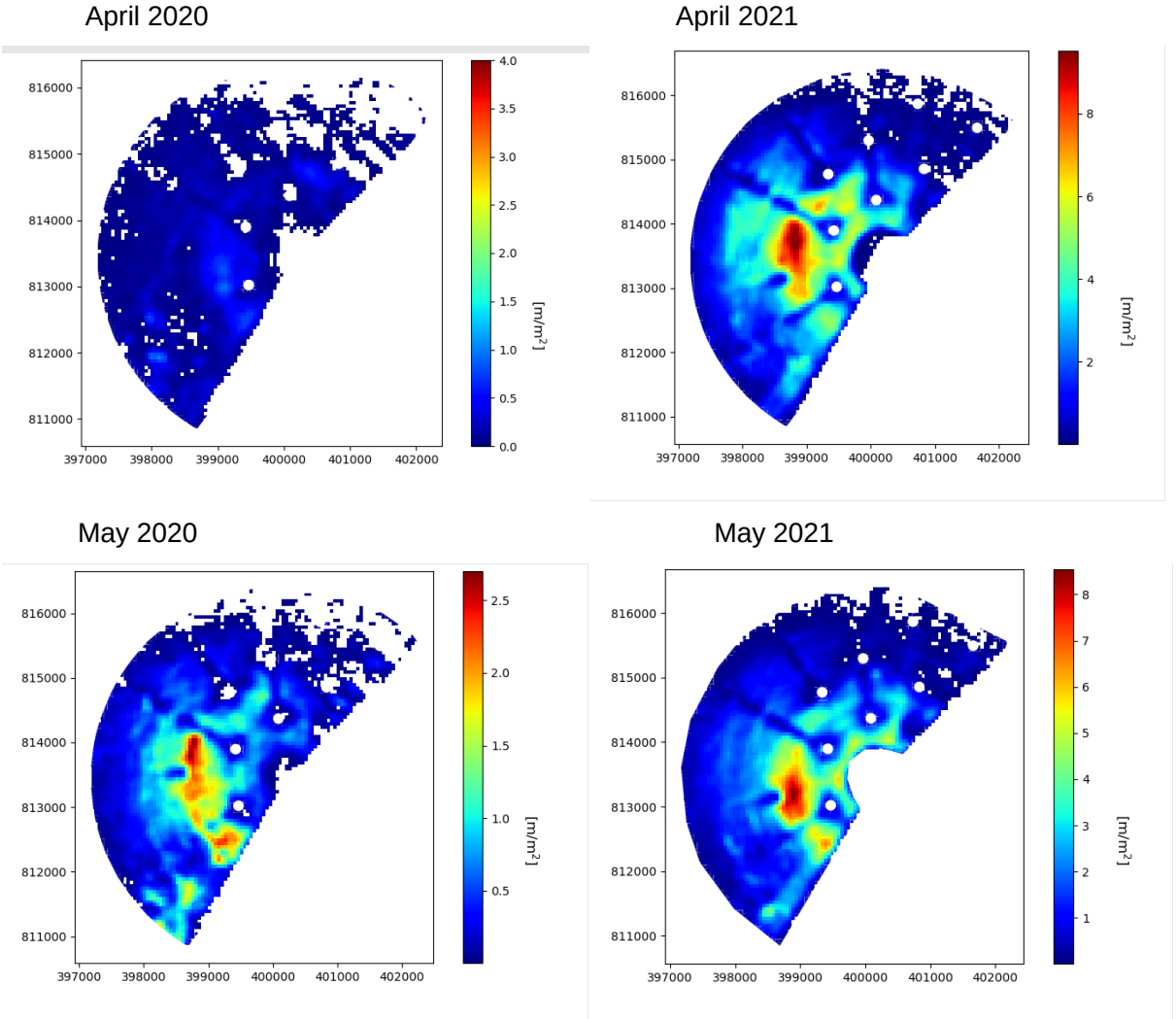

Figure 7-1 Monthly mean track-length densities (m/m^2) during daylight hours. Turbine rotors are indicated by white dots. Please note different colour scales have been applied. Recorded mean density during April 2020 was most likely affected by small number of days when the system was operational

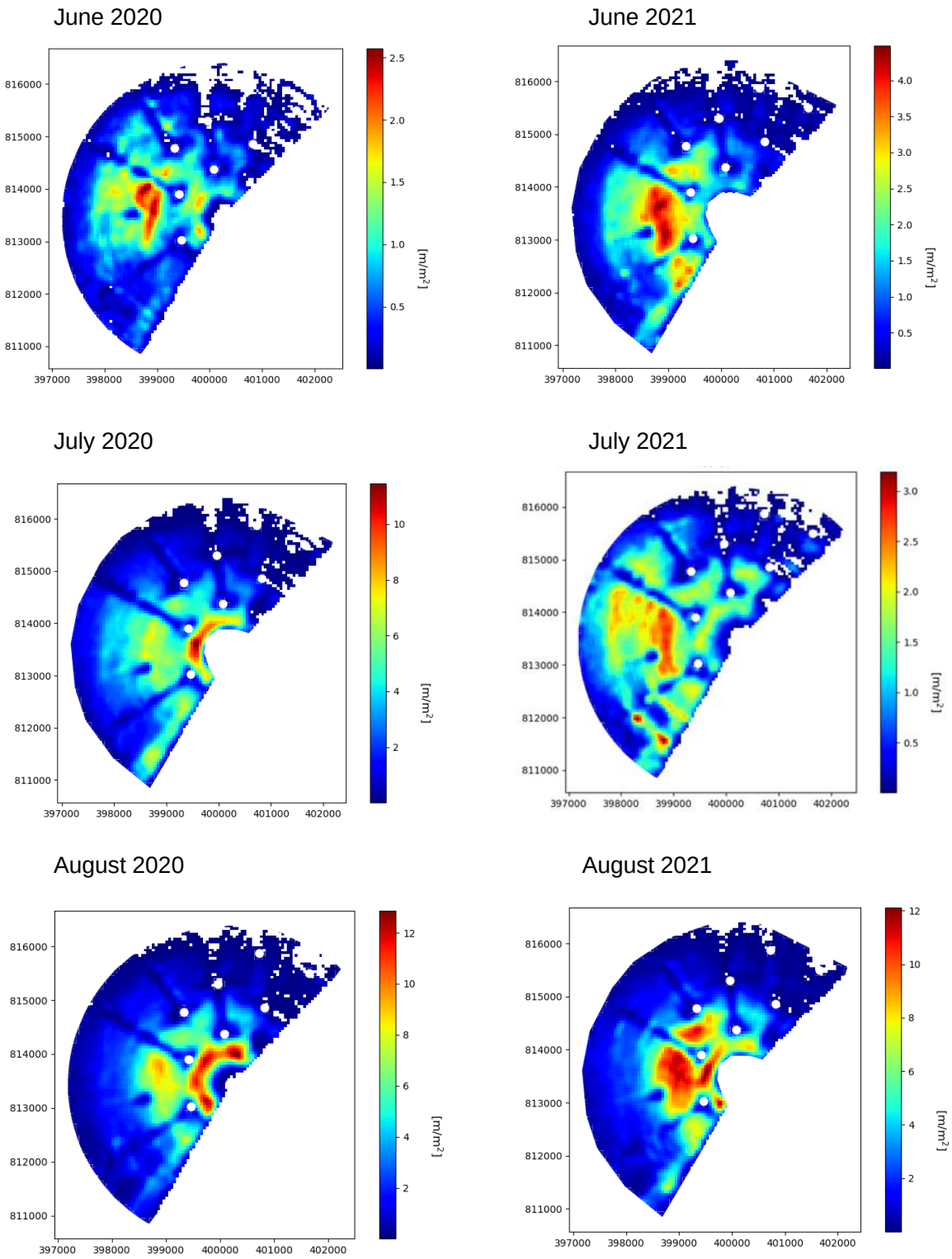

Figure 7-1 (Cont.)

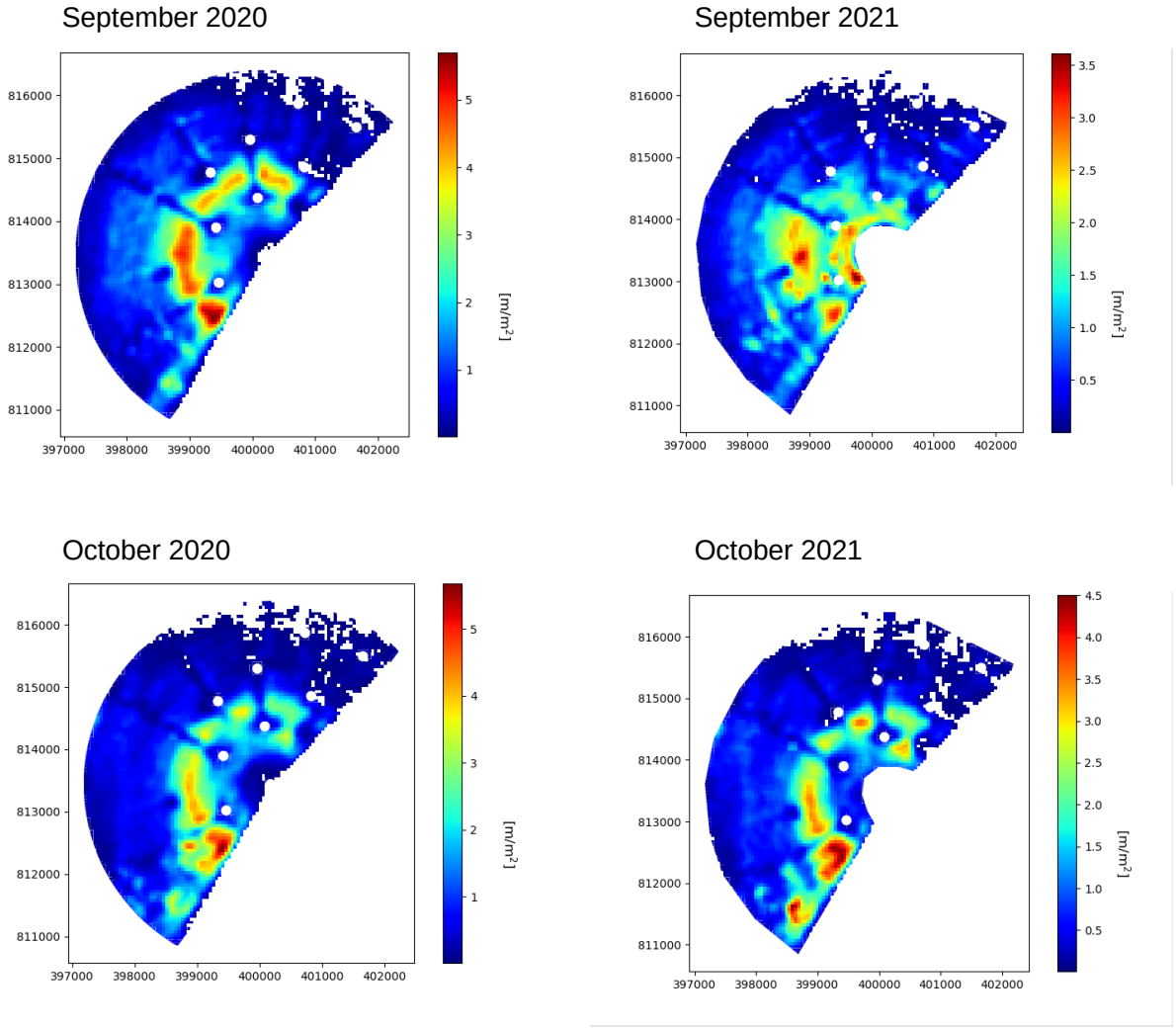

Figure 7-1 (Cont.)

The track-length density plots show a considerable degree of inter-annual variation between months. However, bird activity patterns in spring i.e. in May were quite similar between the two years with the highest track length densities displayed just west of the windfarm area possibly indicating a macro-avoidance response. Another possible explanation to this pattern could be attraction of birds to shoals of fish, however, this seems less likely as the pattern persists across seasons. Moreover, the activity patterns of birds flying inside the windfarm area in April and May show an attraction towards the areas between turbine rows and avoidance close to the turbines and rotor areas indicating a strong avoidance response at the meso scale. Meso-avoidance responses derived from these analyses are further discussed in Section 10.

8 Species composition and dynamics

The video data collected from cameras on AWF06 and AWF10 showed a considerable temporal variation in bird activity over the analysed period from April to October 2020 and 2021. The videos revealed relatively low levels of bird activity during spring continuing until mid-summer (April – July) followed by a prolonged period with higher activity in late summer and autumn (August – October). The level of bird activity was relatively low in April and May with small numbers of large and small gulls, gannets, kittiwakes, great black-backed gulls and few Procellarians (fulmars, shearwaters and storm petrels) and skuas recorded (Figure 8-1to Figure 8-4). Both June and July were also less active than later in the season with small numbers of unidentified large gulls and herring gulls and few procellarians. In August, the level of activity increased considerably with large numbers of unidentified large gulls and herring gulls. Moreover, gannets, kittiwakes, procellarians and skuas were all recorded in small numbers. Overall, September was the peak month for most of the target species recorded at the wind farm. However, there was a noticeable difference in the pattern of occurrence of kittiwakes and gannets between 2020 and 2021. In September 2020 large feeding flocks of kittiwakes were continuously recorded by the cameras resulting in very high kittiwake numbers in the analysed videos, however, this pattern was not observed in 2021, which had the peak of kittiwakes in August. September was also the peak month for gannets in 2020, whereas a similar peak was absent in 2021.

Despite a continued high diversity of species, bird activity in October reduced to a similar level as that recorded in August. Mixed feeding aggregations of auks, kittiwakes and herring gulls were frequently recorded in the wind farm during the period between mid-August and early October.

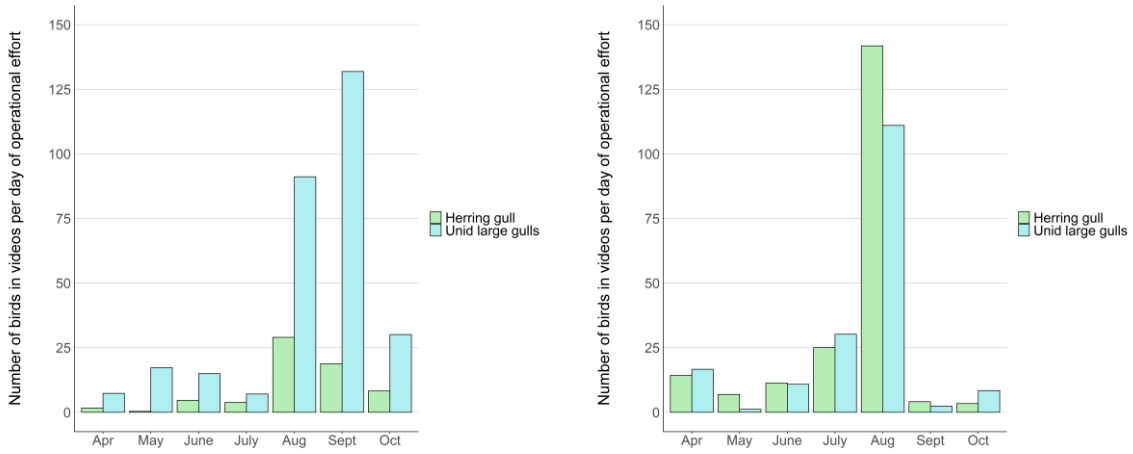

Figure 8-1 Number of unidentified large gulls and herring gulls in bird videos per day of operational effort from April – October in 2020 (left panel) and in 2021 (right panel).

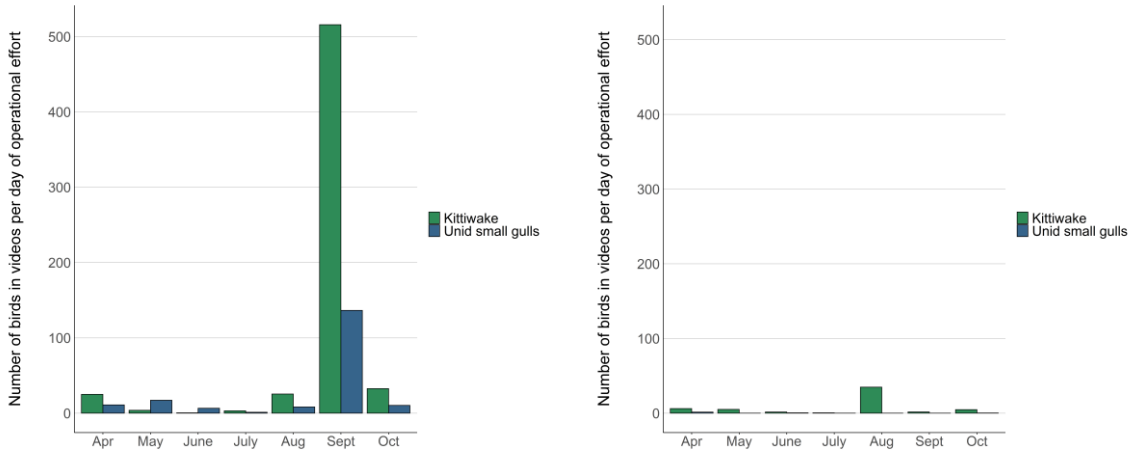

Figure 8-2 Number of unidentified small gulls and kittiwakes in bird videos per day of operational effort from April – October in 2020 (left panel) and in 2021 (right panel).

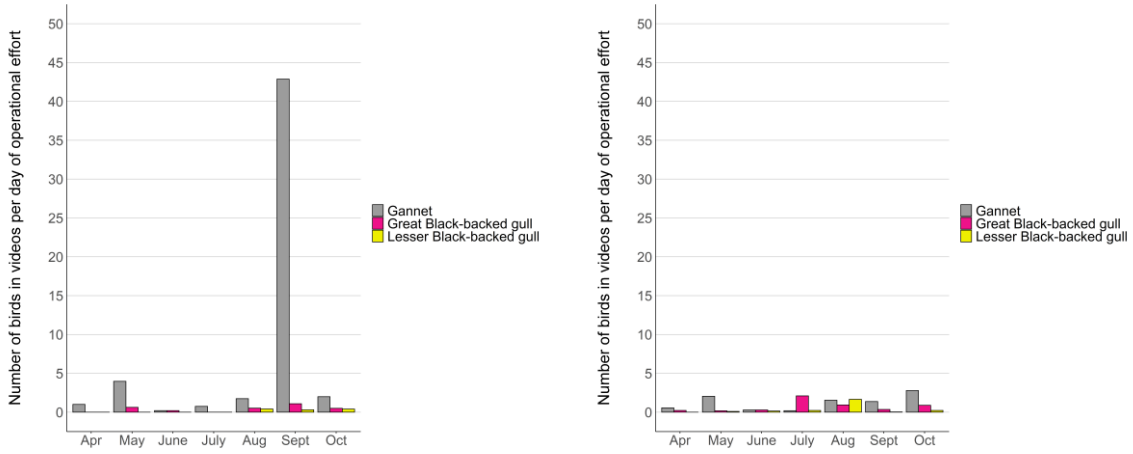

Figure 8-3 Number of gannets, great and lesser black-backed gulls in bird videos per day of operational effort from April – October in 2020 (left panel) and in 2021 (right panel).

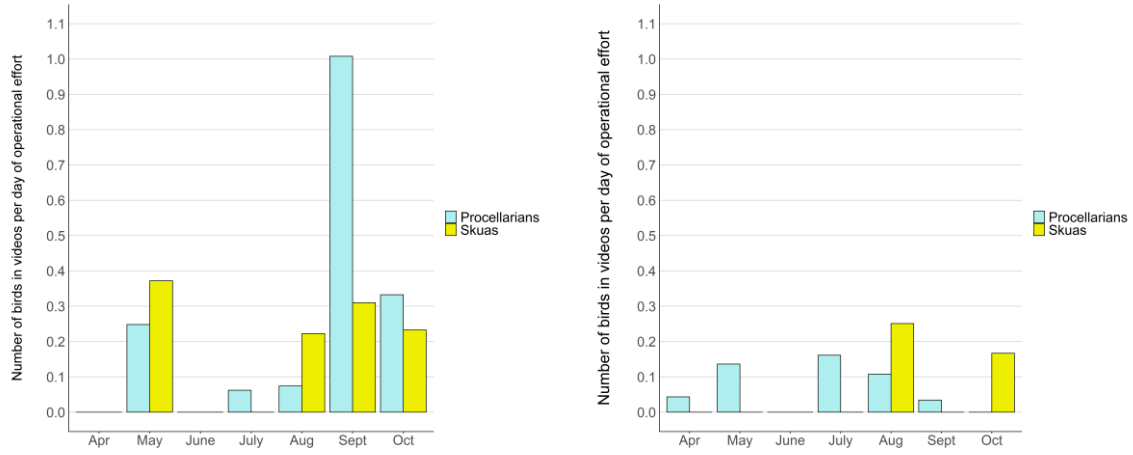

Figure 8-4 Number of procellarians (shearwaters, storm petrels and fulmars) and skuas in bird videos per day of operational effort from April – October in 2020 (left panel) and in 2021 (right panel).

Disregarding the potential difference in the ability of the MUSE system (the radar) to locate and track differently sized birds at high windspeeds and sea-states we analysed the frequencies at which target species appeared in the videos in relation to wind speed. The phenological patterns extracted from the data can therefore be seen as potentially including a bias against high wind speeds and sea states.

The frequency of different bird species recorded during autumn 2020, where bird activity was high, varied with the prevailing speed of the wind. Because some wind speeds may dominate for longer periods of time or be generally more regular than other wind speeds, we accounted for this potential bias in time by computing the number of some of the most commonly recorded species or species groups per hour of wind speed in three classes: <5 m/s, 5-8 m/s and >8 m/s (Figure 8-5 to Figure 8-7). During August – October 2020 the operational performance of the cameras was high (> 86%) and comparable between months, and hence, correction of bird numbers to account for operational performance during the three classes of wind speed was considered unnecessary. Consistently through August – October, unidentified large gulls and herring gulls were mainly recorded in light winds below 8 m/s. In fact, the majority of large gulls were recorded at low wind speeds <5 m/s. During the peak period in September, small gulls and kittiwakes were mainly recorded in medium wind speeds between 5-8 m/s and in strong winds >8 m/s. In contrast to the gulls, the vast majority of gannets were recorded in strong winds.

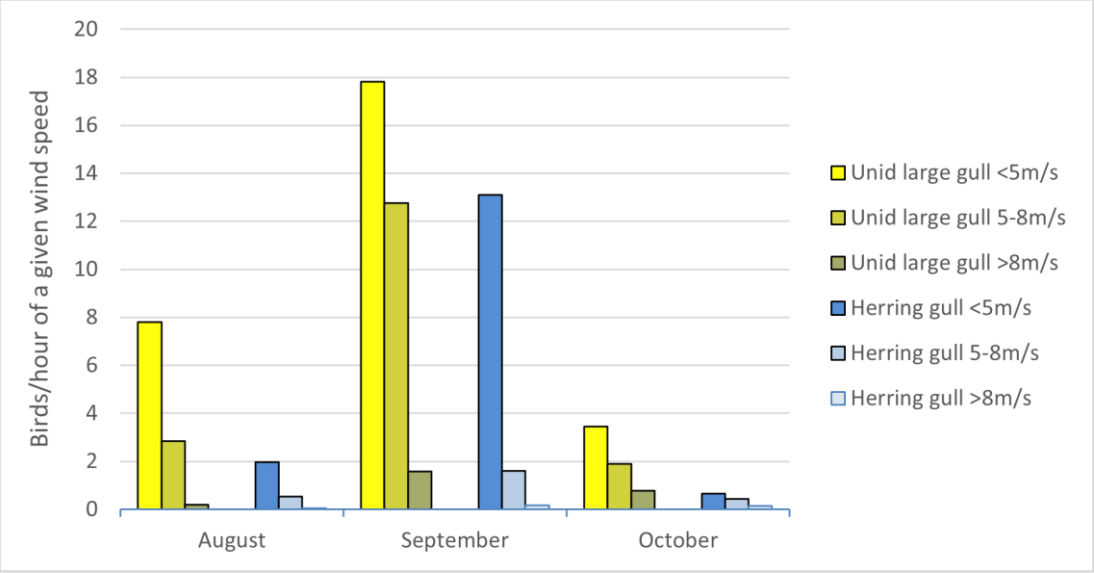

Figure 8-5 Number of unidentified large gulls and herring gulls recorded per hour of wind speed (<5m/s, 5-8m/s, >8m/s) during the months of high bird activity from August – October 2020.

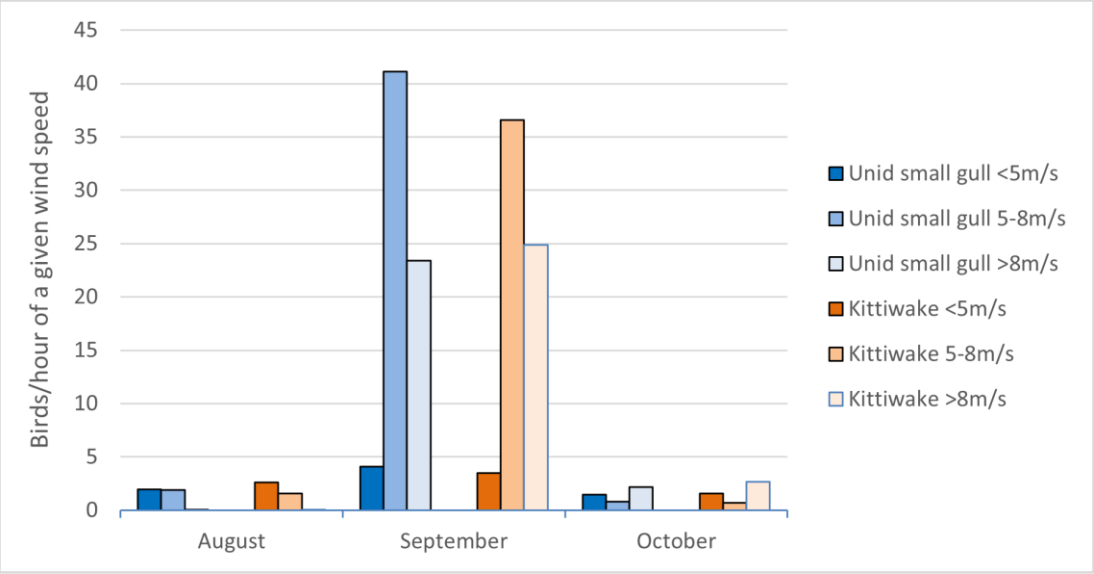

Figure 8-6 Number of unidentified small gulls and kittiwakes recorded per hour of wind speed (<5m/s, 5-8m/s, >8m/s) during the months of high bird activity from August – October 2020.

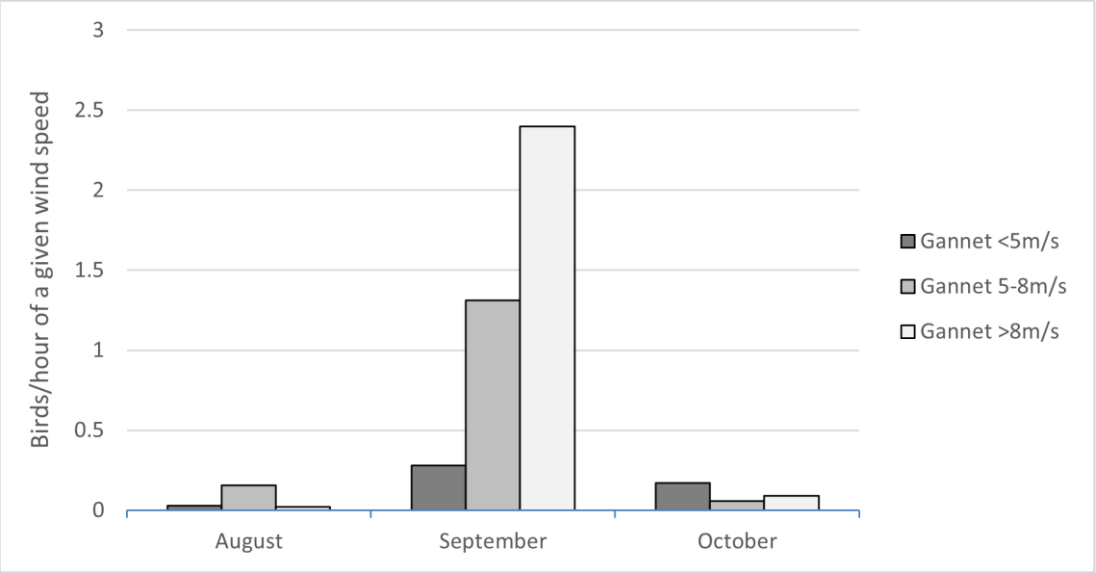

Figure 8-7 Number of gannets recorded per hour of wind speed (<5m/s, 5-8m/s, >8m/s) during the months of high bird activity from August – October 2020.

As a result of the temporal pattern of occurrence and absolute numbers recorded, the monthly composition of species changed noticeably over the study period from April – October (Figure 8-8, Figure 8-9, **Table** 8-1). In April, diversity was relatively low with gulls, kittiwakes and gannets as the predominant species or species groups. Diversity increased in May with small proportions of great and lesser black-backed gulls along with other seabirds such as skuas and terns. In May, the species composition was dominated by large and small gulls, kittiwakes and gannets. Unidentified large and small gulls and herring gulls constituted the largest proportions of birds recorded by the cameras in June (Figure 8-8 and Figure 8-9). July was roughly similar to June in species composition but had a larger proportion of kittiwakes in 2020 and a larger proportion of great black-backed gulls in 2021. In both years, August had a higher diversity compared to previous months with lesser and great black-backed gulls, auks, terns, skuas and cormorants recorded in small proportions (grouped as other seabirds in Figure 8-8 and Figure 8-9). In September, the high

diversity continued but kittiwakes were recorded in a larger proportion of the videos compared to the previous month. In both years, the species composition in October was similar to the species composition recorded for August and a continued high diversity of species.

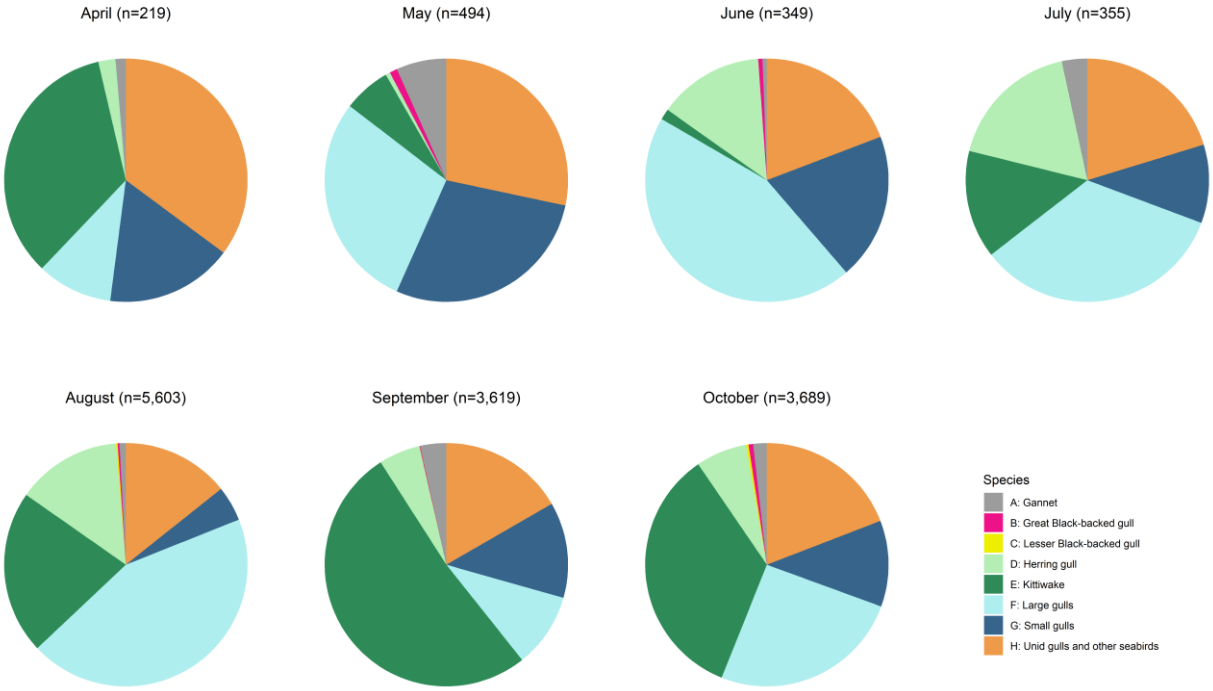

Figure 8-8 Monthly pie charts of proportions of species and species groups in 2020.

Figure 8-9 Monthly pie charts of proportions of species and species groups in 2021.

Table 8-1 Monthly mean track length densities per target species

Species / Species group	Year	Apr	May	Jun	Jul	Aug	Sep	Oct
Northern Gannet	2020	0.02	0.38	0.04	0.38	0.23	0.50	0.21
Northern Gannet	2021	0.22	2.26	0.08	0.08	0.07	1.05	0.51
Great Black-backed gull	2020	0	0.06	0.04	0	0.07	0.01	0.07
Great Black-backed gull	2021	0.08	0.20	0.08	0.81	0.04	0.26	0.16
Lesser Black-backed gull	2020	0	0	0	0	0.05	0	0.04
Lesser Black-backed gull	2021	0	0.10	0.04	0.09	0.08	0.03	0.04
Herring gull	2020	0.03	0.03	0.91	2.02	3.84	0.79	0.79
Herring gull	2021	5.54	7.63	3.26	9.72	6.78	3.14	0.62
Black-legged Kittiwake	2020	0.51	0.36	0.09	1.63	5.97	7.39	4.01
Black-legged Kittiwake	2021	2.38	5.52	0.45	0.16	1.66	1.28	0.86
Large gulls	2020	0.15	1.63	2.91	3.85	12.07	1.42	2.97
Large gulls	2021	6.46	1.31	3.12	11.73	5.30	1.83	1.53
Small gulls	2020	0.25	1.61	1.27	1.19	1.28	1.82	1.33
Small gulls	2021	0.64	0	0.16	0.08	0.01	0	0.17
Unid gulls and other seabirds	2020	0.52	1.61	1.25	2.31	3.92	2.39	2.23
Unid gulls and other seabirds	2021	8.07	0.50	4.74	3.82	16.54	1.59	6.02

9 Feeding activity

The density of seabirds in the AOWFL varies tremendously over time. This variation is mainly due to Mixed Species Feeding Aggregations (MSFAs) which move into the wind farm over shorter or longer periods of time. During the presence of MSFAs the density of seabirds within the array can be very high. Based on the number of MSFAs involving at least 10 individuals of at least one of the target species of seabirds an overview of MSFAs recorded by the cameras is provided in **Table 9-1**. The vast majority of MSFAs during 2020 were recorded in September, while the vast majority during 2021 were recorded during August. There was approximately twice as many recordings of MSFAs during 2020 as compared to 2021.

Table 9-1 The number of MSFAs recorded on the videos within the AOWFL during 2020 and 2021. Table shows total number of MSFAs per month involving at least 10 individuals of at least one of the target species of seabirds

	2020	2021
Apr	2	14
May	2	1
Jun	0	2
Jul	2	4
Aug	36	289
Sep	660	2
Oct	0	9
Total	**702**	**321**

10 Meso-avoidance

In total, 9,998 birds of target species including unidentified small and large gulls were recorded by the cameras in the meso zone (Table 10-1). Video data on meso-avoidance behaviour showed that in 97.7% of the video recordings the target species avoided the RSZ by flying in between the turbines with very few avoiding by changing their flight altitude in order to fly either below or above the rotors (Table 10-1). This pattern of avoidance behaviour was remarkably similar for all three species of large gulls.

Table 10-1 Meso-avoidance behaviour of target species recorded by cameras during 2020 and 2021. Table columns "BELOW ROTOR" and "ABOVE ROTOR" indicate numbers of birds changing their flight height in order to avoid the RSZ.

SPECIES	BIRDS IN MESO ZONE	BELOW ROTOR	ABOVE ROTOR
Unidentified large gull	3388	15	7
Herring gull	2624	22	5
Unidentified small gull	706	2	1
Kittiwake	2178	53	1
Gannet	781	17	0
Great and lesser black-backed gull	321	5	2

Rates of meso-avoidance/attraction were calculated based on species-specific track-length densities in the meso zone (Figure 10-1).

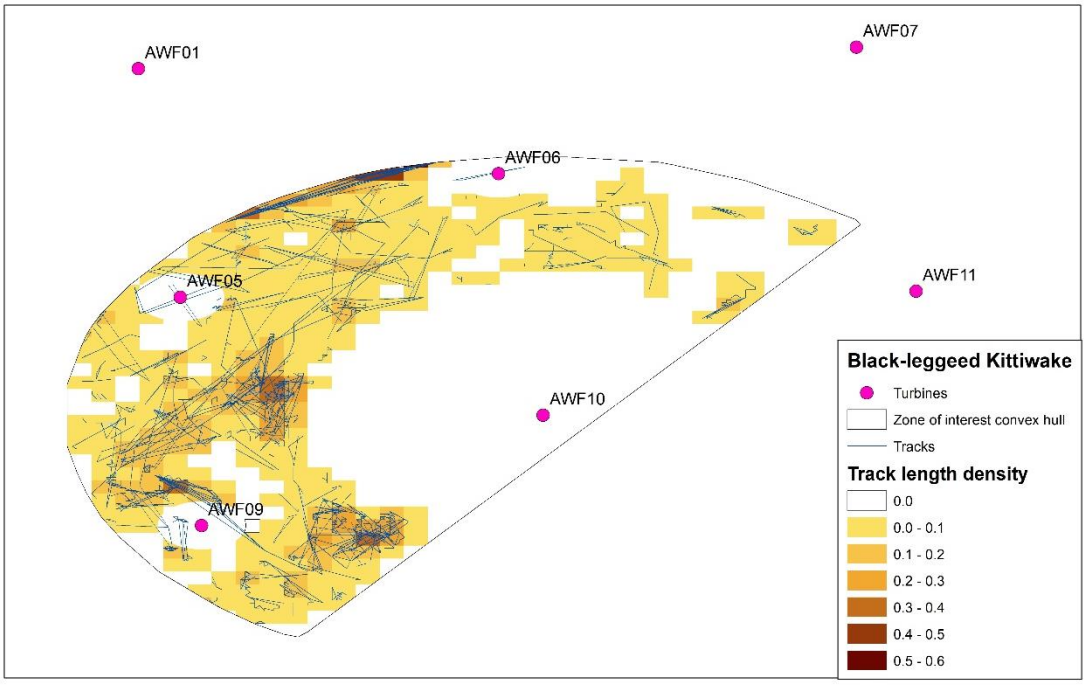

Figure 10-1 Tracks and track length densities of kittiwakes flying in the meso zone in 2021. Track length densities are used to calculate species-specific meso-avoidance/attraction patterns at 10 m intervals in relation to distance from nearest rotor during daytime hours.

The mean meso-avoidance/attraction patterns indicate increasing avoidance within distances of less than 100 m from the tip of the rotor blades (Figure 10-2). As determined from the recorded patterns of track length density, kittiwakes displayed horizontal meso-avoidance from 140-160 m distance from the rotors. Commuting herring gulls showed meso-avoidance from 90-110 m distance and feeding herring gulls from 60-80 m distance. Close to the blades herring gulls showed a maximum avoidance level of 0.70, while kittiwakes showed a maximum avoidance level of 0.5 – for both species this seems to take place at 20-40 m distance. At distances beyond 110-130 m herring gulls displayed negative avoidance levels reflecting attraction to the meso zone between turbines. Kittiwakes displayed negative avoidance rates from a distance of 150-170 m.

Small samples sizes were achieved for gannets and great black-backed gulls and both species displayed a pattern of avoidance/attraction which differed from that of herring gulls and kittiwakes. Gannets only displayed avoidance at distances closer than 40 m from the tip of the rotor blades, while great black-backed gulls showed avoidance at distances closer than 50 m. Maximum avoidance displayed by both species was 0.5. Both species showed attraction to the zone adjacent to the avoidance zone – for gannets from 40 m to 130 m distance and for great black-backed gulls from 55 m to 160 m distance.

Although the data on meso avoidance behaviour of the target species collected in this study were significantly more detailed than obtained in the ORJIP BCA study a comparison was made with the meso avoidance rate as calculated in the ORJIP study (Skov et al. 2018). The meso avoidance rates were calculated as $1 - \frac{N_{in}}{N_{ref}}$, where N_{in} is the mean track length per unit area within the RSZ + a 10 m wide buffer zones and N_{ref} is the mean track length per unit area throughout the sub-area of the wind farm covered by the camera at AWF10 in 2021. The estimated meso avoidance rates are shown in Table 10-2, and show comparable rates with ORJIP for unidentified large gulls and gannet, while slightly lower rates were estimated for herring gulls and great black-backed gulls. The meso avoidance rate estimated for kittiwakes (0.31) was much lower than reported in the ORJIP study.

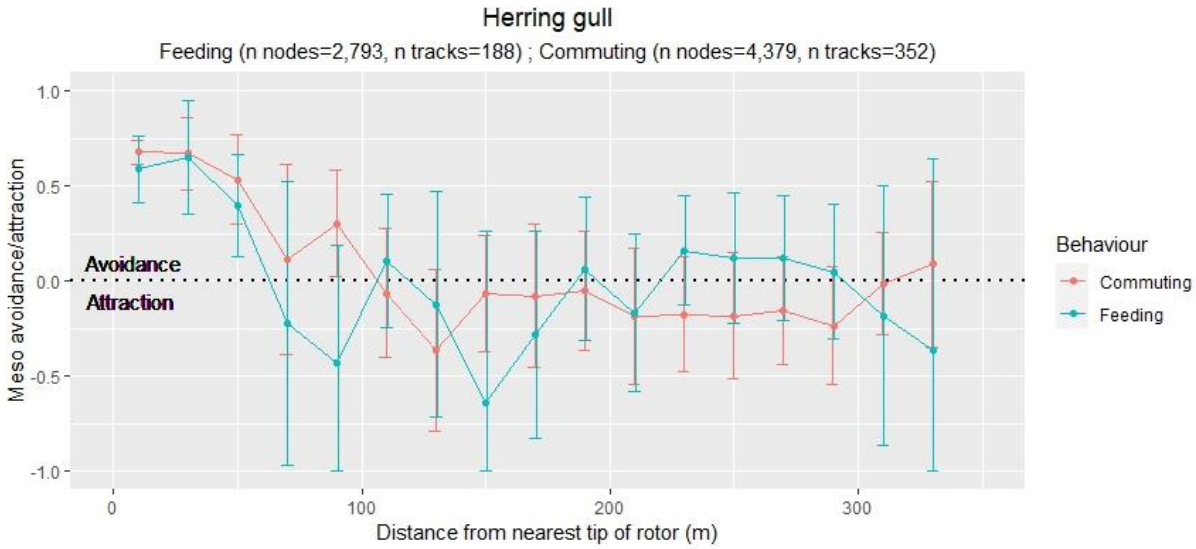

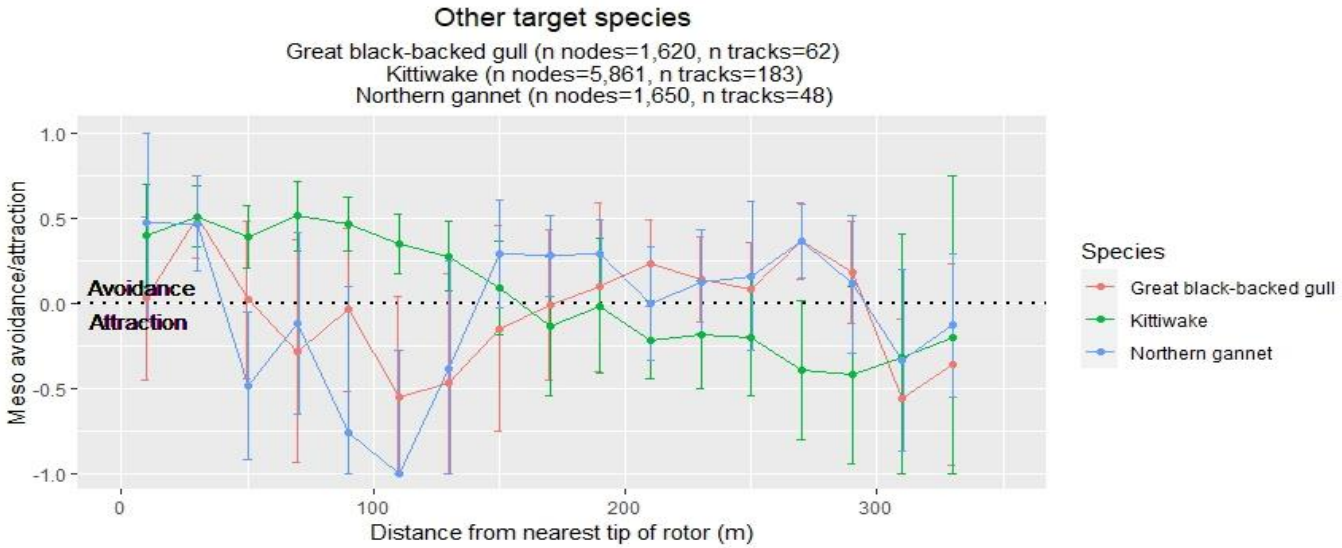

Figure 10-2 Mean meso-avoidance/attraction levels of herring gulls (separated into feeding/commuting behaviour) and other target species calculated at 20 m intervals in relation to distance from nearest rotor during daytime hours. Sample sizes refer to the number of radar track nodes and radar tracks and error bars indicate the SE computed from the variation in track length densities between different turbines (n=4).

Table 10-2 Overall Meso avoidance rates calculated based on a similar methodology as in the ORJIP BCA study (Skov et al. 2018).

SPECIES	Overall Meso EAR
Herring gull	0.69
Unidentified large gull	0.87
Great black-backed gull	0.71
Kittiwake	0.31
Gannet	1

11 Micro-avoidance

In general, gannets, small and large gulls showed a strong tendency to avoid flying into the rotor swept zone defined as a circular area with a radius equivalent to the length of the rotor blades (82 m + 10m buffer). Hence, only 180 occurrences of target species (5.76**%**) flying into the micro zone was recorded. The video analyses highlighted that in the vast majority of the videos classified as entering the micro zone, target species adjusted their flight in order to avoid the spinning rotor (Table 11-1). The most frequently recorded adjustment of the flight was of birds flying along the plane of the rotor which was recorded in 67% of the videos of behaviour in the micro zone. Large gulls adjusted their flight behaviour to cross the rotor either obliquely or perpendicularly more frequently than gannets and kittiwakes. In five videos recorded in the micro zone, target species showed non-avoidance behaviour by crossing the rotor swept area without making adjustments to the spinning rotor in flight behaviour (Table 11-2), leading to high micro-avoidance rates above 0.96 (Table 11-3).

No videos of target species showed a collision with a rotor.

Table 11-1 Species-specific micro-avoidance behaviour of target species recorded by cameras in 2020 and 2021. The proportion of analysed videos showing % of cases where birds were crossing the RSZ in spinning rotor mode. spinning is indicated

SPECIES	VIDEOS IN MICRO ZONE	RETURNS	STOPS BEFORE CROSSING	ALONG ROTOR	CROSSING WITH ADJUSTMENTS	% CROSSING IN ACTIVE ROTOR MODE
Unidentified large gulls	54	6	1	32	13	85%
Herring gull	68	9	1	41	15	66%
Unidentified small gull	7	1	2	4	0	
Kittiwake	28	0	1	24	3	66%
Gannet	10	1	1	8	0	
Great/lesser black-backed gull	13	2	0	9	1	100%
Total	**180**	**19**	**6**	**118**	**32**	**75%**

Table 11-2 Species-specific micro non-avoidance behaviour of target species recorded by cameras in 2020 and 2021. All recordings were made using videos showing rotors spinning. The proportion of analysed videos showing % of cases where birds were crossing the RSZ in spinning rotor mode.

SPECIES	VIDEOS IN MICRO ZONE	CROSSING WITHOUT ADJUSTMENTS	% CROSSING IN ACTIVE ROTOR MODE	COLLISIONS
Unidentified large gulls	54	2	50%	0
Herring gull	68	2	0%	0
Unidentified small gull	7	0		0
Kittiwake	28	0		0

Gannet	10	0		0
Great/lesser black-backed gull	13	1	0%	0
Total	**180**	**5**	**20%**	**0**

Table 11-3 Species-specific micro-avoidance rates of unidentified large gulls, herring gulls and small gulls based on video data collected in 2020 and 2021 (calculated for species/species-groups with sample sizes ≥ 25). All small gulls refer to unidentified small gulls and Kittiwake.

SPECIES	MEAN MICRO-AVOIDANCE RATE	SAMPLE SIZE
Unidentified large gulls	0.963	54
Herring gull	0.971	68
All small gulls	1.0	35
Kittiwake	1.0	28

Figure 11-1 Video sequences showing examples of micro avoidance behaviour. Upper sequence shows a Herring Gull flying along the plane of the rotor. Lower sequence shows a Herring Gull crossing a still rotor perpendicularly without adjustments.

12 Flight altitude

Flight heights in the wind farm array, as derived from the combined radar track and video data, were assessed by histograms (Figure 12-1) and by extracting the mean flight height of all target species in relation to distance from the rotors (Figure 12-2). Examples of 3-D track trajectories are visualised in Figure 12-3.

All the target species of seabirds were predominantly recorded flying at altitudes above the lower tip height of the rotors, but below the hub height with gannets and kittiwakes flying approximately 20 m lower than herring gulls and other large gulls. A weak tendency to increase flight heights when approaching the rotors at distances closer than 150 m was recorded for herring gulls and kittiwakes.

The results of the flight models revealed a high degree of variation in the effect of wind and turbulence conditions on the flight altitude of the target species (Figure 12-4 - Figure 12-7). Turbulence affected the flight height of all target species more than other weather parameters with the tendency to increase flight height on approach to the rotor being identified only during situations with high turbulence levels. Wind speed affected the distance at which the increase in flight height took place as the response took place well beyond 100m distance at low wind speeds. Superimposed on these trends there was a predicted tendency for all target species to fly at higher altitudes during tail winds in situations with a combination of low turbulence and high wind speed. These trends were apparent irrespective of whether the birds were recorded as feeding or commuting.

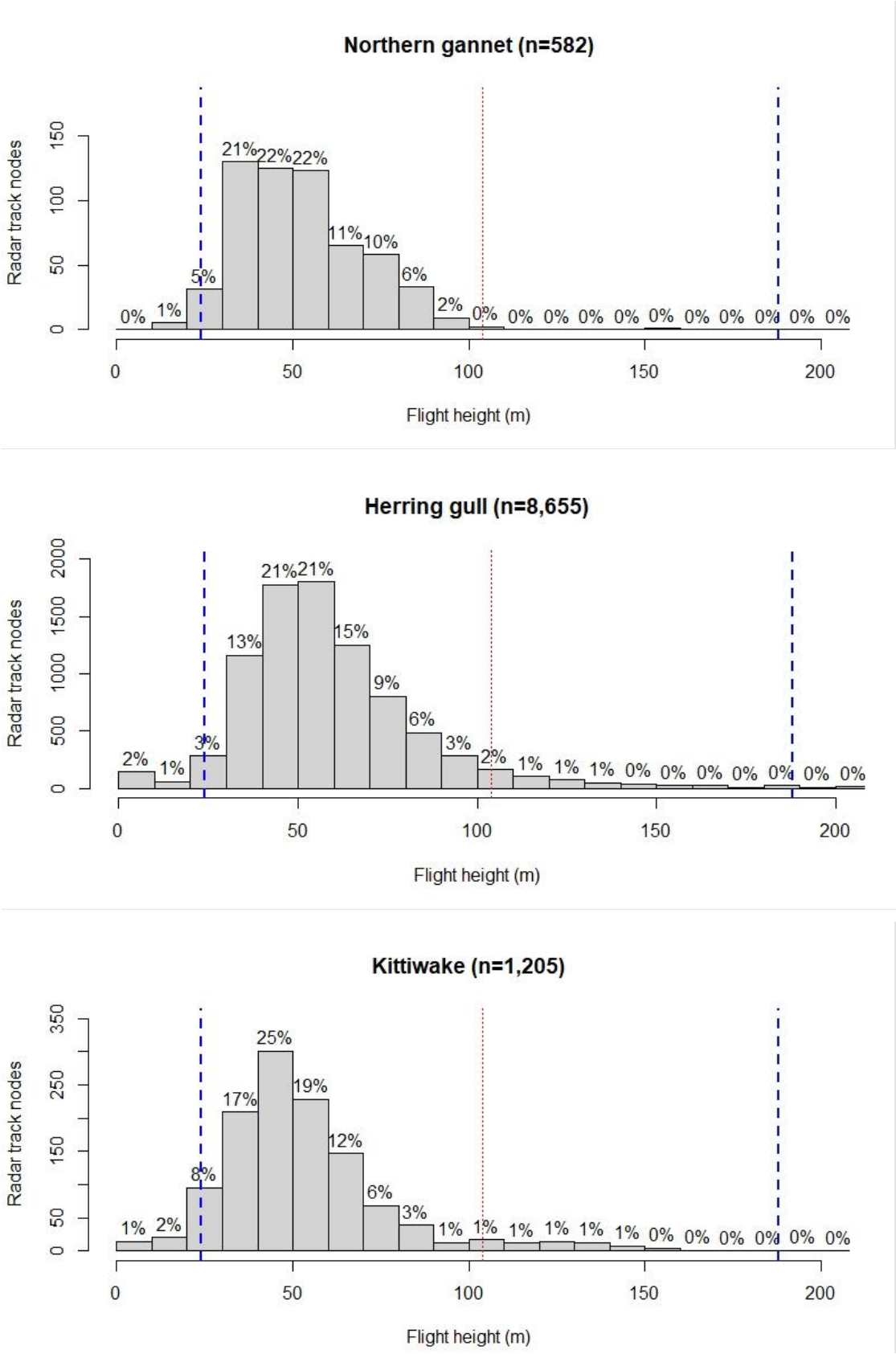

Figure 12-1 Histograms of flight heights of target species in 2021. Lower and upper boundaries of the RSZ and hub height of turbines are indicated.

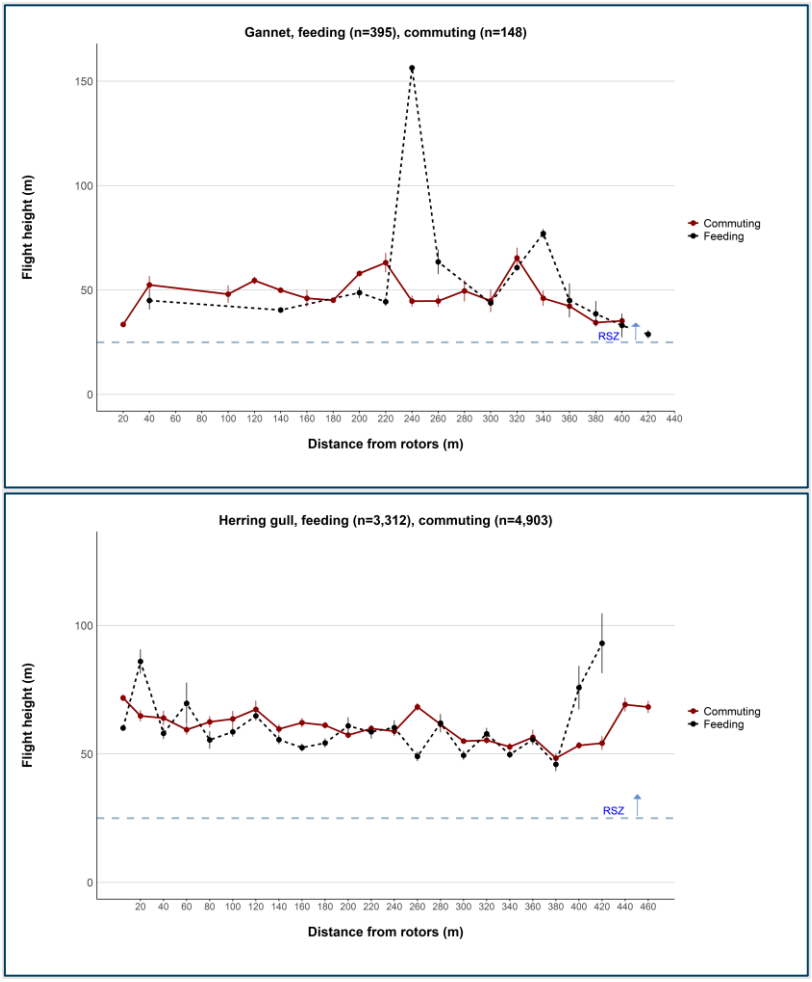

Figure 12-2 Mean observed flight heights of target species (using triangulation) and shown in relation to distance from nearest turbine during daytime hours in 2021. Lower boundary of the RSZ indicated with a blue long-dashed line.

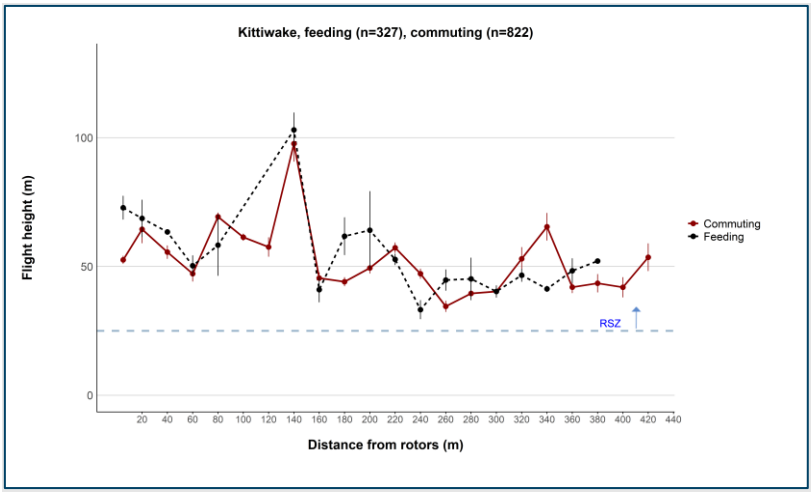

Figure 12-2 (Cont).

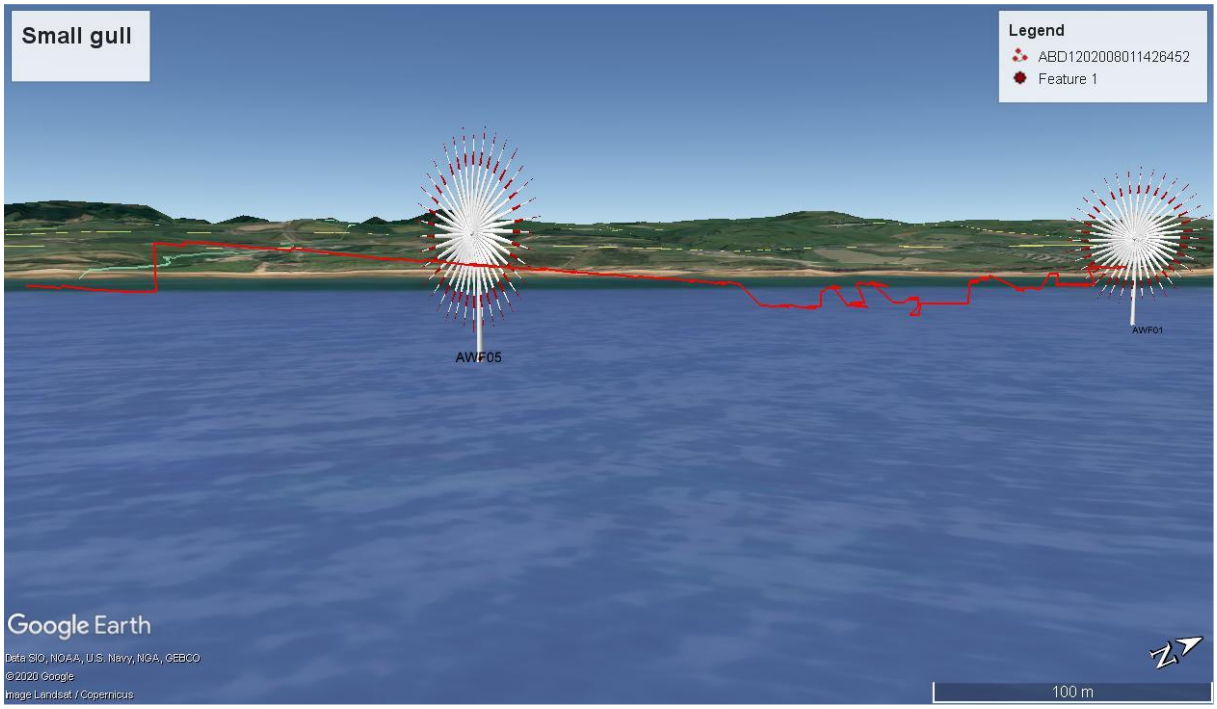

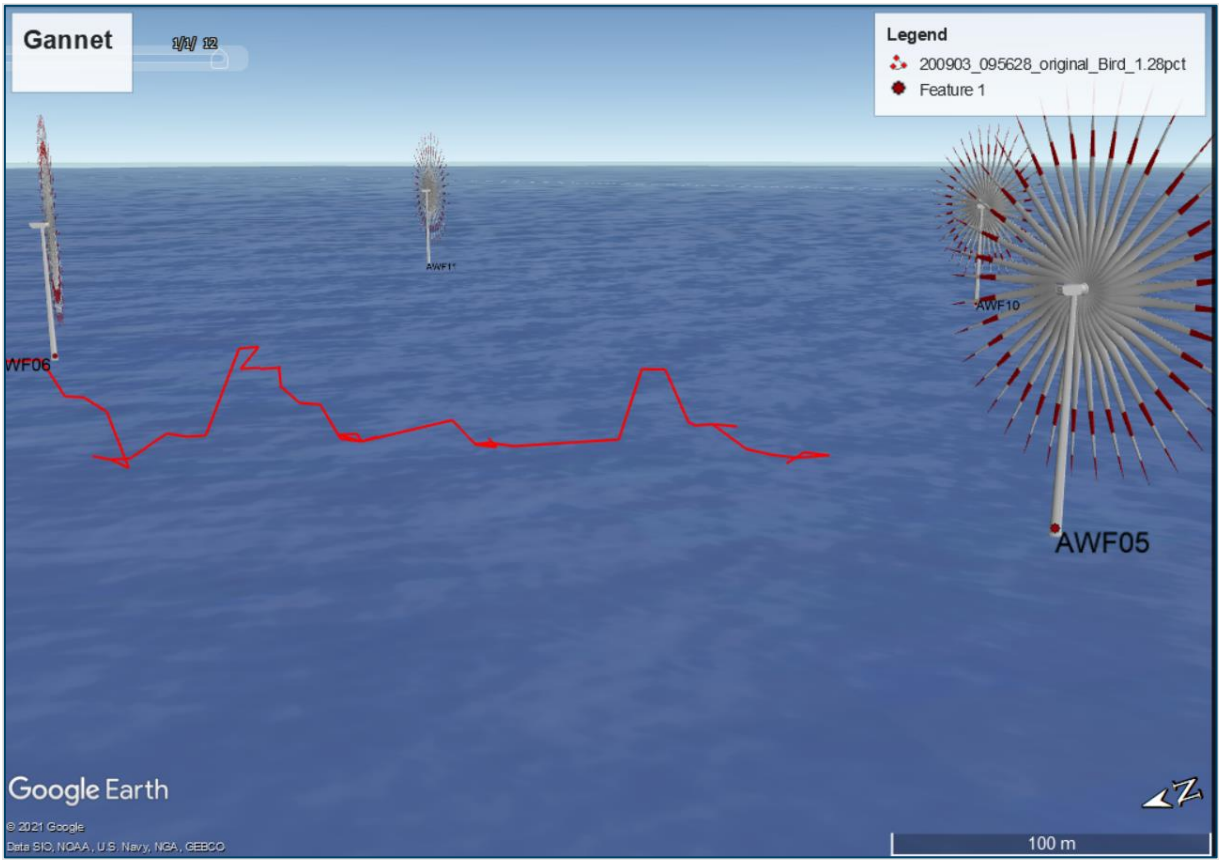

Figure 12-3 Examples of 3-D trajectories visualised with virtual turbines designed with correct dimensions and rotor orientation

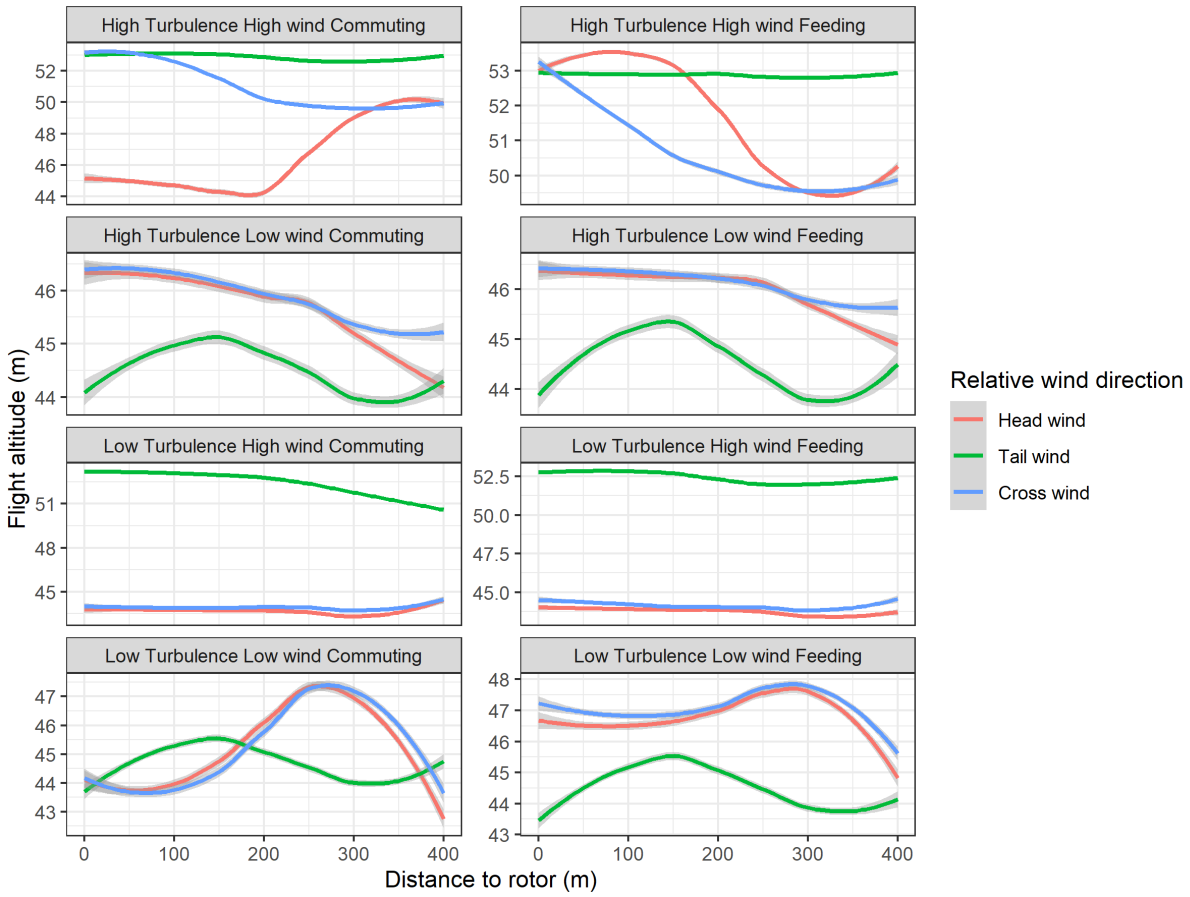

Figure 12-4 Predicted mean profiles of flight height of gannets viewed from the edge of the RSZ to the centre of the areas between turbines. The mean profiles are visualised for commuting and feeding birds in relation to relative wind direction and levels of wind speed and turbulence. See text for definitions of low and high levels of wind speed and turbulence.

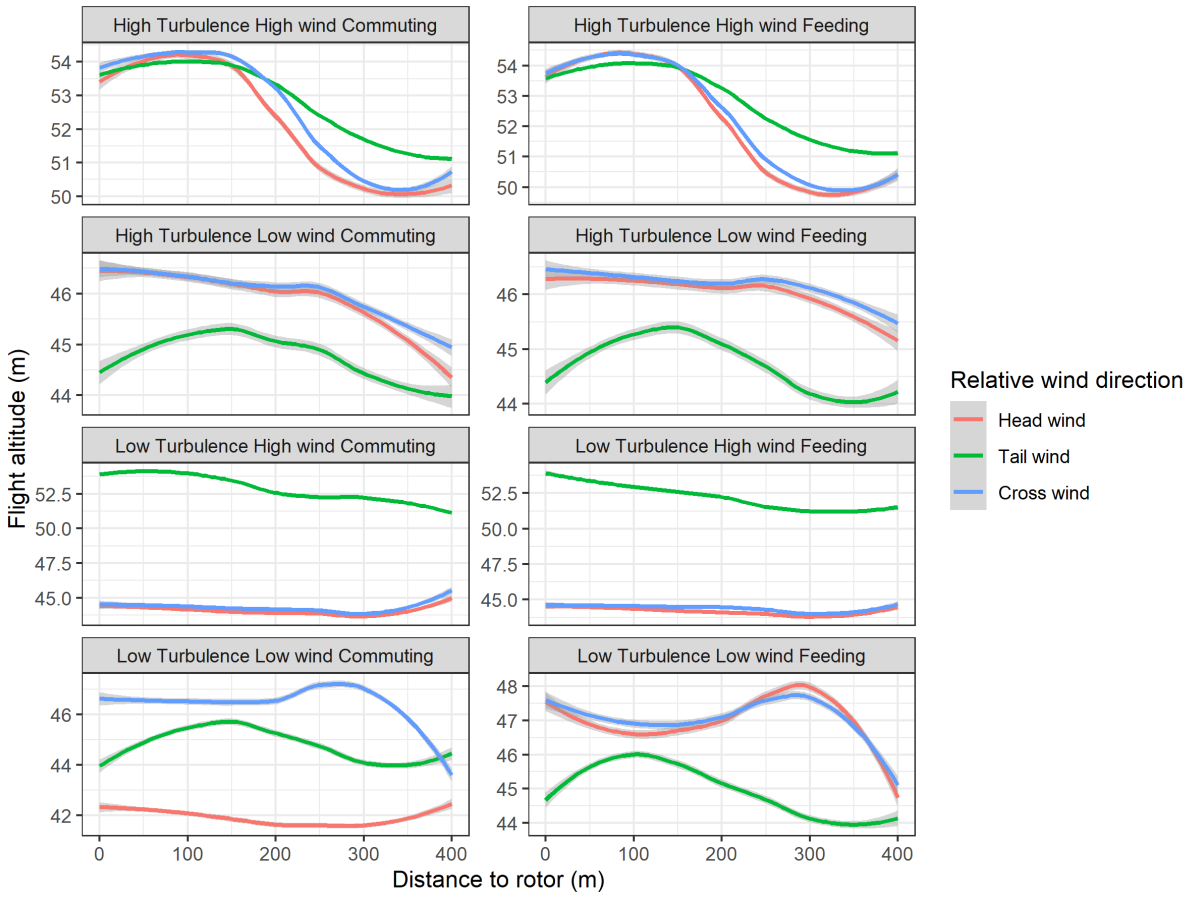

Figure 12-5 Predicted mean profiles of flight height of herring gulls viewed from the edge of the RSZ to the centre of the areas between turbines. The mean profiles are visualised for commuting and feeding birds in relation to relative wind direction and levels of wind speed and turbulence. See text for definitions of low and high levels of wind speed and turbulence.

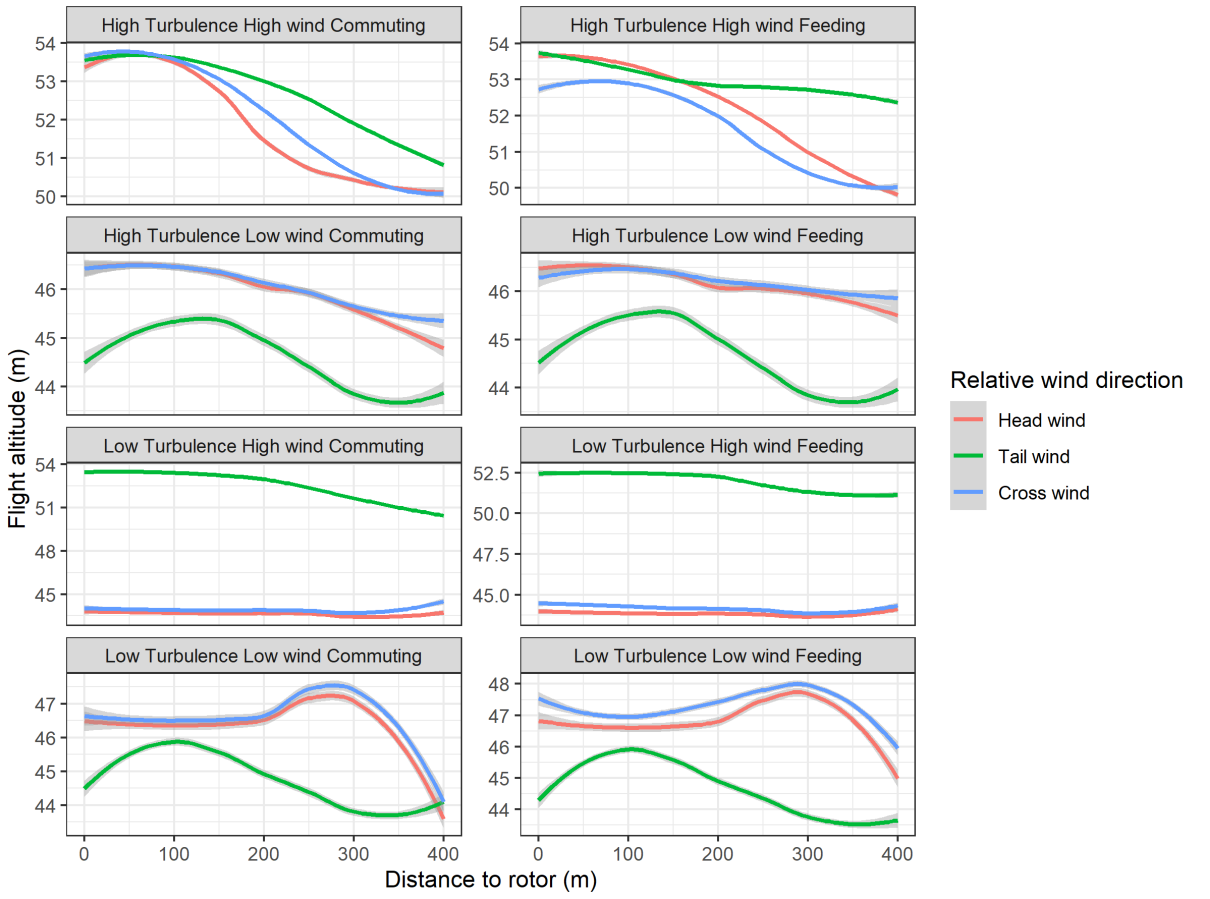

Figure 12-6 Predicted mean profiles of flight height of great black-backed gulls viewed from the edge of the RSZ to the centre of the areas between turbines. The mean profiles are visualised for commuting and feeding birds in relation to relative wind direction and levels of wind speed and turbulence. See text for definitions of low and high levels of wind speed and turbulence.

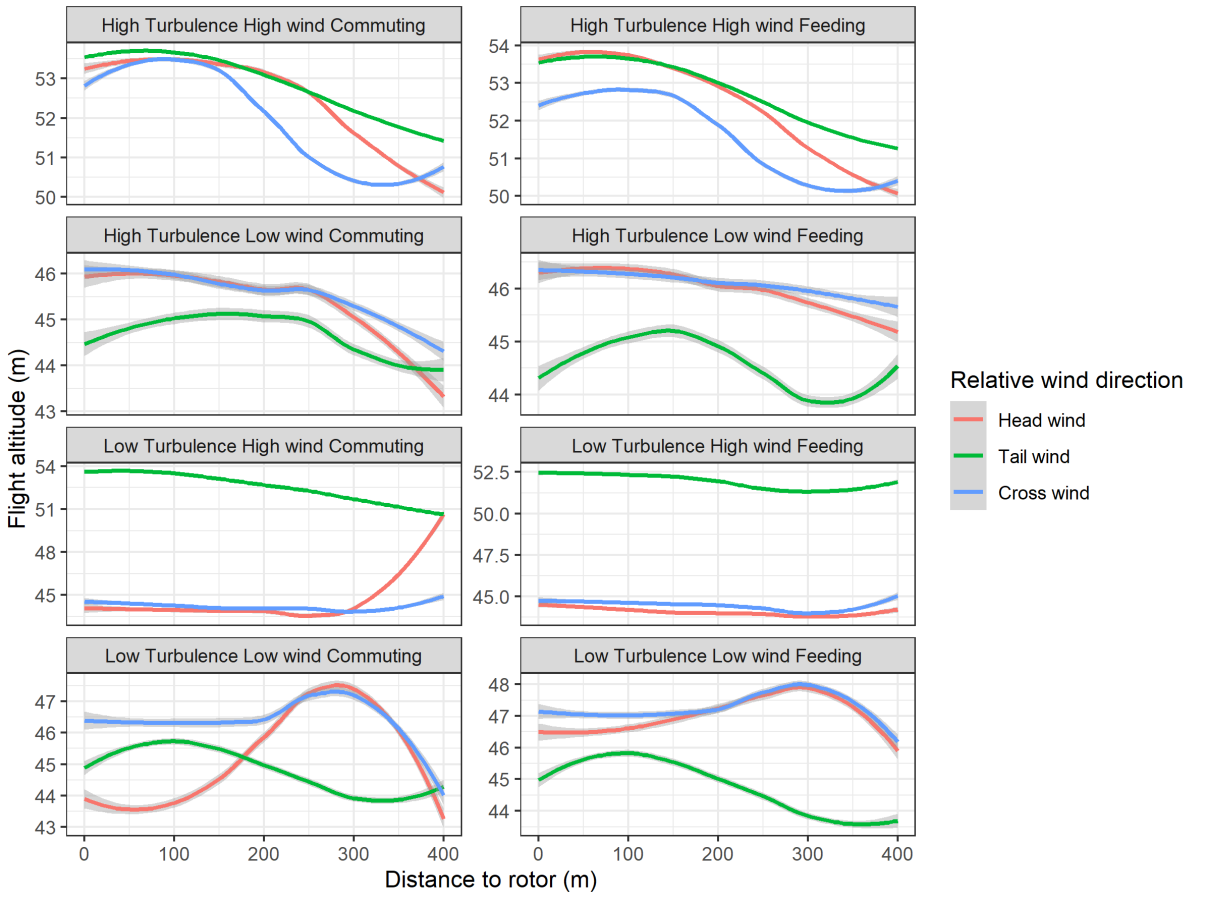

Figure 12-7 Predicted mean profiles of flight height of kittiwakes viewed from the edge of the RSZ to the centre of the areas between turbines. The mean profiles are visualised for commuting and feeding birds in relation to relative wind direction and levels of wind speed and turbulence. See text for definitions of low and high levels of wind speed and turbulence.

13 Flight speed

Combined radar track and video data also allowed for estimation of mean flight speed of the target species (Figure 13-1). For all target species recorded flight speeds were most frequently in the range between 3 and 8 m/s. Feeding gannets were flying with lower speeds than commuting gannets at all distance from the rotors (Figure 13-2). No differences in flight speed were recorded between commuting and feeding birds for the other target species. Close to the rotors target species were recorded flying with slightly lower speed. The reduction in flight speed is initiated at 100 m distance for the gannets, at 120 m distance for herring gulls and unidentified large gulls and at 200 m distance for kittiwakes.

The results of the flight models in relation to flight speed are shown in Figure 13-3 - Figure 13-6 and seemingly resolved the drivers behind the reduction in flight speed for all target species. For all target species turbulence had a strong effect on the flight speed profile, as the tendency to reduce speed on approach to the rotor was most clear in situations with low levels of turbulence. Wind speed mainly affected the distance at which the birds started reducing their flight speed at further distances during low wind speeds. The flight models did not reveal any clear influence of relative wind directions and feeding/commuting behaviour on flight speed.

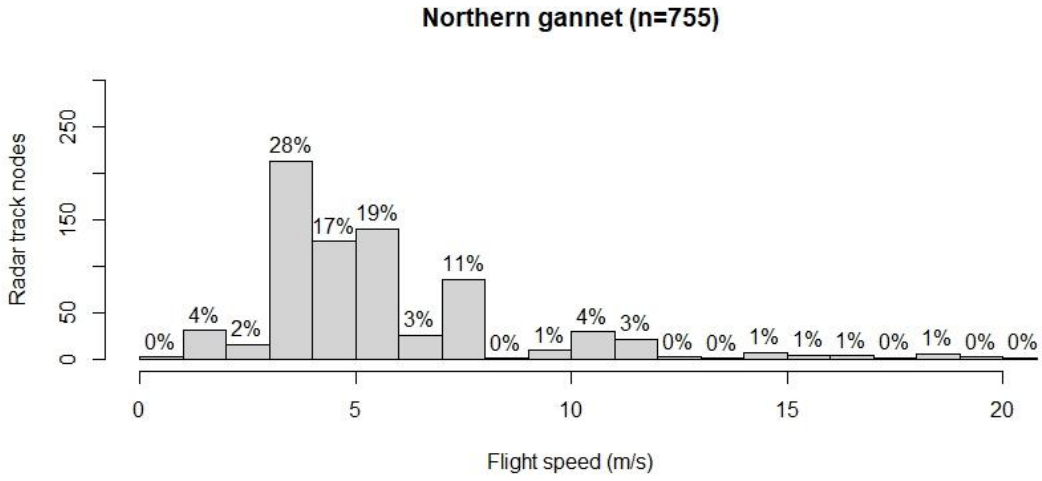

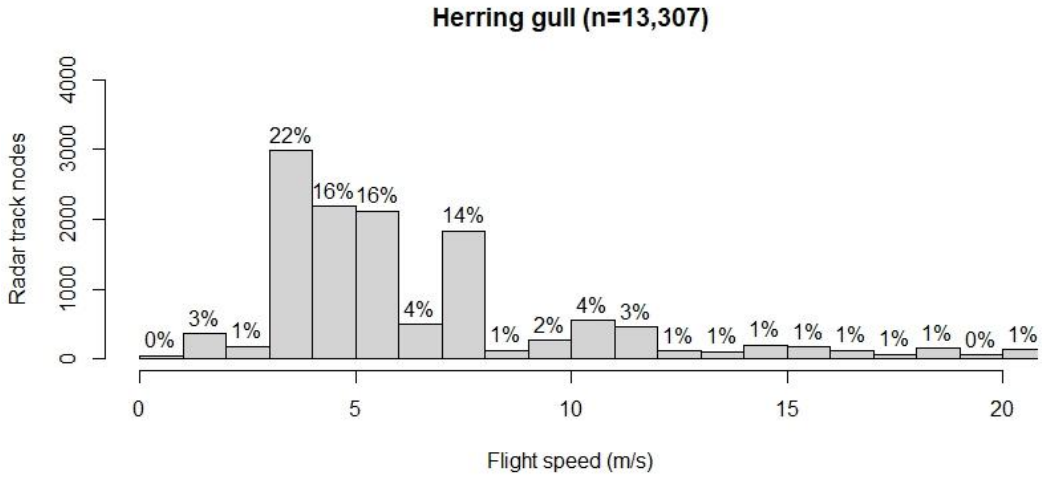

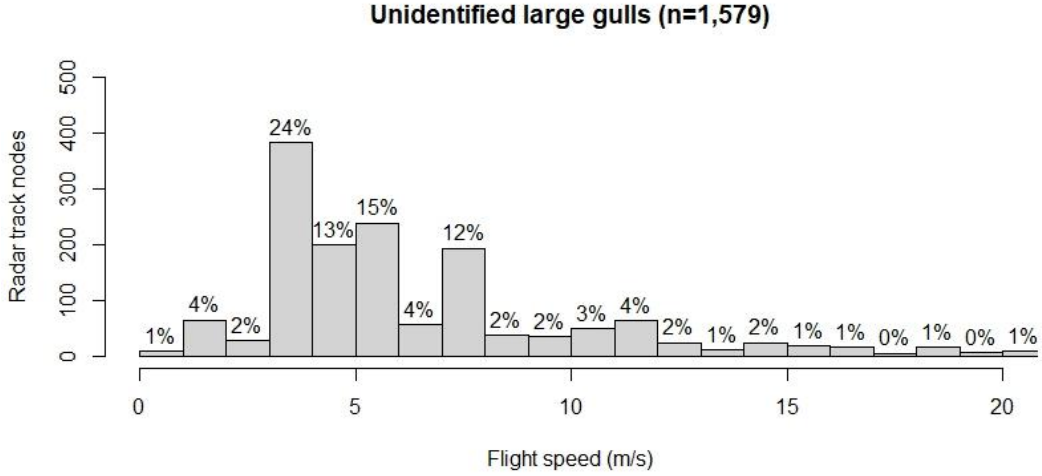

Figure 13-1 Histograms of flight speeds of target species in 2021.

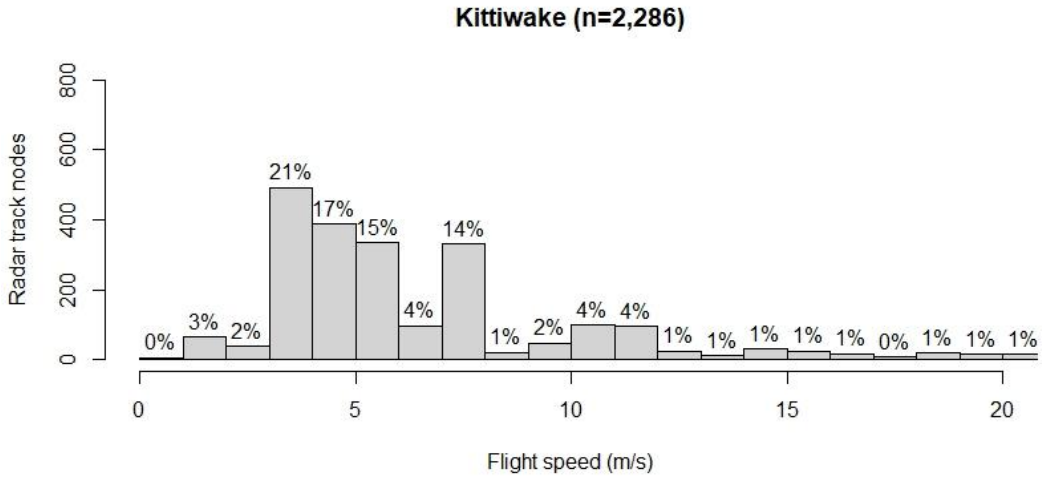

Figure 13-1 (Cont.)

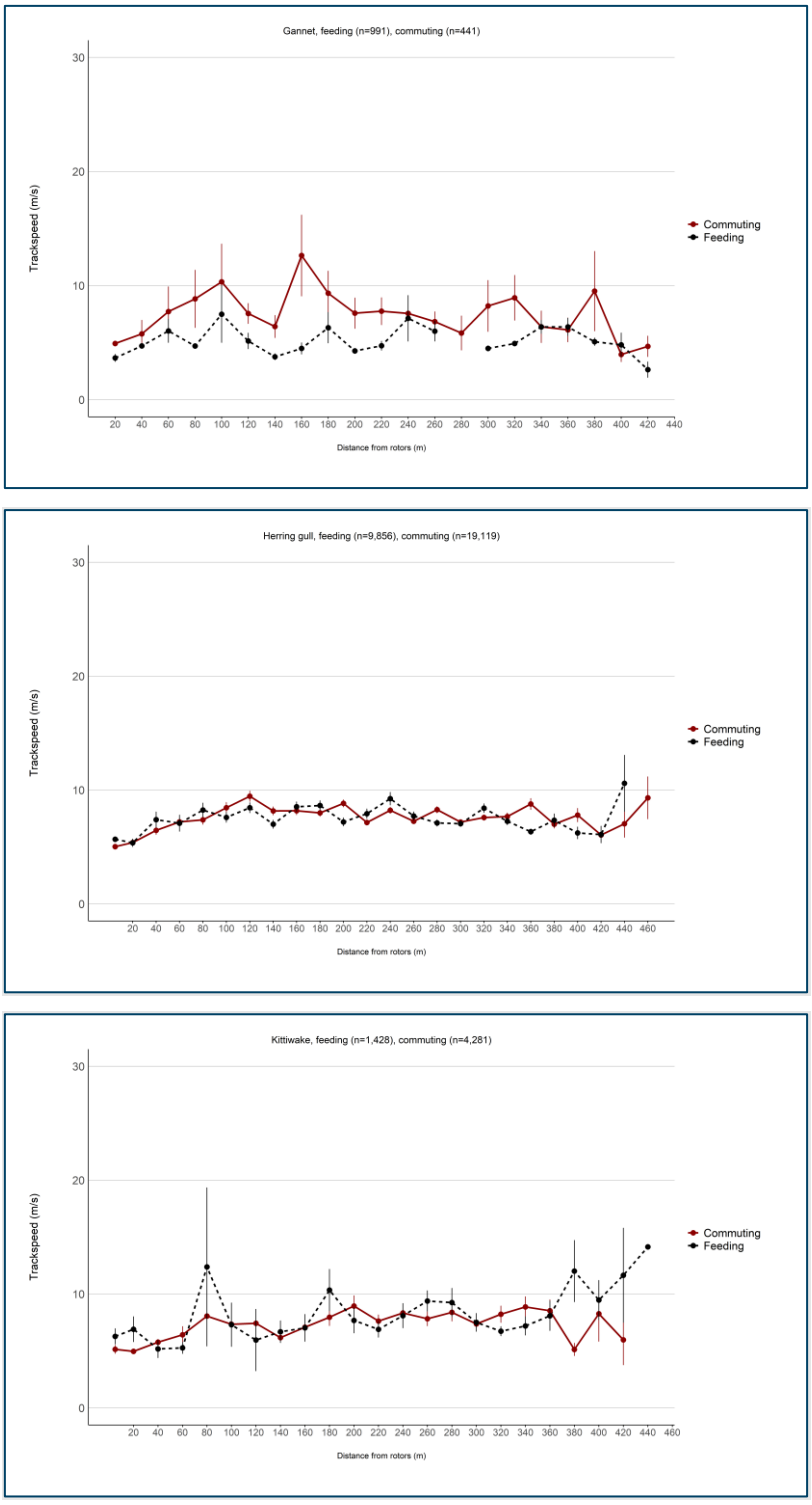

Figure 13-2 Mean observed flight speed of target species in relation to distance from nearest turbine during daytime hours in 2021.

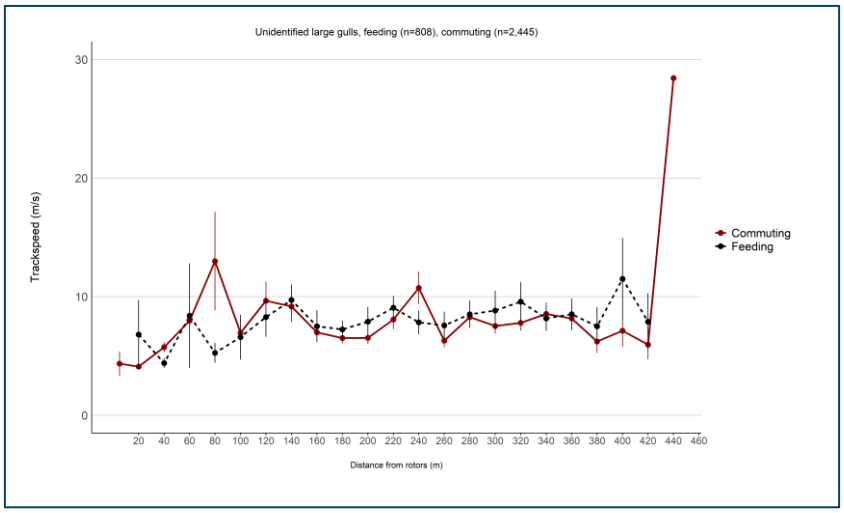

Figure 13-2 (Cont.)

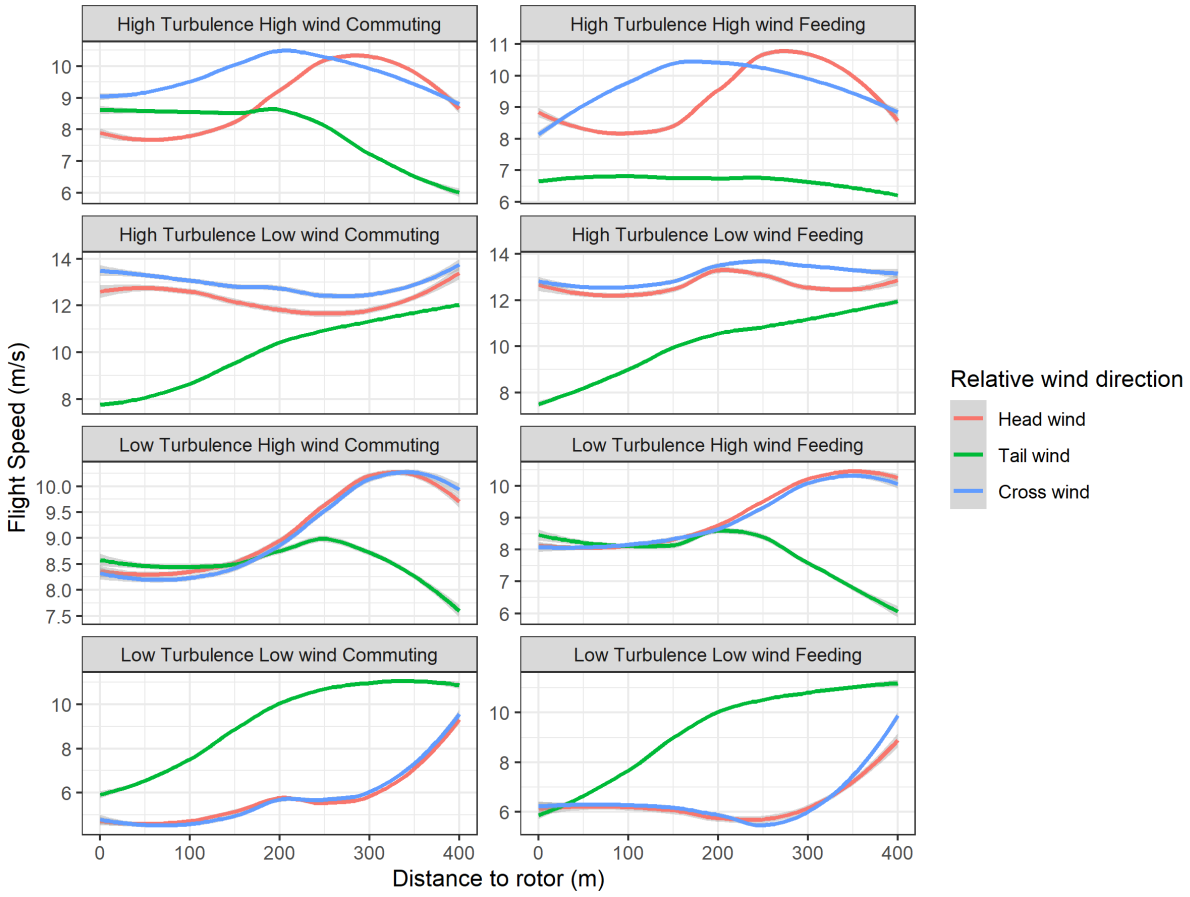

Figure 13-3 Predicted mean profiles of flight speed of gannets viewed from the edge of the RSZ to the centre of the areas between turbines. The mean profiles are visualised for commuting and feeding birds in relation to relative wind direction and levels of wind speed and turbulence. See text for definitions of low and high levels of wind speed and turbulence.

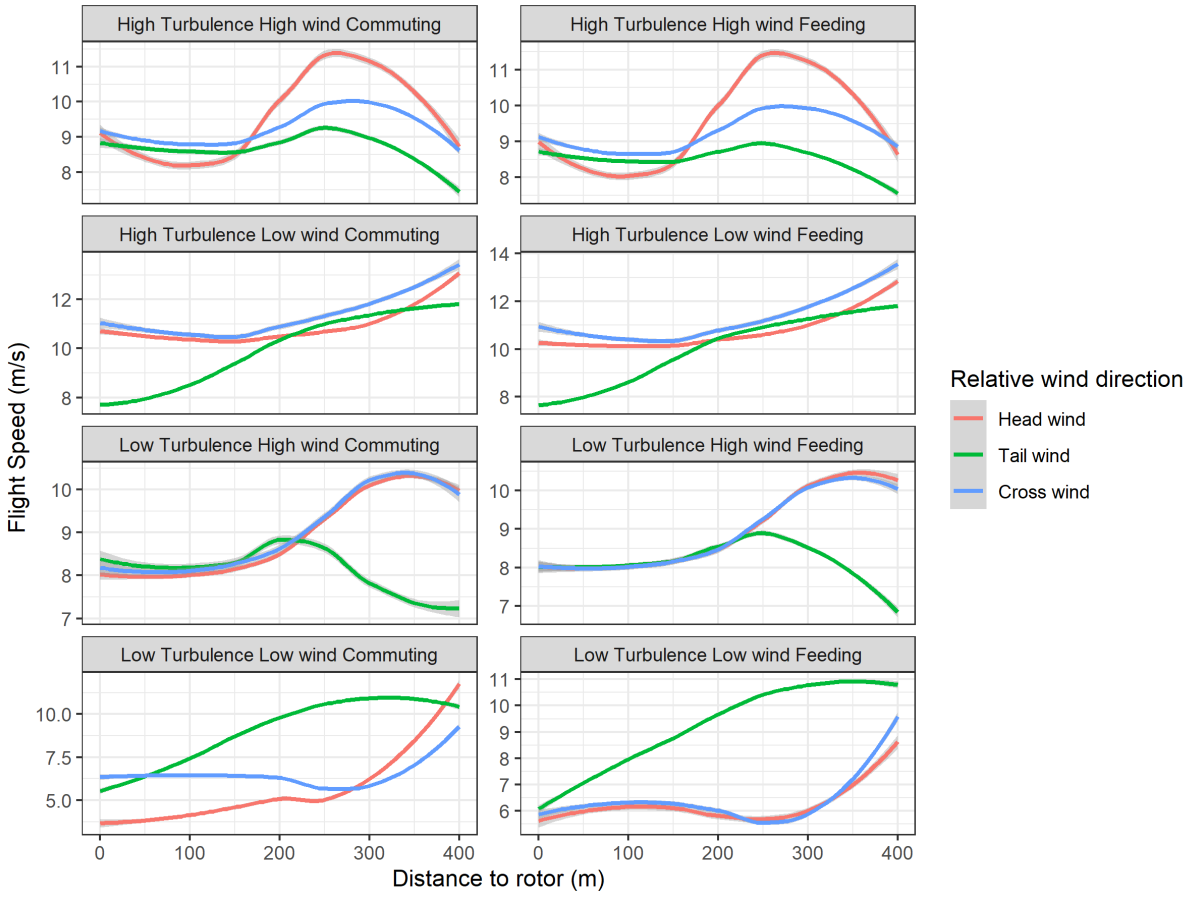

Figure 13-4 Predicted mean profiles of flight speed of herring gulls viewed from the edge of the RSZ to the centre of the areas between turbines. The mean profiles are visualised for commuting and feeding birds in relation to relative wind direction and levels of wind speed and turbulence. See text for definitions of low and high levels of wind speed and turbulence.

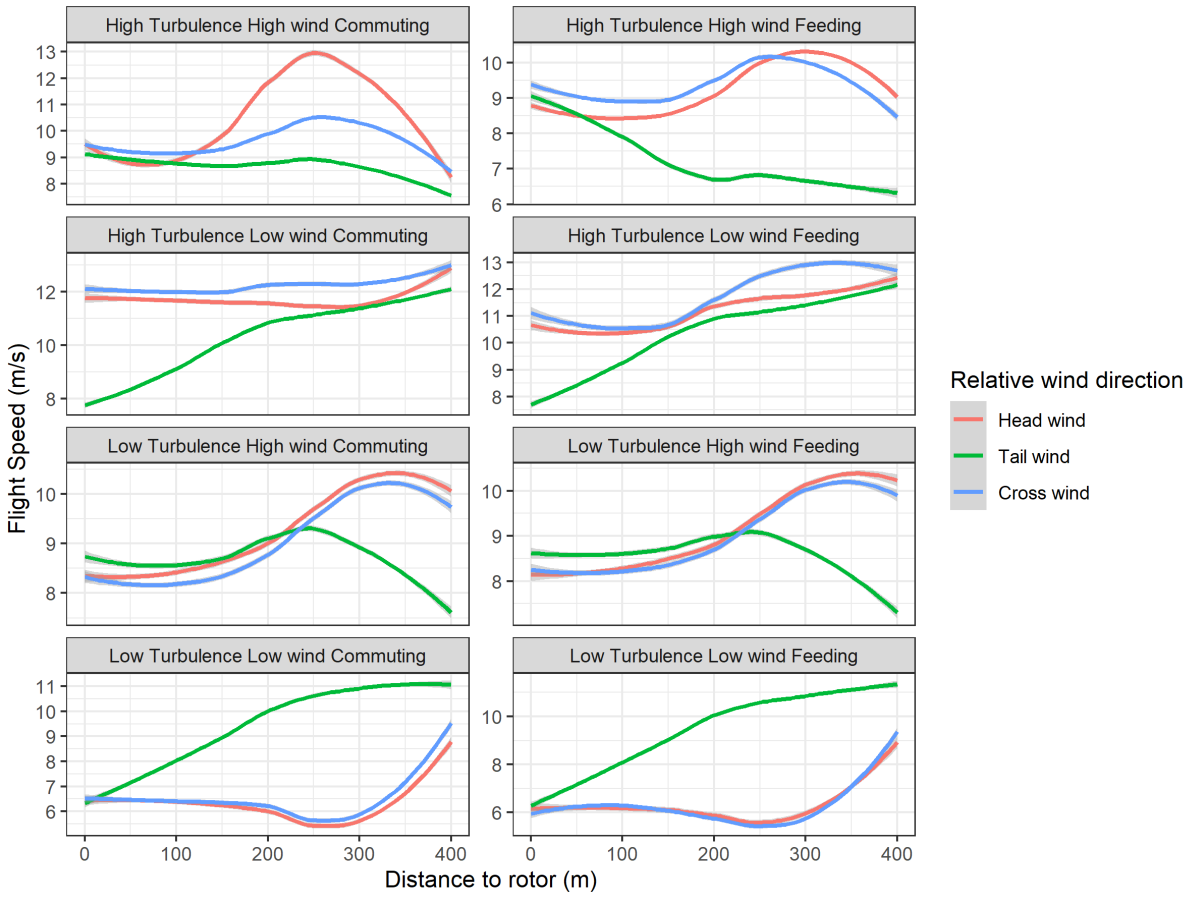

Figure 13-5 Predicted mean profiles of flight speed of great black-backed gulls viewed from the edge of the RSZ to the centre of the areas between turbines. The mean profiles are visualised for commuting and feeding birds in relation to relative wind direction and levels of wind speed and turbulence. See text for definitions of low and high levels of wind speed and turbulence.

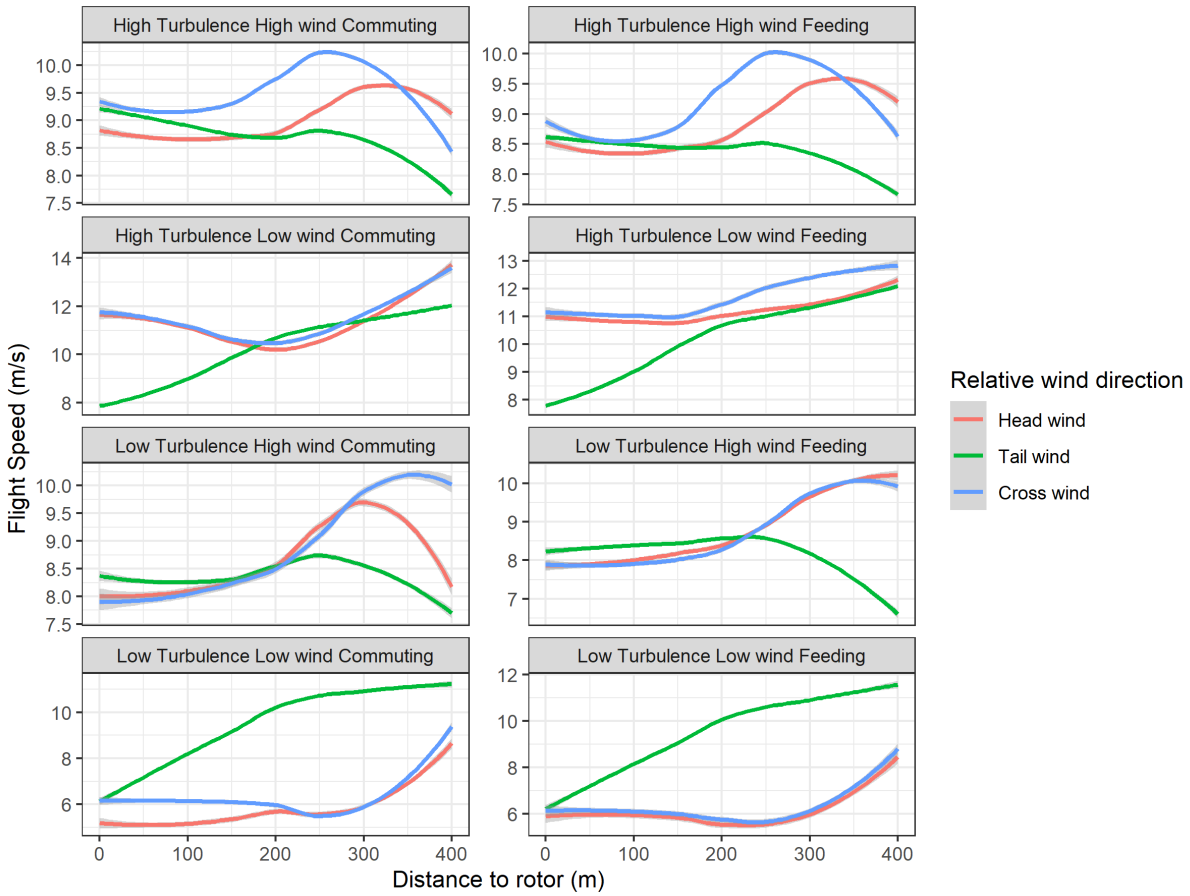

Figure 13-6 Predicted mean profiles of flight speed of kittiwakes viewed from the edge of the RSZ to the centre of the areas between turbines. The mean profiles are visualised for commuting and feeding birds in relation to relative wind direction and levels of wind speed and turbulence. See text for definitions of low and high levels of wind speed and turbulence.

14 Flight direction

Combined radar track and video data also allowed for estimation of changes in the flight direction of the target species in relation to distance from the rotors. Estimated changes in flight direction relative to the orientation of the rotor are indicated in Figure 14-2. The results indicated that commuting gannets appeared to deflect around 80 m distance from the rotors, whereas herring gulls showed a weaker mean deflection at 50 m. No mean deflection pattern was evident for kittiwakes.

The results of the flight models in relation to flight direction relative to the orientation of the rotor are shown in Figure 14-3 - Figure 14-6. The flight models revealed similar patterns for all target species, as flight direction was affected more or less equally for the different target species. A clear deflection profile towards the rotor was identified for situations with a combination of high turbulence level and low wind speed but was not clear during other combinations of wind speed and turbulence levels. Relative wind direction was an important factor as all target species were predicted to fly at smaller angles to the rotor during head and cross winds as compared to tail winds. These trends were apparent both for commuting and feeding birds.

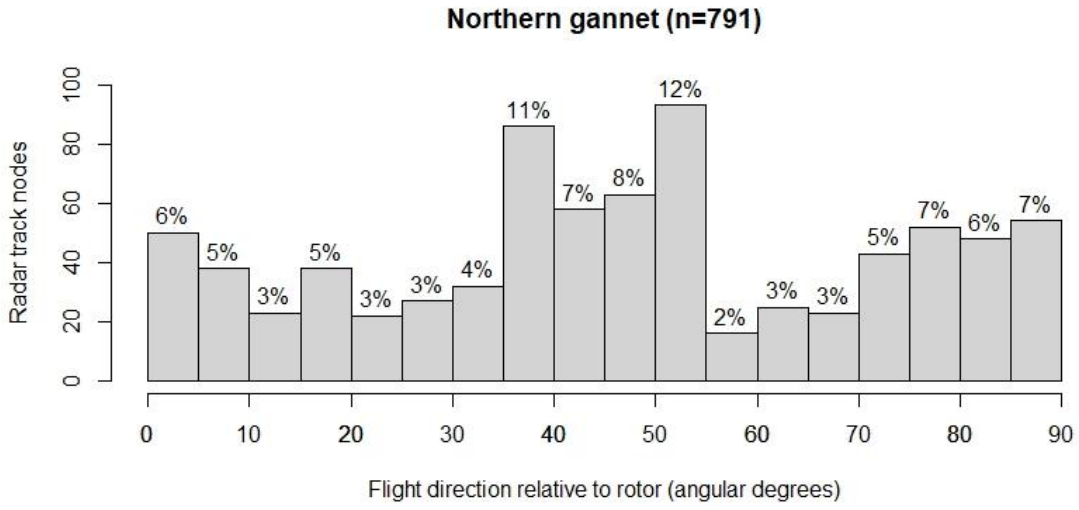

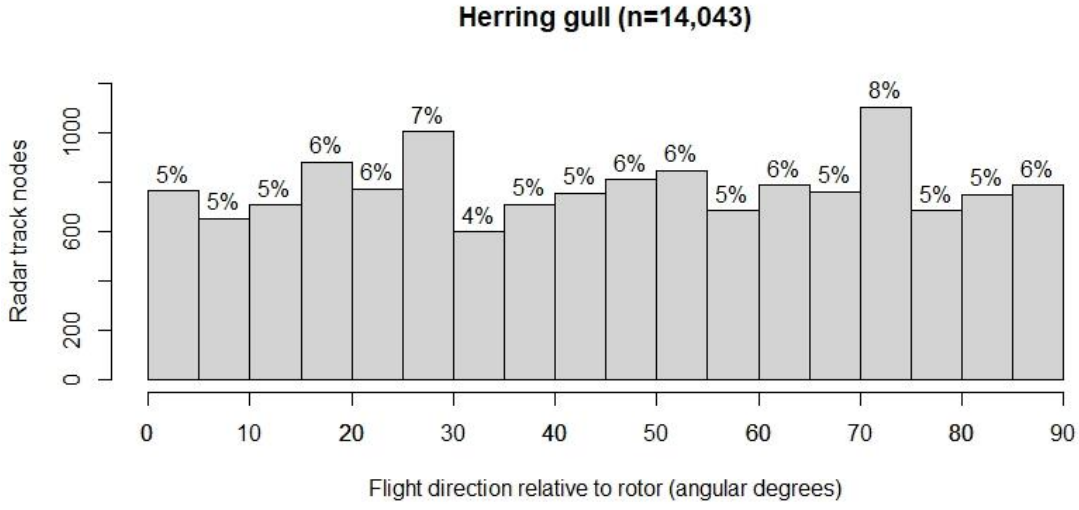

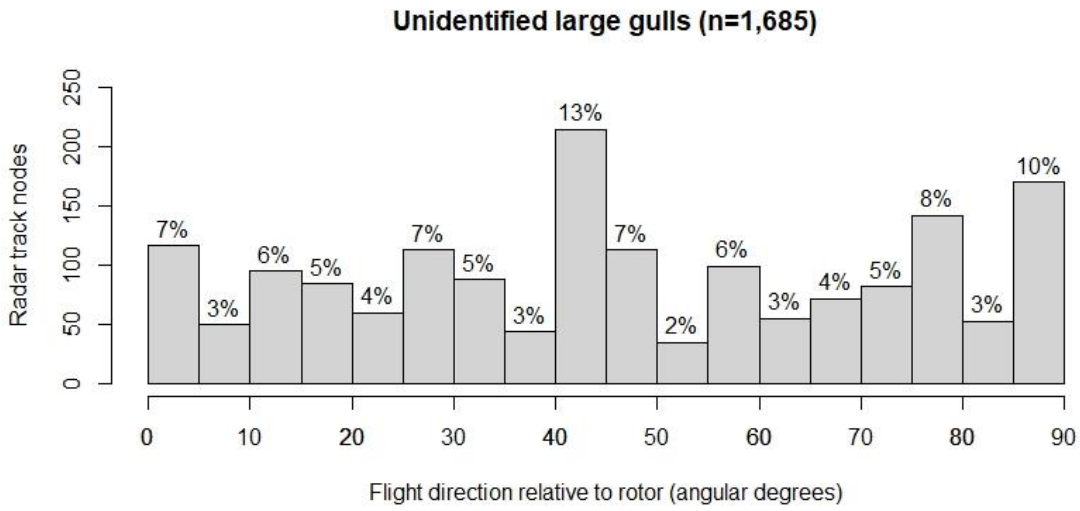

Figure 14-1 Histograms of flight directions of target species in 2021.

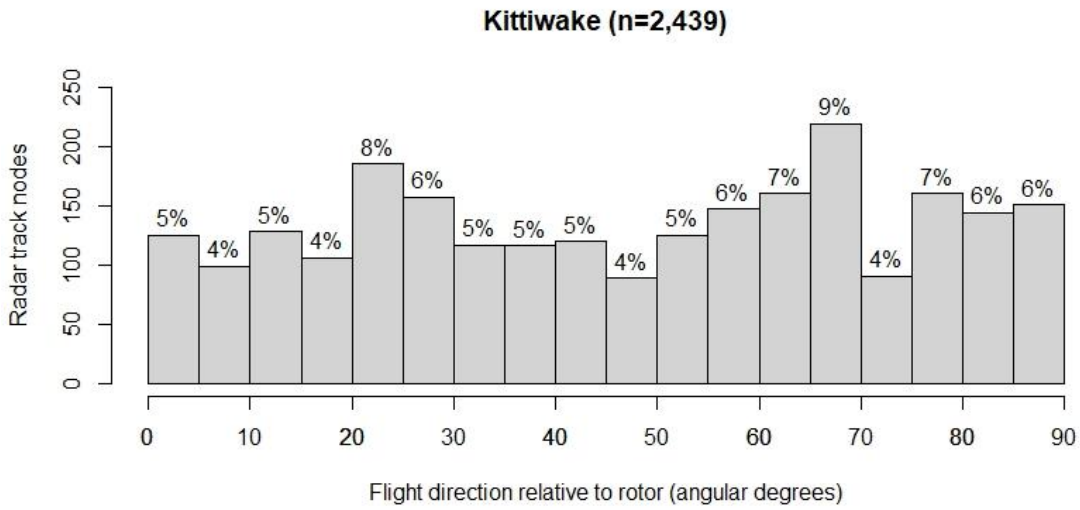

Figure 14-1 (Cont.).

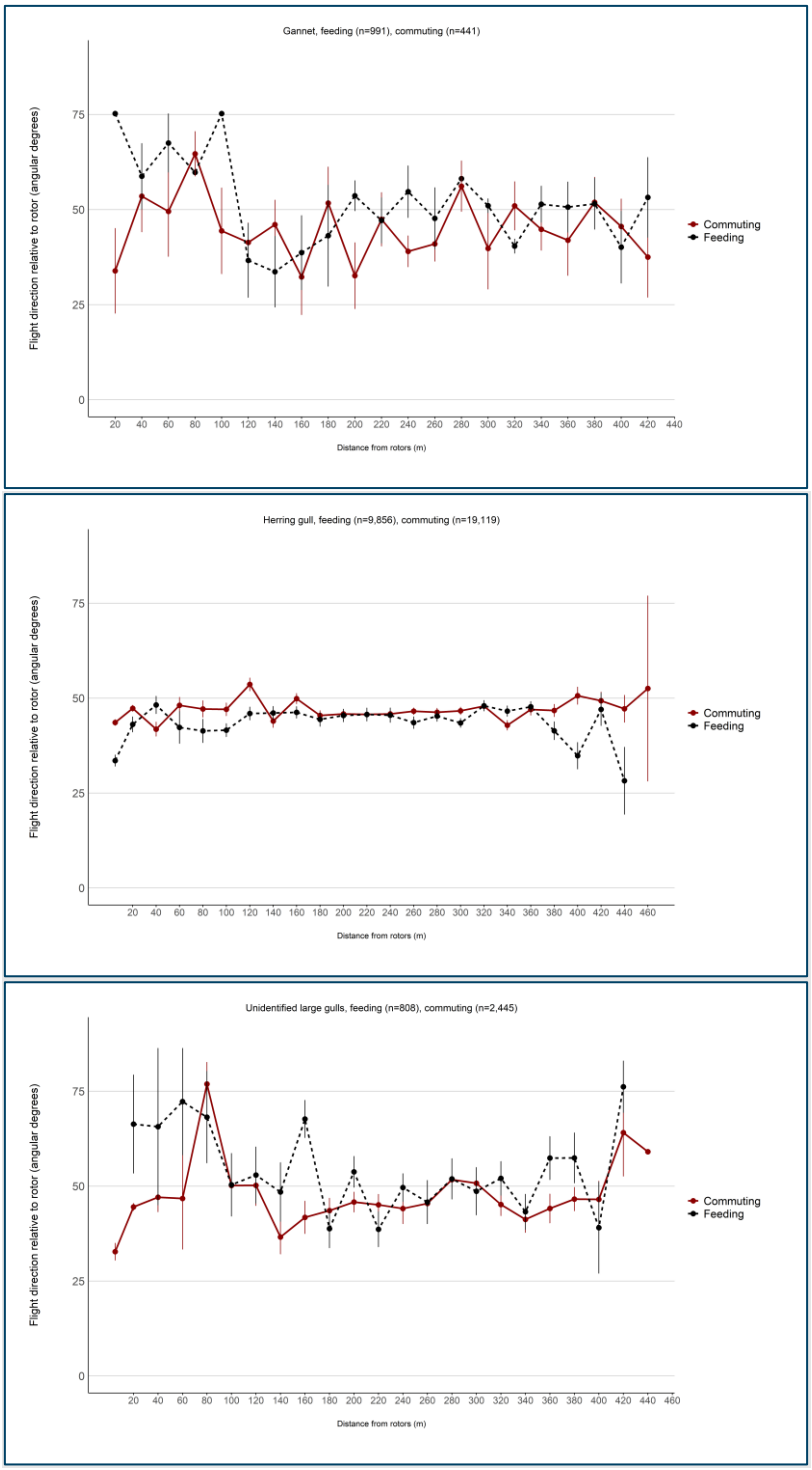

Figure 14-2 Mean observed flight directions relative to the orientation of the rotor estimated for each target species in relation to distance from nearest turbine during daytime hours in 2021.

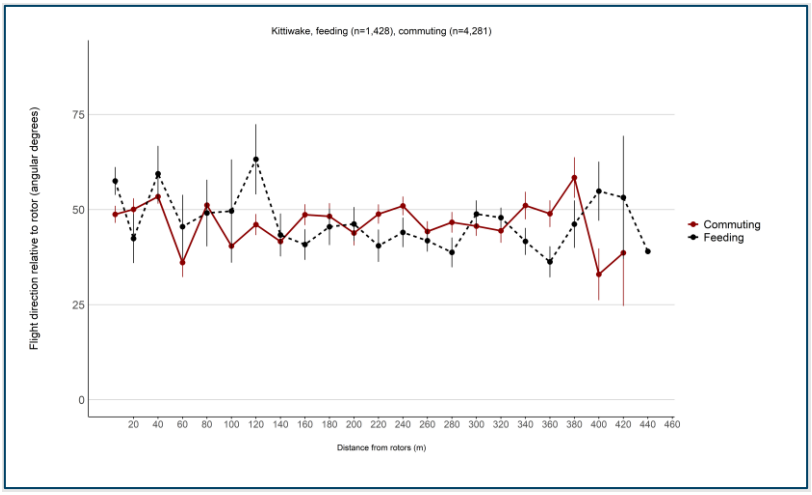

Figure 14-2 (Cont.)

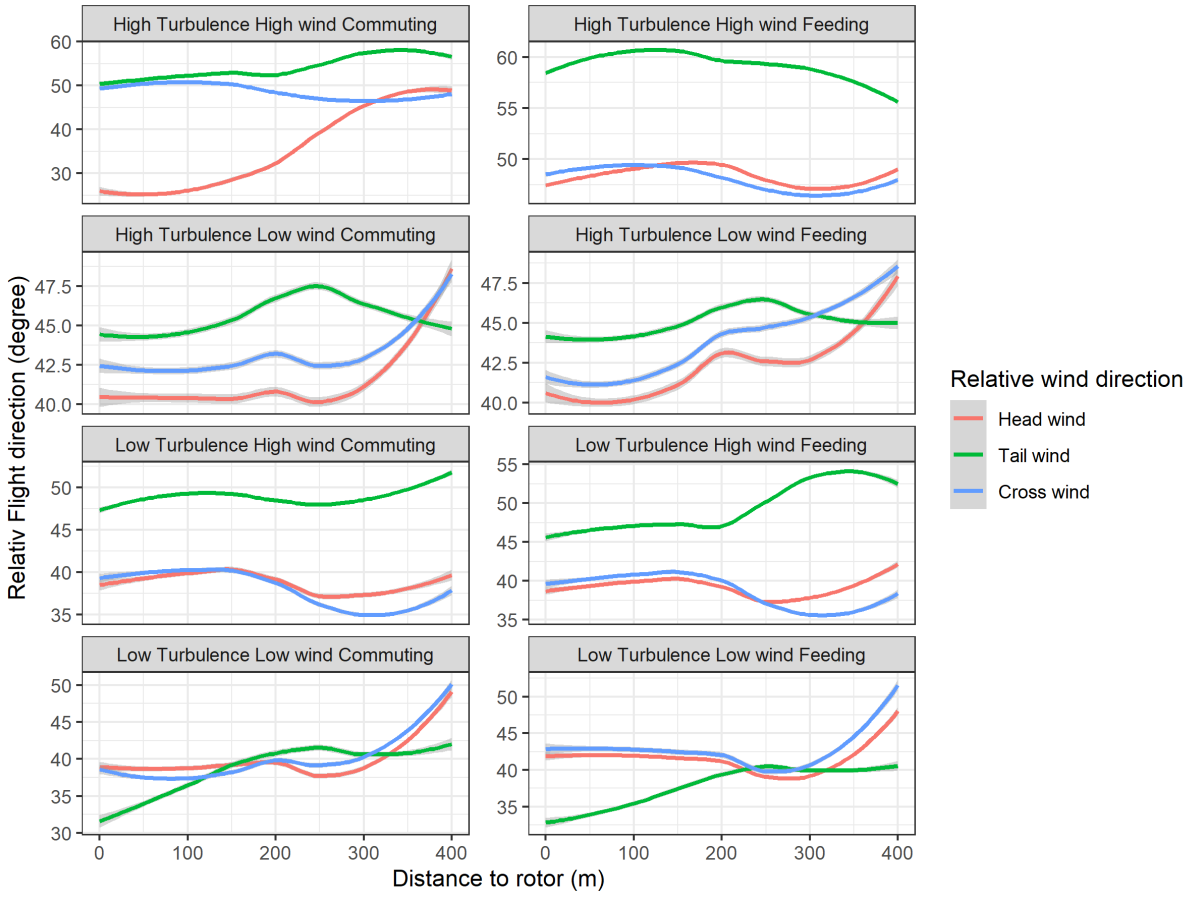

Figure 14-3 Predicted mean profiles of flight direction of gannets viewed from the edge of the RSZ to the centre of the areas between turbines. The mean profiles are visualised for commuting and feeding birds in relation to relative wind direction and levels of wind speed and turbulence. See text for definitions of low and high levels of wind speed and turbulence.

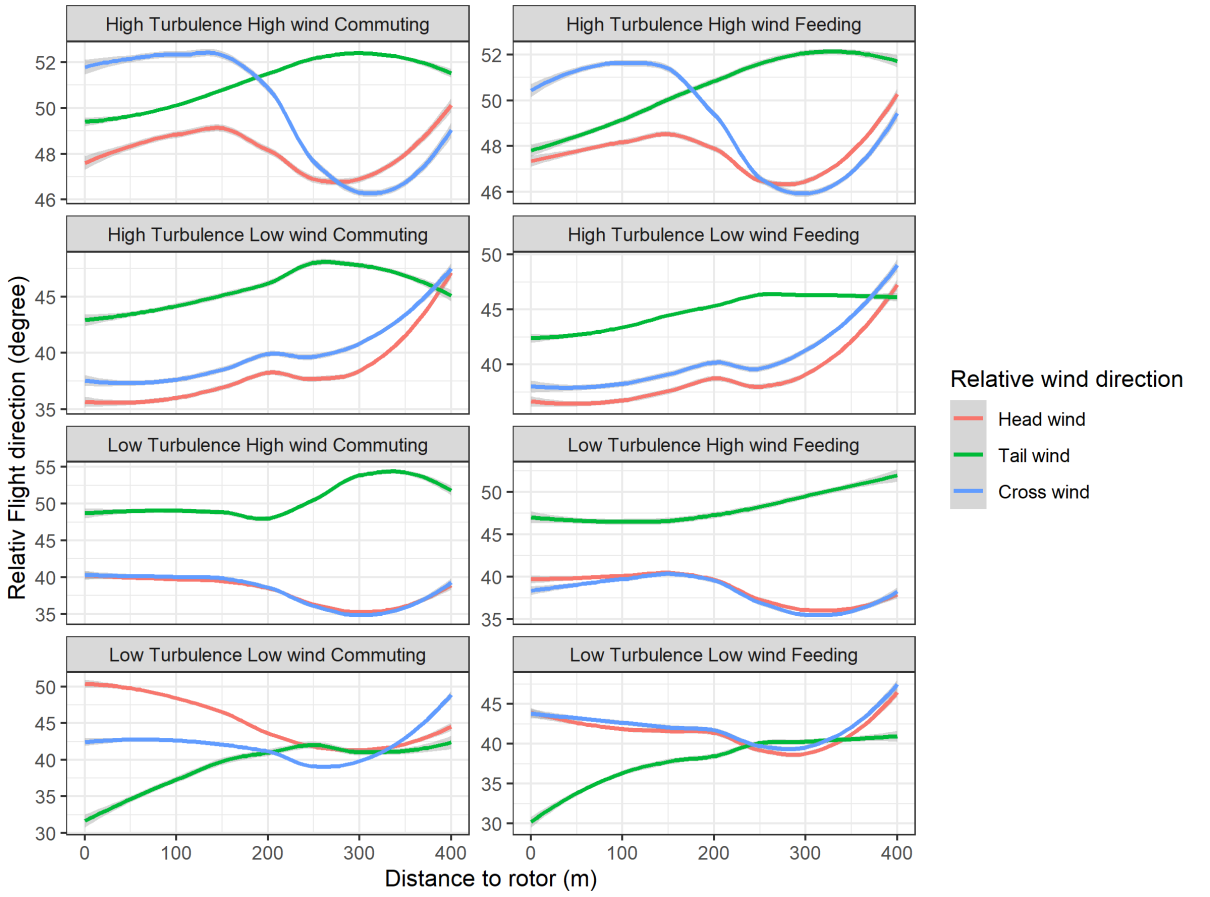

Figure 14-4 Predicted mean profiles of flight direction of herring gulls viewed from the edge of the RSZ to the centre of the areas between turbines. The mean profiles are visualised for commuting and feeding birds in relation to relative wind direction and levels of wind speed and turbulence. See text for definitions of low and high levels of wind speed and turbulence.

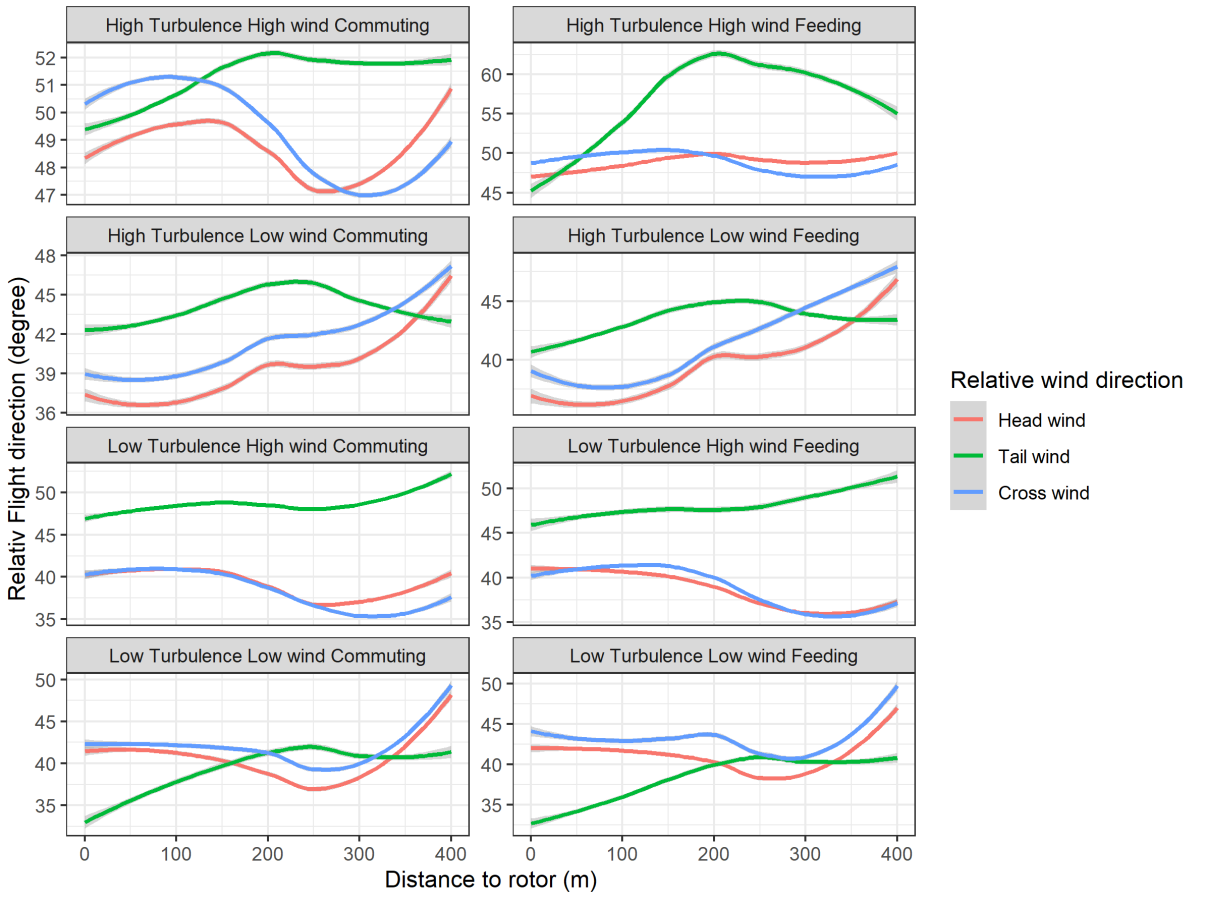

Figure 14-5 Predicted mean profiles of flight direction of great black-backed gulls viewed from the edge of the RSZ to the centre of the areas between turbines. The mean profiles are visualised for commuting and feeding birds in relation to relative wind direction and levels of wind speed and turbulence. See text for definitions of low and high levels of wind speed and turbulence.

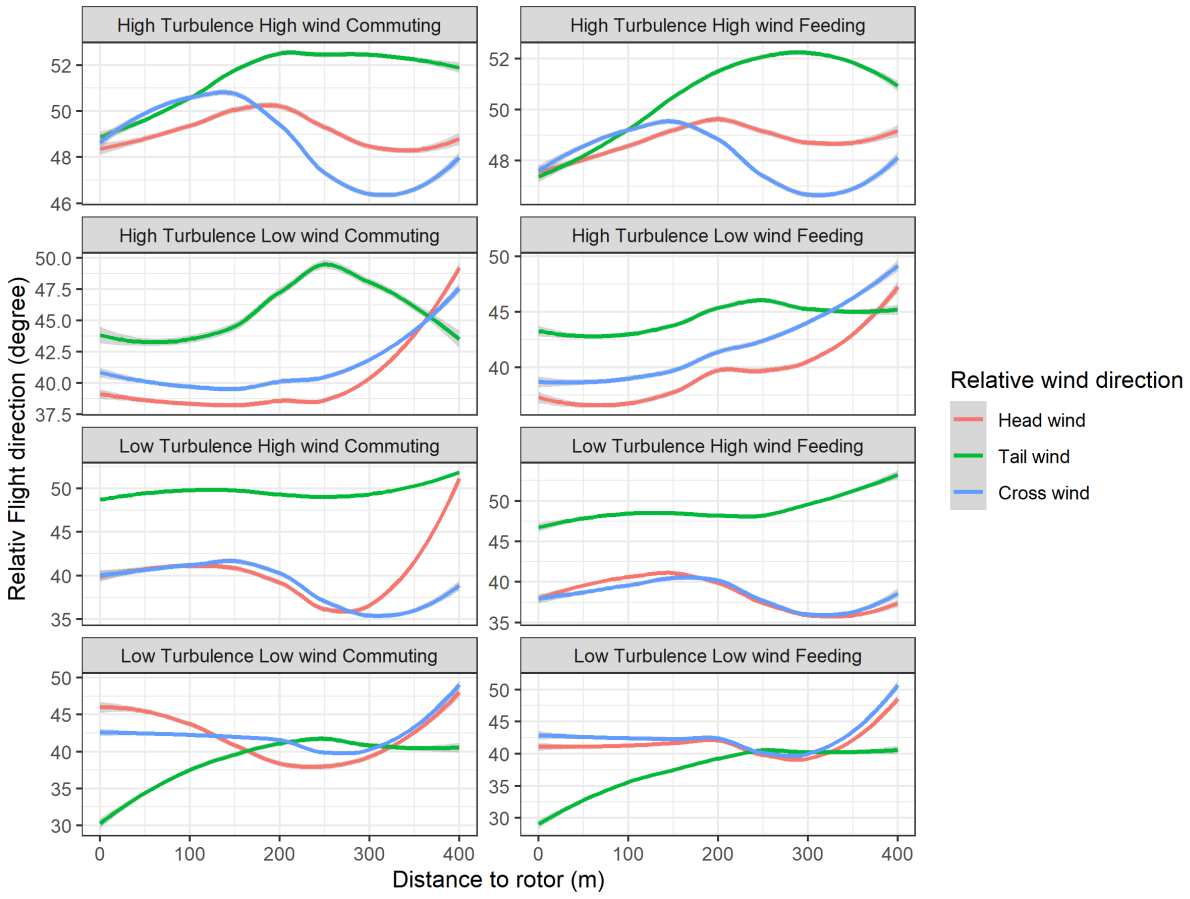

Figure 14-6 Predicted mean profiles of flight direction of kittiwakes viewed from the edge of the RSZ to the centre of the areas between turbines. The mean profiles are visualised for commuting and feeding birds in relation to relative wind direction and levels of wind speed and turbulence. See text for definitions of low and high levels of wind speed and turbulence.

15 Discussion

15.1 Sensor equipment and design

During 2020, the temporal coverage of the monitoring equipment was overall 59% with the best coverage achieved from July onwards. The coverage increased in 2021 to 76% with high coverage remaining throughout the season. High densities of flying seabirds were recorded within the wind farm during both seasons. The number of recorded radar tracks was higher in 2021 than 2020, but frequency was lower (357 tracks/hr in 2020; 268 tracks/hr in 2021). The full integration of radar and cameras and the operation of moving cameras resulted in a large number of videos of target species recorded. During 2021, an upgrade of the video tracking software to apply AI-based tracking resulted in fewer videos, but better quality and few false positives. The integrated nature of the radar and camera tracking made it possible to couple a number of video camera recordings of seabird movements to a sample of their radar tracks. It was possible to match video camera recordings of seabird movements to a sample of their radar tracks. A total of 1,753 coupled tracks were recorded during 2020 and 1,370 coupled tracks during 2021, which was beyond expectations and formed the basis for robust assessments of flight behaviours of target species in different parts of the wind farm array.

Despite the high number of videos obtained during the 2020 season the video tracker which was based on motion detection rather than AI technology was judged as suboptimal in situations with high densities of flying seabirds which occur frequently during August to October. In these situations, the tracker may shift targets when there is more than one bird in the field of view. In addition, the motion detection tracker does not have the same capacity to always keep the tracked bird in the centre of the field of view and hence may produce inaccurate estimates of flight height of the target bird. It was therefore decided to upgrade the video tracker on both cameras before the 2021 season to a new version which uses deep learning algorithms to separate flying seabirds from other flying objects and has the capability to keep the tracked bird in the centre of the field of view and record the tracks for longer periods. The smoother footage of birds recorded using the upgraded tracker with associated high-level zoom also facilitated better identification of target species in 2021.

The quality of the collected video data was judged by the video analysts as acceptable. However, the RVision camera does not produce videos with the same high definition as the FLIR M400 camera. The lower resolution of the RVision videos affected the number of videos being recorded by the new AI-tracker from that camera.

The estimated flight heights of gannets based on triangulation between radar and camera data with the AI-tracker in 2021 revealed results which show higher flight altitudes compared with results from tracking studies. Cleasby et al. (2015) showed a median flight height of commuting gannets at 12 m and feeding birds at 27 m compared with an average flight height of commuting gannets at 50 m and feeding gannets at 45 m in this study at the EOWDC. These differences between the flight heights recorded during the EOWDC study and those reported from tagging studies may be due to both site-specific differences and the potential bias in the AI-based video tracker. The tracker performance is sensitive to the amount and quality of video data used for training the bird species recognition model. The AI-based tracker has been trained using videos with both the sky and the sea as a background. As such, the tracker version in this study should be generic with a moderate risk of a bias.

The estimated flight heights for kittiwakes indicated that all birds (both commuting and feeding) were flying at rotor height. The reported flight heights in literature are diverse and according to the review by Furness et al. (2013) varies in different studies between 0-38% at rotor height, which is clearly lower than found in this study at the EOWDC during 2021. However, the proportion of birds flying at rotor height recorded in OWEZ was 45% (Krijgsveld et al. 2011) and in the ORJIP BCA study it was found to be 77% (Skov et al. 2018). At the Alpha Ventus offshore wind farm, kittiwakes were observed to prefer flight heights between 10 to 20 m (Mendel et al. 2014). Evidence from visual surveys in proposed development areas in the UK assessed flight height of 62,975 kittiwakes

suggesting that 15% of flights occurred at collision risk height (Johnston et al. 2014). The higher flight altitudes for kittiwakes recorded in the EOWDC may be related to the lower level of feeding activity during 2021 compared with 2020. During the 2020 season, data from the motion detection tracker indicated that 44% were flying at rotor height (Tjørnløv et al. 2021).

The estimated flight heights of large gulls indicated that all commuting and feeding herring gulls and unidentified large gulls were flying at rotor height. Furness et al. (2013) indicated that there is a large variation in defined percentage of large gull species flying at rotor height with maximum values at 90%.

The measured flight speeds from the radar track data in the wind farm are generally lower than flight speeds recorded from GPS studies outside wind farms. These studies are generally, however, large scaled and therefore also include “transition flights” from colonies to feeding grounds, long sustained directional flights. Pettex et al. (2012) reported a mean flight speed of about 13.5 m/s for gannet in comparison to the 6-8 m/s measured in this study. Flight speed of lesser black-backed gulls based on GPS measurements (Gyimesi et al. 2016) from two different studies was 12.5 m/s and 10.7 m/s compared with 5-8 m/s measured for herring gulls and unidentified large gulls in this study. GPS flight speed for kittiwake was reported by Kotzerka et al. (2010) and Elliot et al. (2014) to be 9.2 m/s and 10.6 m/s respectively compared with 6.5-7.0 m/s measured in this study.

The coupled radar-camera track data recorded in this project offer species-specific empirical data on flight speeds in an offshore wind farm measured at a rather high temporal resolution (2.5 secs). As such, the data are a valuable source of information on more realistic mean flight speeds and associated variability in offshore wind farms necessary for improving estimates of the flux of birds for the species in question. It should be noted that currently only one speed measurement is used in the Band model although the model uses the speed for calculating both the flux and collision risk when flying through the rotor (PColl, Band et al. 2012). For the flux calculation, the track speed would more appropriate and for PColl estimation the flight speed would be more appropriate. Both track and flight speeds can be extracted from the combined radar-camera tracks data; the flight speed recorded close to the tip of the rotor blades should be applied.

15.2 Avoidance behaviour of seabirds

The target sample size of 250 per species for assessment of meso-avoidance was exceeded as a result of the large number of combined radar and video tracks collected by the system over the two study periods in 2020 and 2021. As the calculation of the meso-avoidance rates is based on proportional statistics the results for meso-avoidance are judged as unbiased even if it is based on a subset of all tracks. The same holds true even if a lower proportion of the birds are recorded by the radar during high sea states (> Beaufort 4) due to the use of dynamic clutter filtering. As determined from the recorded patterns of track length density kittiwakes displayed horizontal meso-avoidance within 140-160 m distance from the rotors. Commuting herring gulls showed meso-avoidance within 90-110 m distance and feeding herring gulls within 60-80 m distance. Herring gulls showed maximum meso-avoidance of 0.7 close to the blades, and kittiwakes showed maximum avoidance of 0.5. As expected, they also displayed attraction to the areas in between the turbine rows. Gannets only displayed avoidance at distances closer than 40 m from the tip of the rotor blades, and great black-backed gull only within 50 m distance. Both species had maximum avoidance levels at 0.5.

For comparison with the the ORJIP BCA study meso avoidance rates were estimated in the EOWDC study using the same algorithm and the results showed comparable rates with ORJIP for unidentified large gulls and gannet, while slightly lower rates were estimated for herring gulls and great black-backed gulls, and much lower rates were calculated for kittiwakes. In the ORJIP BCA study, the meso-avoidance rates were estimated at 0.961 (±0.175 SD) for herring gull, 0.921 (± 0.174 SD) for gannet, 0.916 (±0.177 SD) for kittiwake, 0.894 (± 0.174 SD) for lesser and great black-backed gull combined and 0.842 (±0.177 SD) for great black-backed gull (Skov et al. 2018).

The only other empirical study which has reported on meso-avoidance is the monitoring study in the OWEZ OWF in the Netherlands where Krijgsveld et al. (2011) reported a meso-avoidance rate of 0.66 for all species combined. Cook et al. (2018) reviewed existing evidence from monitoring

programs and suggested that meso-avoidance rates may vary between sites. The results from the EOWDC study strongly indicates that seabirds' avoidance response towards turbines mainly takes place within 100-120 m distance from rotors and that the response intensifies as the seabirds approach the rotor blades. In proximity to the rotors, the recorded meso-avoidance response behaviour for all target species was manifested as a complex 3-dimensional pattern. Commuting gannets appeared to reduce flight altitude, whereas herring gulls and kittiwakes displayed a slight increase in mean flight height as they approached the rotor blades. When approaching the rotor blades all target species showed a marked decrease in mean flight speed. When assessing the recorded flight orientation of the birds relative to the rotors commuting gannets and kittiwakes appeared to deflect around 80 m distance from the rotors and herring gulls at 50 m.

The flight models revealed that turbulence and wind speed had the strongest effect on the profiles of flight behaviour of all target species. The tendency to increase flight height on approach to the rotor was identified only during situations with high turbulence levels. Wind speed affected the distance at which the increase in flight height took place as the response took place well beyond 100m distance at low wind speeds. Superimposed on these trends there was a predicted tendency for all target species to fly at higher altitudes during tail winds in situations with a combination of low turbulence and high wind speed.

Turbulence had a strong effect on the flight speed profile, as the tendency to reduce speed on approach to the rotor was most clear in situations with low levels of turbulence. Wind speed mainly affected the distance at which the birds started reducing their flight speed at further distances during low wind speeds. A clear deflection profile towards the rotor was identified for situations with a combination of high turbulence level and low wind speed but was not clear during other combinations of wind speed and turbulence levels.

Relative wind direction as compared to the flight direction of the birds was only an important factor in relation to the tendency of deflection as all target species were predicted to fly at smaller angles to the rotor during head and cross winds as compared to tail winds. The trends resolved by the flight models were apparent irrespective of whether the birds were recorded as feeding or commuting.

The change in orientation means that micro-avoidance is very strong as seabirds are rarely recorded crossing the spinning rotors. Large gulls adjusted their flight behaviour to cross the rotor either obliquely or perpendicularly more frequently than gannets and kittiwakes. The recorded micro-avoidance rates were very high (> 0.96) for all target species. A similar micro-avoidance rate (0.957 ± 0.115 SD) was estimated for large gulls in the ORJIP BCA study using the same methods as in this project (Skov et al. 2018). These flight characteristics translate into a very low risk of collision.

Despite the evidence of the low risk of collision by seabirds in the EOWDC, the Random Forest flight models revealed that the mean avoidance response pattern may break down during specific weather conditions. The model results indicate that all target species show different flight profiles towards the rotor. The models also revealed that the avoidance behaviour displayed as a reduction in flight speed on approach to the turbines did not seem to take place during situations with strong turbulence. The avoidance behaviour manifested as a deflection of the flight path along the plane of the rotor only occurred during situations with high turbulence level and low wind speed.

15.3 Implications for assessments of seabird collision risk

Assessment of collision risk to birds constitutes one of the key elements of the consenting process of all wind projects, and the challenge of obtaining realistic quantifications of the bird collision risk has become a central theme for onshore and offshore projects worldwide. For offshore projects, the technical difficulties to measure bird avoidance behaviour within an offshore wind farm has aggravated the situation resulting in the emergence of potentially overly precautionary assessments leading to concern over population level effects (Green et al. 2016, Gibson et al. 2017). However, the high levels of micro and meso-avoidance recorded in the Thanet Offshore Wind Farm by the ORJIP BCA study 2014-2016 pointed towards the fact that gulls seem to have very low risk of collision despite their low macro-avoidance behaviour (Skov et al. 2018).

Technical improvements of the monitoring equipment and especially the ability to track seabirds inside the array and measure meso-avoidance with higher confidence made it possible during this project to collect a comprehensive and robust amount of meso-avoidance data at the species level. Together with the recorded high levels of micro-avoidance in all target species (> 0.96) it is now evident that seabirds in most weather and turbulence conditions will be exposed to very low risks of collision in offshore wind farms. This is also substantiated by the fact that no collisions or even narrow escapes were recorded for the analysed 10,000+ bird flights during the two years of video recordings.

In order to obtain collision risk estimates, collision risk modelling is typically undertaken using the Band model (Band 2012). Although widely used the Band model has severe limitations regarding estimation of realistic collision rates based on empirical data like telemetry data or radar-camera tracking data. This is due to the lack of flexibility of the Band model which quantifies collision risks with fixed and theoretical values for avoidance rates and flight speeds and assumes perpendicular crossing of the rotors (Bowgen & Cook 2018). It should therefore be seen as a priority for advancing the credibility of assessments of seabird collision risk to develop a spatially explicit collision risk model capable of applying empirical behavioural monitoring data on seabirds.

Rather than calculating collisions in the absence of avoidance prior to application of avoidance rates an individual based modelling technique would enable a new generation collision risk model for simulation of collision scenarios and cumulative assessments, integration of area-specific habitat displacements, inclusion of spatial gradients and individual variability. Importantly an IBM-based collision model would be capable of describing seabird flight behaviour inside a wind farm using realistic flight parameter values for flight speed, orientation, and height. IBM-based collision risk models have recently been developed for migrating red knot (Calidris canutus) (Gordon & Nations 2016) and lesser black-backed gull (van Bemmelen et al. 2021).

15.4 Conclusions

The main aim of the EOWDC Bird Collision Avoidance Study has been to improve our understanding of seabird flight behaviour inside an offshore wind farm. The technical improvements of the monitoring equipment employed in the Aberdeen Offshore Wind Farm made it possible to track seabirds inside the array and measure meso-avoidance more confidently than before. Due to the high temporal resolution of the track data (2.5 secs) the meso-avoidance behaviour could be assessed in unprecedented detail that has not been possible to date in other studies of bird flight behaviour within wind farms.

As a result of the full integration of radar and video tracks collected by the system over the two study periods in 2020 and 2021 It has been possible to couple a large number of video camera recordings of seabird movements to a sample of their radar tracks. A total of 1,753 coupled tracks were recorded during 2020 and 1,370 tracks during 2021, which was beyond expectations and formed the basis for robust assessments of flight behaviours of target species in different parts of the wind farm array.

The target sample size for species-specific meso-avoidance of 250 was reached for all key species. The level of meso-avoidance recorded was between 0.5 and 0.7, and together with the recorded high levels of micro-avoidance in all target species (> 0.96) it is now evident that the studied species of seabirds will be exposed to very low risks of collision in offshore wind farms during daylight hours. This was also substantiated by the fact that no collisions or even narrow escapes were recorded in over 10,000 bird videos during the two periods of monitoring.

The detailed assessments of the flight behaviour of the studied species of seabirds inside the array indicated that the meso avoidance response was in fact composed of three behavioural responses which take place on approach to the spinning rotors. Within distances of less than 100 m the seabirds responded by changing flight height, by reducing flight speed and reducing the difference between their flight direction and the orientation of the rotor. The application of multivariate Random Forest flight models revealed that these avoidance responses were relatively unaffected by wind direction and whether the seabirds were commuting or feeding. However, increasing turbulence and wind speed seemed to break down the strength of the avoidance responses in all species.

The large number of high-resolution species-specific tracks obtained for the target species inside the wind farm constitutes a unique dataset. This dataset would in combination with high-resolution tracking data provide calibration data for development of an improved collision risk modelling approach based on individual-based modelling. Thus, a future CRM IBM model approach is within reach and will be capable of describing seabird flight behaviour inside a wind farm using realistic flight parameter values for flight speed, orientation, and height. To further boost the availability of species-specific flight track data additional meso avoidance studies using integrated high resolution radar and powerful PTZ cameras are recommended for these target species as well as for other species.

Unlike for meso avoidance, the target sample size for species-specific micro-avoidance behaviour (100) was not achieved for any of the target species, - a situation which could be attributed to the strong meso avoidance behaviour of these species. The calculated micro-avoidance rate was above 0.96 or similar to Skov et al. (2018). As the analyses of micro-avoidance in the AOWFL were undertaken using similar methods as the ORJIP BCA project it is feasible to assess micro avoidance of the target species using the combined recordings from both projects. Accordingly, the total sample size for unidentified large gulls exceeds 100, but reliable assessment of the micro avoidance of gannets, kittiwakes and herring gulls still requires more video data collected for these species. Future studies of micro avoidance behaviour in these target species and other species of seabirds are therefore recommended, preferably using the same classification scheme for assessing micro avoidance as in this and the ORJIP study.

16 References

Andersen, S., Sørensen, J., Ivanell, S. & R. Mikkelsen. 2013. Comparison of Engineering Wake Models with CFD Simulations, Journal of Physics: Conference Series 524: 012161

Band, B. 2012. Using a Collision Risk Model to Assess Bird Collision Risks for Offshore Wind Farms. Report by British Trust for Ornithology (BTO), Bureau Waardenburg bv and University of St Andrews.

Bowgen, K. & Cook, A. 2018. Bird Collision Avoidance: Empirical evidence and impact assessments. JNCC Report No. 614, JNCC, Peterborough, ISSN 0963-8091.

Breiman, L. 2001. Random forests. Mach. Learn. 45(1): 5–32.

Camphuysen, C. & Garthe, S. 2004. Recording foraging seabirds at sea: Standardised recording and coding of foraging behaviour and multi-species foraging associations. Atlantic Seabirds. 6. 1-32.

Cook, A.S.C.P, Humphreys, E.M., Bennet, F., Masden, E.A., Burton, N.H.K. 2018. Quantifying avian avoidance of offshore wind turbines: Current evidence and key knowledge gaps. Mar Environ Res. 140: 278-288. doi: 10.1016/j.marenvres.2018.06.017.

Cleasby, I.R., Wakefield, D.E., Bearhop, S., Bodey, T.W., Votier, S.C. and Hamer, K.C. 2015. Three-dimensional tracking of a wide-ranging marine predator: flight heights and vulnerability to offshore wind farms. Journal of Applied Ecology 52: 1-9.

DHI. 2017. Verification Compliance Statement. MUSE Detection System. DHI Internal.

Elliot, K.H., Chivers, L., Bessey, L., Gaston, A.J., Hatch, S.A., Kato, A., Osborne, O., Ropert-Coudert, Y., Speakman, J.R. and Hare, J.F. 2014. Windscapes shape seabird instantaneous energy costs but adult behaviour buffers impacts on offspring. Movement Ecology 2014, 2: 1-15.

Furness, R., Wade, H. and Masden, E. 2013. Assessing vulnerability of marine bird populations to offshore wind farms. Journal of Environmental Management 119: 56–66.

Gibson, L., Wilman, E.N. & Laurance, W.F., 2017. How Green is “Green” Energy? Trends in ecology & evolution, 32(12): 922–935.

Gordon, C. E., & C. Nations, 2016. Collision Risk Model for “rufa” Red Knots (Calidris canutus rufa) Interacting with a Proposed Offshore Wind Energy Facility in Nantucket Sound, Massachusetts. US Department of the Interior, Bureau of Ocean Energy Management, Sterling, Virginia. OCS Study BOEM 2016-045. 90 pp. + frontmatter and appendix.

Green, R.E., Langston, R.H.W., McCluskie, A., Sutherland, R. & Wilson, J.D., 2016. Lack of sound science in assessing wind-farm impacts on seabirds. Journal of Applied Ecology, 53(6):1635-1641.

Gögmen, T., v. d. Laan, P., Réthoré, P.-E., Pena, A. & G. Larsen. 2016. Wind turbine wake models developed at the technical university of Denmark: a review. Renewable and Sustainable Energy Reviews 60: 752-769.

Gyimesi, A., Boudewijn, T.J., Buijs, R.J., Shamoun-Baranes, J.Z. and others. 2016. Lesser black-backed gulls Larus fuscus thriving on a non-marine diet. Bird Study 63: 241-249.

Jensen, N. 1983. A note on wind generator interaction, Risø M-2411, Roskilde.

Johnston, A., Cook, A.S.C.P., Wright, L.J., Humphreys, E.M. and Burton, N.H.K. 2014. Modelling flight heights of marine birds to more accurately assess collision risk with offshore wind turbines. Journal of Applied Ecology 51: 31-41.

Kotzerka, J., Garthe, S. and Hatch, S.A. 2010. GPS tracking device reveal foraging strategies of Black-legged Kittiwakes. Journal of Ornithollogy 151: 459-467.

Krijgsveld, K.L., Fijn, R., Japink, M., Van Horssen, P., Heunks, C., Collier, M., Poot, M.J.M., Beuker, D., Dirksen, S. 2011. Effect studies offshore wind farm Egmond aan Zee. Final Report on fluxes, flight altitudes and behaviour of flying birds. Bureau Waardenburg bv. Nordzee Wind. 330pp.

Mendel, B., Kotzerka, J., Sommerfeld, J., Schwemmer, H., Sonntag, N. and Garthe, S. 2014. Effects of the Alpha Ventus offshore test site on distribution patterns, behaviour and flight heights of seabirds. In: Federal Ministry for the Environment, Nature Conservation and Nuclear Safety (Eds.) Ecological Research at the Offshore Windfarm alpha ventus, pp95 – 110. DOI: 10.1007/978-3-658-02462-8_11.

Pettex, E., Lorentsen, S.H., Gremillet, D., Gimenez, O., Barrett, R.T., Pons, J.B., Le Bohec, C. and Bonadonna, F. 2012. Multi-scale foraging variability in Northern Gannet (Morus bassanus) fuels potential foraging plasticity. Marine Biology 159: 2743-2756.

Segal, M. & Xiao, Y. 2011. Multivariate random forest. WIREs Data Mining and Knowledge Discovery 1.

Skov, H. and Heinänen, S. 2013. Predicting the weather-dependent collision risk for birds at wind farms. In Hull C, Bennet E, Stark E, Smales I, Lau J, Venosta (Eds): Wind and wildlife 2012. Proceedings from the Conference on Wind Energy and Wildlife Impacts. Spinger.

Skov, H., Heinänen, S., Norman, T., Ward, R.M., Méndez-Roldán, S. & Ellis, I. 2018. ORJIP Bird Collision and Avoidance Study. Final report – April 2018. The Carbon Trust. United Kingdom. 247 pp..

Tjørnløv, R.S., Skov, H., Armitage, M., Barker, M., Cuttat, F. & Thomas, K. 2021. Resolving Key Uncertainties of Seabird Flight and Avidance Behaviours at Offshore Wind Farms. Annual report for April 2020 – October 2020. Project No. DHI: 11820296; RPS: ECO00516.

van Bemmelen, R.S.A., F.H. Soudijn, D. Benden, A. Potiek, C. Chen, N. Hintzen, T. Wilkes, T. van Kooten & A. Gyimesi. 2020. Individual-based model lesser black-backed gulls in the Netherlands. Report number 21-168. Bureau Waardenburg, Culemborg.

Zhang, L. et al. 2019. Classification and regression with random forests as a standard method for presence-only data SDMs: a future conservation example using China tree species. – Ecol. Inform. 52: 46–56.

APPENDICES

Appendix 1 FAR-3000 radar specifications

Technical and functional specifications of the FAR-3000 radar

Technical	Specification	Reference
Radar brand	FAR-3000	
Dimensions antenna	3900 mm	
Height	80 cm	
Weight	150 kg	
Minimal height above sea level	10 m	Furuno
Power supply (V,A)	230 VAC 13 A	
Cable connection (type, diameter, length)	Ø 32 mm 30 m	Furuno
Internal network speed	100 Mbits	Furuno
Bandwidth data connection	1.4 Mbits/s	Furuno
Frequency	3.1 GHz	Furuno
Additional hardware signal processing	FPGA - DHI proprietary	DHI
Software used	Tracker DHI and sensor fusion proprietary	DHI
Operating software	WINDOWS/Linux	
Maintenance needs	Annual inspection	DHI
Power backup	UPS	DHI
Waterproof classification (IP code)	Antenna/Gear IP 65 /Computer IP50	Furuno
Operational wind force limit	Up to 100 knots	Furuno
Magnetron / Solid state	Solid state S Band	Furuno
Power (kW)	250W	Furuno
Rotational speed (rpm)	24/42	Furuno
Horizontal scan of 360º	Yes	Furuno
Data sampling frequency	100 Msamples/S	DHI
Pulse emission frequency	600-3000 Hz	Furuno
Beam width (degrees)	1.8	Furuno
Beam height (degrees)	25	Furuno
Suppression of wave clutter	Very good	DHI field tests
Suppression of rain clutter	Excellent	DHI field tests
Expected false positive detection rate	< 5-25% on average	DHI field tests
Expected false negative detection rate	< 15% on average	DHI field tests
Resolution, capacity to separate two close bird targets	Good. Due to pulse compression the radar has a higher resolution than expected with S band. This allows for separation of close bird targets like individual seabirds flying in a flock.	DHI field tests
Side lobe suppression	Good. Very few ‘false’ detections in blind sectors.	DHI field tests

Technical	Specification	Reference
Capability to correct for volume sampling bias	Yes. Scanned area can be defined rather accurately.	DHI field tests
Horizontal range / spatial coverage	Coverage of up to 4 km for individual passerines, 7 km for wader-type birds, 10 km for goose-type birds and 25 km for a flock of birds.	Radar performance simulations (CARPET) and field tests
Correction for distance sampling bias	Standardised dB-values for certain echo sizes, even detection probability for seabirds within 6 km distance	Radar performance simulations (CARPET) and field tests
Accuracy / smallest RCS (radar cross section) detection at 3 nm distance	10 cm	Radar performance simulations (CARPET) and field tests
Max number of simultaneously tracked bird targets	3000 instantaneous	Furuno
Automatic database registration	Included, MUSE software (tracks saved in csv. format with location, direction and speed)	DHI
Automatic bird tracking software	Included	DHI
Distinguish between Birds / Aircrafts ?	Yes, through bird classification algorithm (MUSE software)	Field tests
Capability to measure and take account of static clutter	Clutter areas are mapped and masked from data processing	Field tests
Capability to measure and take account of dynamic clutter from waves and rain	Dynamic selection of clutter-free sections	Field tests
On-site calibration for specific conditions and detection of target bird species	Yes	DHI
Capability for remote fine-tuning of setup	Yes	DHI
Species (Species-group) specific information	Yes, by coupling to digital camera through sensor fusion software	DHI
Data distributing capabilities / Protocols	TCP-IP	
Data storage	Locally, with daily backups of radar track data via net	DHI

Appendix 2 FLIR M400 camera specifications

Specifications for the FLIR M400 Camera

Thermal Imaging Specifications (optional)	
Sensor Type	Uncooled VOx microbolometer
Focal length	35-105 mm
Array Format	640 x 480
Field of view	18° to 6° HFOV / 1.5° HFOV with E-Zoom
Optical Zoom 1× to 4×	Optical Zoom 1× to 4×
E-Zoom 1× to 4×	E-Zoom 1× to 4×
Daylight Imaging Specifications	
Sensor	Long-range colour daylight and low-light viewing
Effective pixels (H x V)	1920 x 1080
Focal length / Hor. field of view	129 mm to 4.3 mm (30 optical zoom)/ 64° to 2.3°
Sensitivity	>0.5 lux at 50 IRE / .05 lux in ICR Mode (B/W)
Video format	
Analogue Video Output	NTSC or PAL, <9 Hz
Digital Zoom and Pan	Region of interest; E-zoom from 1X – 4X
Pan/Tilt	
Pan (Azimuth)	360° continuous
Tilt (Elevation)	+- 90°
Mechanical	
Overall dimensions (H/W/L)	458.7 mm x 273.1 mm x 397.6 mm with top down riser
Net weight	12.7 kg
Environmental	
Operating voltage	24 VDC
Power consumption	<50 W nominal; 130 W peak
Chock/vibrations	Vibration IEC 60945; MIL-STD-810E and chock 15 g vertical, 9 g horizontal

Appendix 3 RVision camera specifications

Specifications for the RVision MiniHP day-light camera

Camera specifications	
Item	***Specification***
Pan Range	Continuous
Tilt Range	180°
Pan/Tilt Speed	180°/s
Weight	7.1 lbs.
Housing Material	6061-T6 Machined Aluminium
Operating Temperature	-40°C to +70°C
Control Interface	RS232/RS422
Command Protocol	RVision, Pelco-D
Video Format	NTSC / PAL
Zoom - Colour	36x Optical, 12x Digital
HFOV - Colour	57.8° - 1.7°
Sensitivity - Colour	0.1 lux 0.01 lx NIR
Voltage	12-30 VDC
Voltage	12-30 VDC

Appendix 4 ERA Wake model description

In this section the methodology behind the estimated turbine wakes within the offshore wind farm (OWF) is described.

Kinetic energy from the incoming wind is converted to electrical energy by the wind turbine. From a wind perspective the consequence is a downstream wake of reduced wind speed and enhanced turbulence. In the current project the characterization of the size and strength of this wake is important and will be addressed in the section. The interplay of more than one turbine and hence the superposition of turbine wakes complicates the picture. In this study we use an iterative method [1] across the full OWF in order to capture this effect.

The layout of the “Aberdeen” OWF is presented in Figure A4- 1 with 11 wind turbines names AWF01 to AWF11.

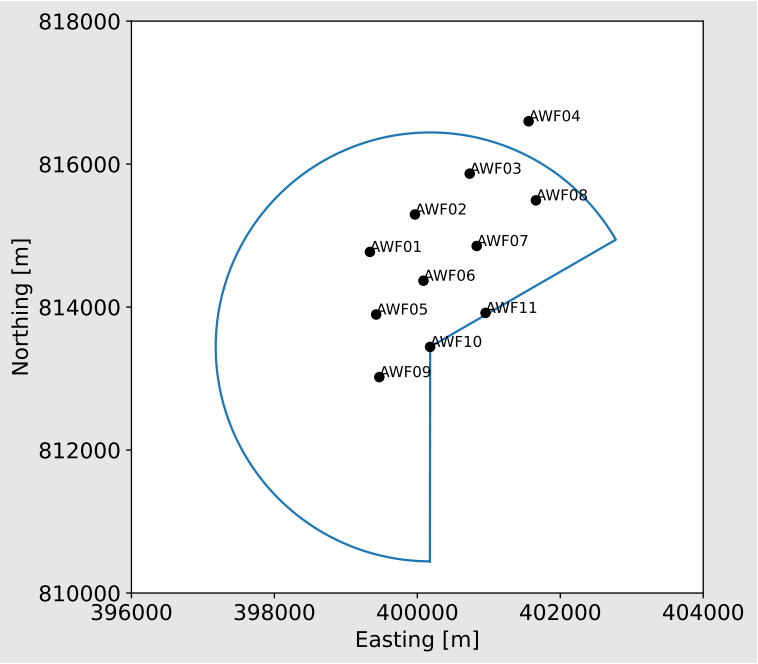

Figure A4- 1 OWF layout in British National Grid. Turbines named from AWF01-AWF11. Radar scan area shown as polygon.

Wind speed, direction, and time series

The wind speed over the area covering the OWF – but without considering the effect of the turbines - is assumed to be homogeneous. AOWFL has delivered wind speed and direction at each turbine location measured at the nacelle of the turbine. Often measurements like these are not accurate due to presence of the rotor in front of the anemometer, and hence flow distortion reduced wind speed and enhanced turbulence, but also possible speed-up effect from the nacelle it-self. The timeseries consist of two periods as given in Table A4- 1.

Table A4- 1 Timeseries used in study

Name	Period start	Period end
Period 2020	2020-04-01 00:00:00	2020-10-30 23:00:00
Period 2021	2021-04-01 00:00:00	2021-10-30 23:00:00

The wind speed and direction measured simultaneous from the 11 turbines (AWF01 to AWF11) shown in Figure A4- 2 often varies more than 3 m/s and more than 20 degrees from turbine to turbine. Any wakes produced with a steady-state wake model forced with this wind would therefore show very fluctuating wake directions (but also speed) between consecutive time steps. By using the maximum

wind speed over the 11 turbines in each time step (10 min averaged to 1 h) and wind direction from the associated turbine, it is implicitly assumed that this wind speed best represents the undisturbed wind speed when no turbines are present (disregarding blocking effect as discussed later). Using this approach, we still encounter jumps in the wind direction between consecutive time steps. A wind rose plot of the resulting time series of wind speed and wind direction is shown in Figure A4- 2: the main wind direction is from the south, and this is also the direction with the strongest winds of 23-24 m/s.

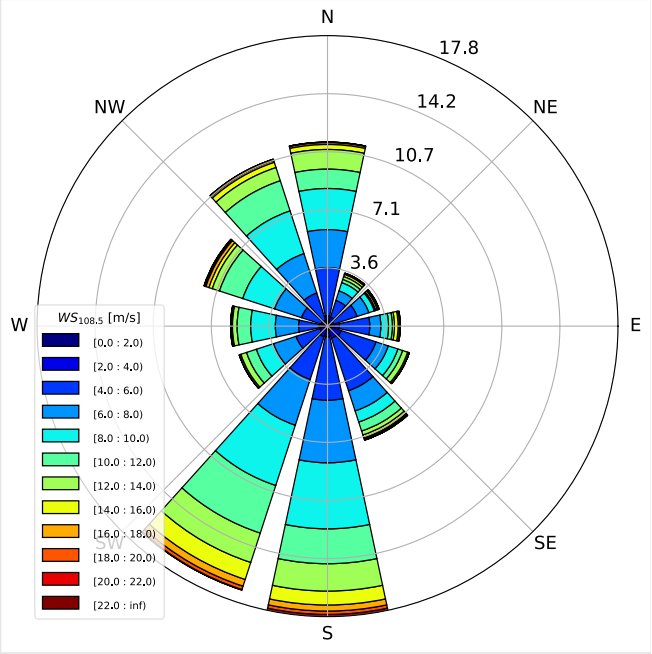

Figure A4- 2 **Wind rose of OWF measured wind speed and wind direction The OWF measurements is taken as the maximum wind speed of all turbine readings in the OWF and its associated wind direction.**

We have therefore decided to use a wind model, in this case the atmospheric reanalysis model ERA5[3]. This model offers a grid resolution of ~30 km and hourly time scales, i.e., the flow is smooth which will guarantee smoothly varying wakes. A scatter plot comparison with ERA5 wind is presented in Figure A4- 3 and Figure A4- 4 for wind speed and wind direction, respectively. For the wind speed the scatter index (si=0.20) and root-mean-square-error (rmse=2.18) are low and the correlation coefficient (cc=0.88) is high. There is a bias of -1.26 m/s, i.e., the values of the measurements are lower than those of ERA5. Since this bias is most pronounced for higher wind speed (above turbine rated speed ~12 m/s) the effect on the strength of the wakes is small. For wind direction the circular bias is small (3.59°) and the correlation coefficient is high (0.88). Based on this comparison we decided to go on with the ERA5 model.

[3] Atmospheric Re-Analysis 5 (ERA5) developed by the European Centre for Medium Range Weather Forecasts (ECMWF) . ERA5 | ECMWF.

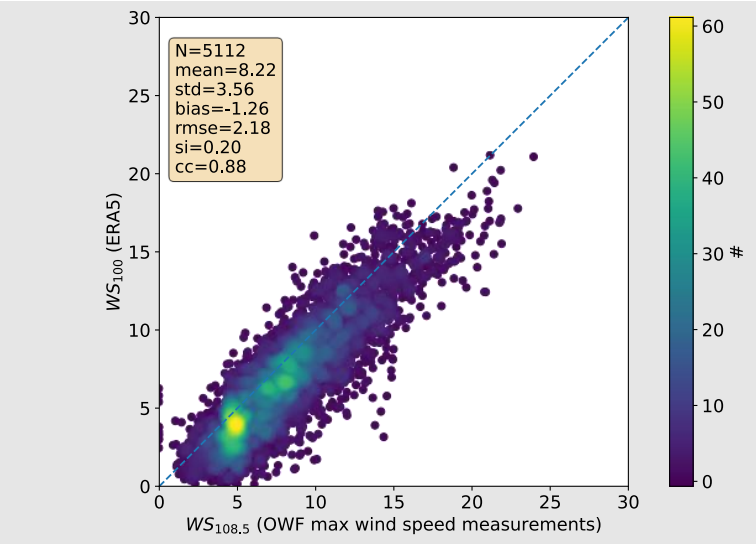

Figure A4- 3 **Scatter plot of 1h wind speed of OWF measurements at 108.5 mMSL and ERA5 at 100 mMSL. The OWF measurements is taken as the maximum wind speed of all turbine readings in the OWF. Statistics added: Mean value of 1h measurements, standard deviation of 1h measurements, bias, root-mean-square-error (rmse), scatter index (si) and correlation coefficient (cc) added.**

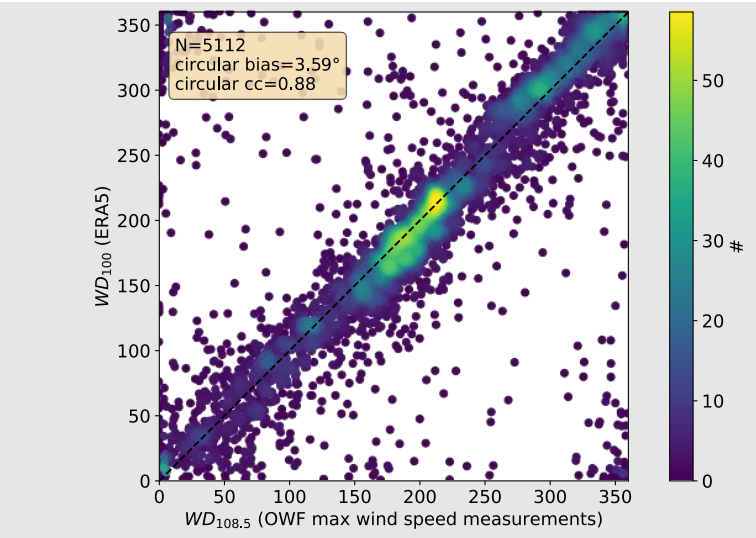

Figure A4- 4 **Scatter plot of 1h wind direction of OWF measurements at 108.5 mMSL and ERA5 at 100 mMSL. The OWF measurements is taken as the wind direction of the turbine with the maximum wind speed of all turbine readings in the OWF. Statistics added: Circular bias and circular corelation coefficient.**

Wind turbine wake models

The turbine layout and turbine dimensions have been provided by AOWFL (Table A4- 2). In reality nine of the turbines are 8.4 MW and the other two are 8.8 MW. As a compromise a rated power of 8.6 MW has been chosen for this study (it has been verified that the effect on the final results is negligible).

Table A4- 2 **Turbine key dimensions**

Turbine hub height	108.5mMSL
Rotor Diameter	164m
Rated Power	8.6 MW

For the turbine thrust coefficient curve (ct-curve), values from the DTU 10 MW test turbine have been used [2]. The rated speed is 11 m/s, i.e., the wind speed at which the thrust coefficient levels off, and the rated power of 8.6 MW is achieved.

The wake model consist of several sub models: a wake deficit model to account for the reduced wind speed downstream of the rotor; a turbulence model to account for the enhanced turbulence level downstream of the rotor; a blockage deficit model to account for the reduced wind speed just in from of the rotor due to the rotor induced pressure gradient force, and speed-up along the sides of the downstream wake; and a superposition model to account for mixing if wakes from nearby turbines.
The complete wake model used has been implemented using the DTU Wind Energy Open Source PyWake Package v.2.2.0 [1] [3] using the engineering wake models listed in Table A4- 3

Table A4- 3 Engineering wale models

Wake deficit model	Zong Gaussian model [4]
Turbulence model	Frandsen model [5]
Superposition model	Linear sum [1]
Blockage deficit model	Rathmann model [1]

The majority of wake deficit models are developed with wind resource assessment studies in mind, where often accurate modelling of the far field is most relevant. In this study, however, near wake distances are equally important and hence the Zong Gaussian model is a very good candidate, and hence chosen for this study. A comparison of the chosen model with the canonical Niels Otto Jensen (NOJ) model [6] on the centerline is shown in Figure A4- 5. The strength of the wake is defined through WS_{ratio}, which is the ratio between the local wind speed and the incoming wind speed (upstream where the wind is unaffected by turbines). In the presence of wakes $WS_{ratio}<1$. In the figure it is observed that the Zong Gaussian model used in this study has a smaller maximum deficit compared to the NOJ model, and it is located further downstream which is more realistic [7], and of importance for this study in particular. Also, by including a blocking model the wind speed is reduced in front of the turbine. Due to the varying thrust coefficient (ct) with wind speed, the wake strength (WS_{ratio}) is also dependent on wind speed.

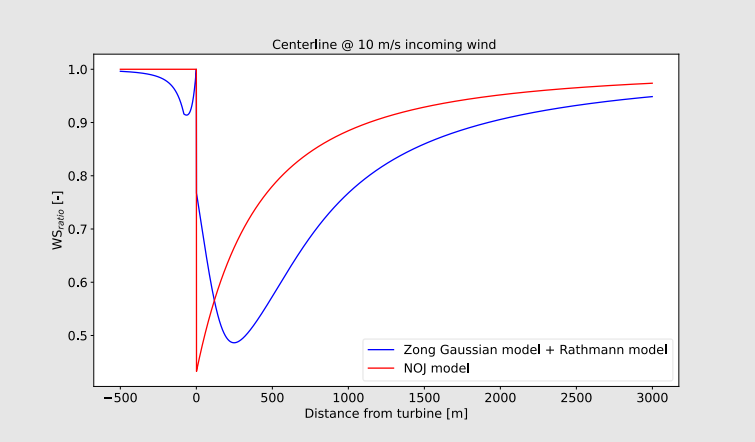

Figure A4- 5 Centerline comparison between the Zong Gaussian model + Rathmann model (utilized in this study) with the canonical NOJ model. The wind speed ratio (WS_{ratio}) is plotted as function of distance from turbine (turbine at distance=0).

The time series described above based on the measurements within the park is used to force the wake combined model. The resulting flow field is obtained from an iteration procedure until convergence of the effective wind speed is obtained at all turbine positions in AOWFL. An example of the resulting wind speed ratio (WS_{ratio}) across the radar scan area is shown in Figure A4- 6.

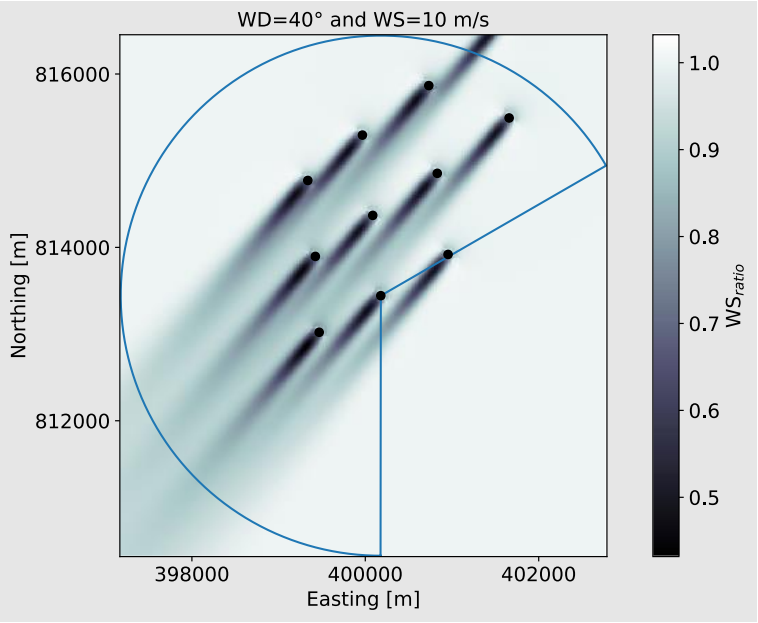

Figure A4- 6 **Wind speed ratio (WS_{ratio}) of "Aberdeen" OWF. Radar scan area shown as polygon. Wind speed is 10 m/s and wind direction is 40°. Coordinates in British National Grid.**

References

[1] DTU Wind Energy, »https://topfarm.pages.windenergy.dtu.dk/PyWake/index.html,« [Online].

[2] C. Bak, F. Zahle, R. Bitsche, T. Kim, A. Yde, L. Henriksen, M. Hansen, J. Blasques, M. Gaunaa og N. A, »The DTU 10-MW Reference Wind Turbine,« DTU Wind Energy, 2013.

[3] T. Gögmen, P. v. d. Laan, P.-E. Réthoré, A. Pena og G. Larsen, »Wind turbine wake models developed at the technical university of Denmark: a review,« Renewable and Sustainable Energy Reviews, årg. 60, pp. 752-769, 2016.

[4] H. Zong og F. Porté-Agel, »A momentum-conserving wake superposition method for,« Journal of Fluid Mechanics , årg. 889, p. A8, 2020.

[5] S. Frandsen, »Turbulence and turbulence-generated structural loading in wind turbine clusters,« Risø-R-1188(EN), Roskilde, 2007.

[6] N. Jensen, »A note on wind generator interaction,« Risø M-2411, Roskilde , 1983.

[7] S. Andersen, J. Sørensen, S. Ivanell og R. Mikkelsen, »Comparison of Engineering Wake Models with CFD Simulations,« Journal of Physics: Conference Series, årg. 524, p. 012161, 2014.

Appendix 5 Random Forest flight models – validation

Northern Gannet

Table A5- 1 Results from multivariate random forest on Northern Gannet flight behaviour, Flight height (top), flight speed (middle), relative flight direction (bottom)

```
                         Sample size: 201
                    Number of trees: 200
          Forest terminal node size: 1
      Average no. of terminal nodes: 99.775
No. of variables tried at each split: 5
              Total no. of variables: 5
              Total no. of responses: 3
        User has requested response: Height
      Resampling used to grow trees: swor
   Resample size used to grow trees: 127
                           Analysis: mRF-R
                             Family: regr+
                     Splitting rule: mv.mse *random*
      Number of random split points: 10
                    (OOB) R squared: 0.80352982
  (OOB) Requested performance error: 51.83181502
```

```
                         Sample size: 201
                    Number of trees: 200
          Forest terminal node size: 1
      Average no. of terminal nodes: 99.775
No. of variables tried at each split: 5
              Total no. of variables: 5
              Total no. of responses: 3
        User has requested response: Speed
      Resampling used to grow trees: swor
   Resample size used to grow trees: 127
                           Analysis: mRF-R
                             Family: regr+
                     Splitting rule: mv.mse *random*
      Number of random split points: 10
                    (OOB) R squared: -0.0296744
  (OOB) Requested performance error: 27.17982437
```

```
                         Sample size: 201
                    Number of trees: 200
          Forest terminal node size: 1
      Average no. of terminal nodes: 99.775
No. of variables tried at each split: 5
              Total no. of variables: 5
              Total no. of responses: 3
        User has requested response: Relativ_direction
      Resampling used to grow trees: swor
   Resample size used to grow trees: 127
                           Analysis: mRF-R
                             Family: regr+
                     Splitting rule: mv.mse *random*
      Number of random split points: 10
                    (OOB) R squared: 0.48808242
  (OOB) Requested performance error: 298.73392544
```

Comparison of observed and predicted variables

Overall there was a good correspondence when comparing predicted flight parameters with observed ones, with a correlation between observed and predicted parameters on average at 0.98 (Flight height 0.99, Flight speed 0.96, Flight direction 0.98) (Figure A5- 1).

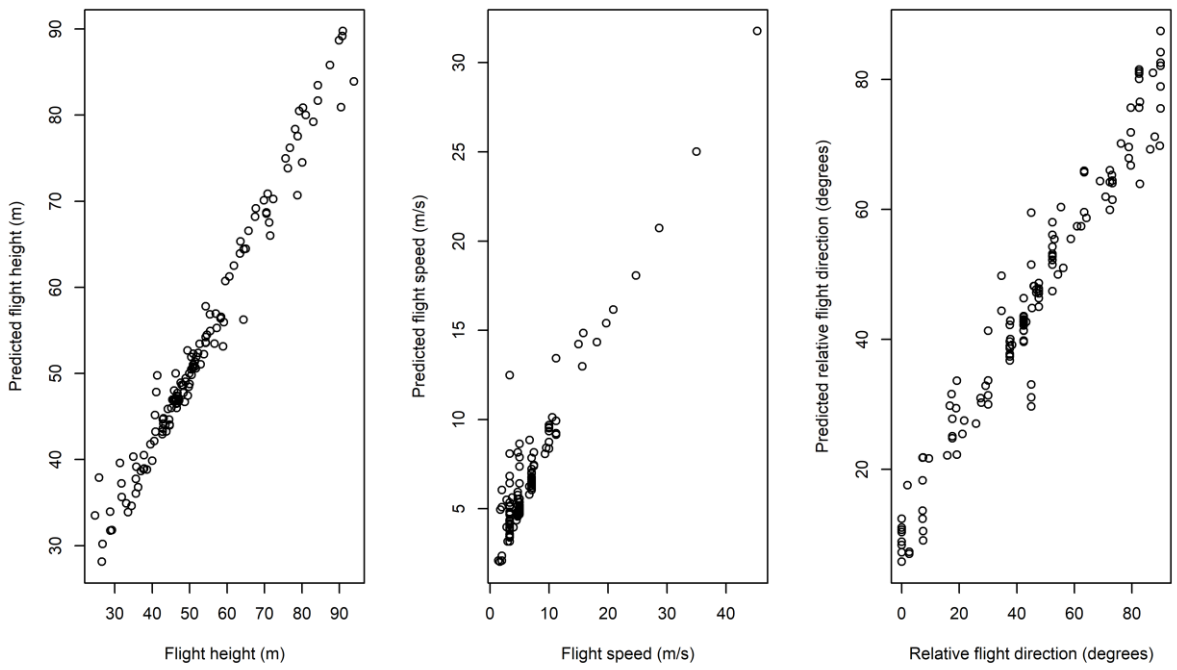

Figure A5- 1 Comparison between observed and predicted variables

Additionally, no significant autocorrelation was evident in the residuals from the model.

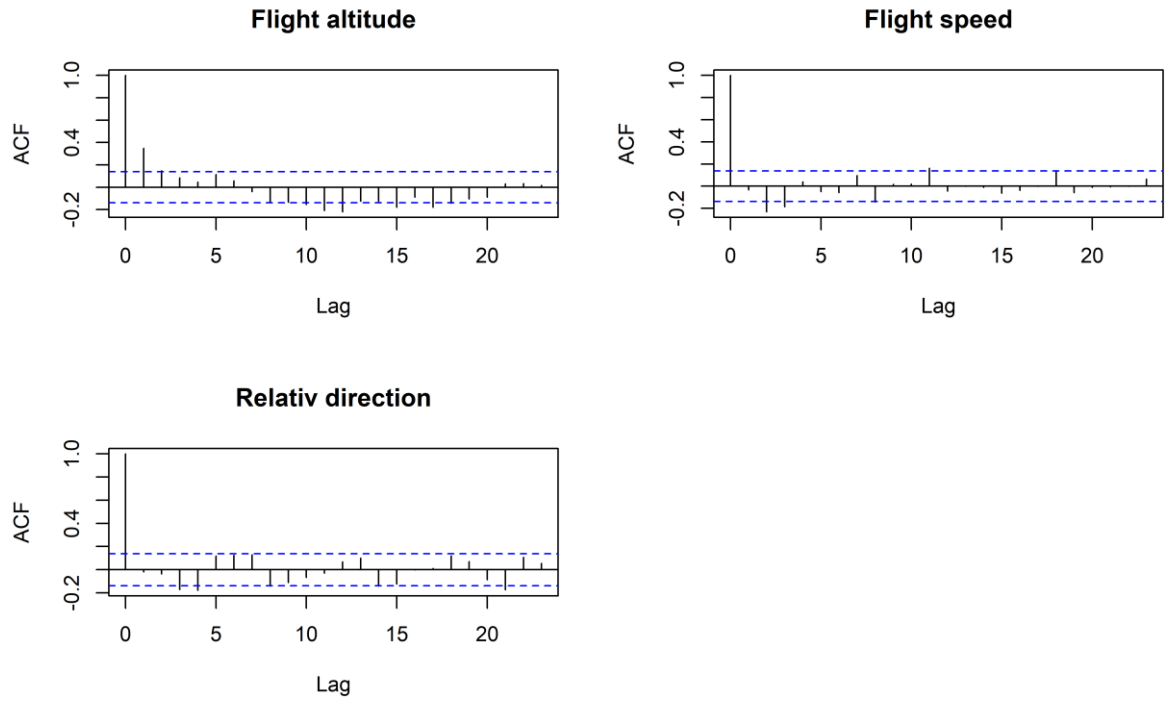

Figure A5- 2 ACF plots of residuals.

From the analysis of importance (Figure A5- 3) it was evident seen that it was not the same variables that drove each behaviour. Flight speed was primarily driven by wind speed and the distance to rotor, while flight height has determined by turbulence, wind speed and distance to rotor. Most factors determined the relative flight direction.

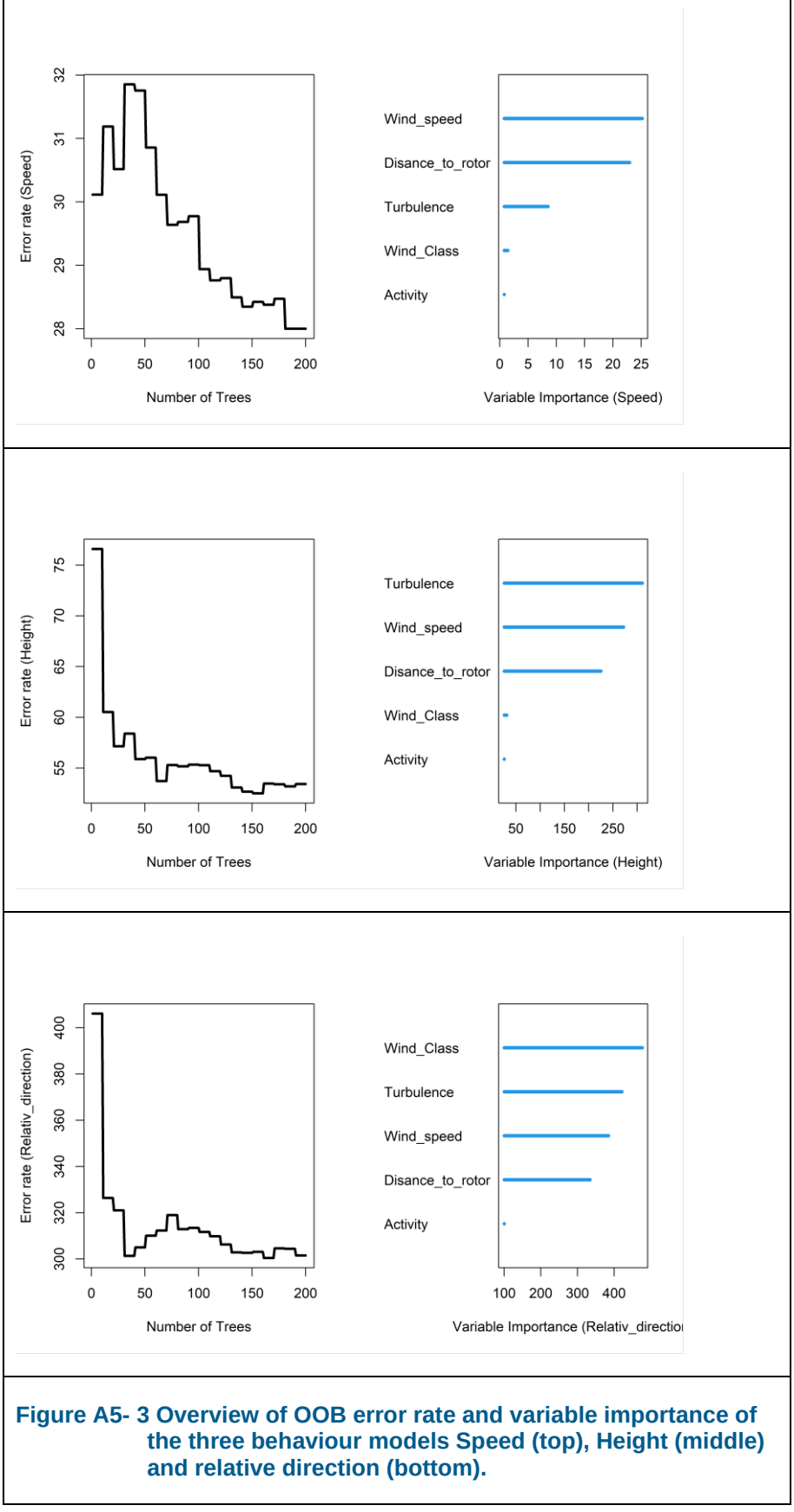

Figure A5- 3 Overview of OOB error rate and variable importance of the three behaviour models Speed (top), Height (middle) and relative direction (bottom).

Black-legged Kittiwake

```
                         Sample size: 401
                      Number of trees: 200
           Forest terminal node size: 1
       Average no. of terminal nodes: 237.07
No. of variables tried at each split: 4
              Total no. of variables: 5
              Total no. of responses: 3
        User has requested response: Height
       Resampling used to grow trees: swor
    Resample size used to grow trees: 253
                            Analysis: mRF-R
                              Family: regr+
                      Splitting rule: mv.mse *random*
       Number of random split points: 10
                      (OOB) R squared: 0.64385459
   (OOB) Requested performance error: 197.26708051
```

```
                         Sample size: 401
                      Number of trees: 200
           Forest terminal node size: 1
       Average no. of terminal nodes: 237.07
No. of variables tried at each split: 4
              Total no. of variables: 5
              Total no. of responses: 3
        User has requested response: Speed
       Resampling used to grow trees: swor
    Resample size used to grow trees: 253
                            Analysis: mRF-R
                              Family: regr+
                      Splitting rule: mv.mse *random*
       Number of random split points: 10
                      (OOB) R squared: -0.02828739
   (OOB) Requested performance error: 47.82691919
```

```
                         Sample size: 401
                      Number of trees: 200
           Forest terminal node size: 1
       Average no. of terminal nodes: 237.07
No. of variables tried at each split: 4
              Total no. of variables: 5
              Total no. of responses: 3
        User has requested response: Relativ_direction
       Resampling used to grow trees: swor
    Resample size used to grow trees: 253
                            Analysis: mRF-R
                              Family: regr+
                      Splitting rule: mv.mse *random*
       Number of random split points: 10
                      (OOB) R squared: 0.17350047
   (OOB) Requested performance error: 488.20965246
```

Figure A5- 4 Results from multivariate random forest on Black-legged kittiwake flight behaviour, Flight height (top), flight speed (middle), relative flight direction (bottom)

Comparison of observed and predicted varables

Overall there was a good correspondence when comparing predicted variables with observed ones, with a correlation between observed and predicted variables on average at 0.97 (Flight height 0.98, Flight speed 0.97, Flight direction 0.97) (Figure A5- 5).

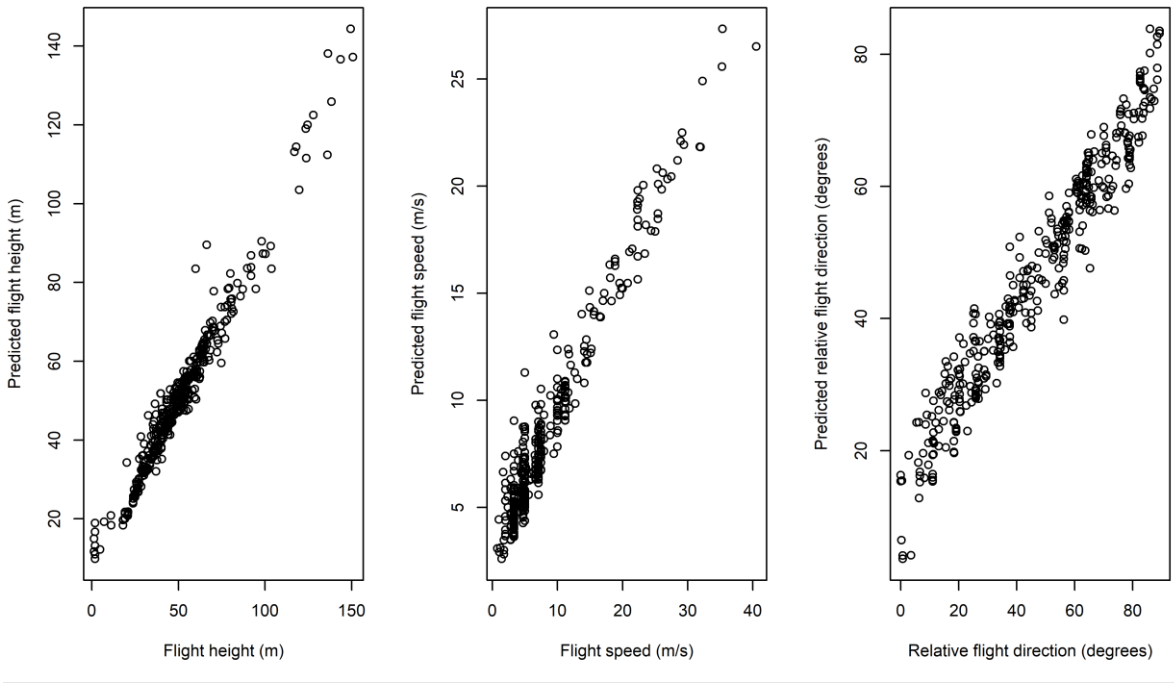

Figure A5- 5 Comparison between observed and predicted variables

Additionally, no significant autocorrelation was evident in the residuals from the model.

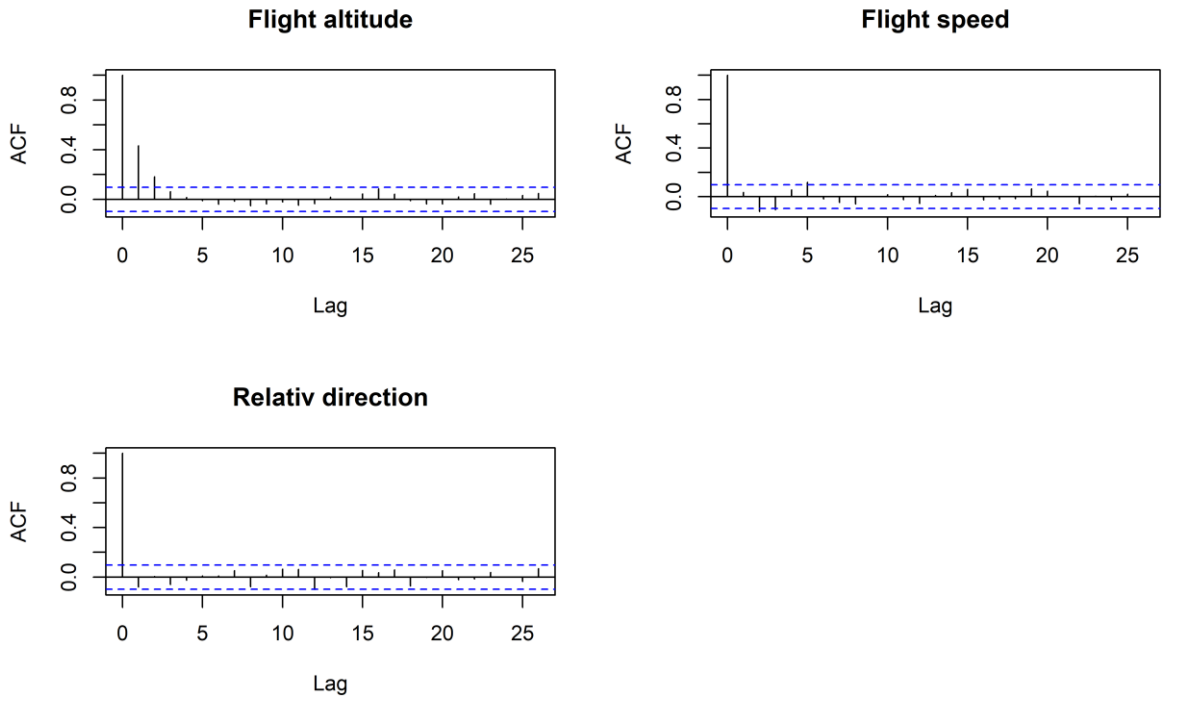

Figure A5- 6 ACF plots of residuals.

From the analysis of importance (Figure A5- 7) it was evident seen that it was not the same variables that drove each behaviour. Flight speed was primarily driven by turbulence and wind speed, while flight height has determined by turbulence, distance to rotor and wind speed. Most factors determined the relative flight direction, except activity.

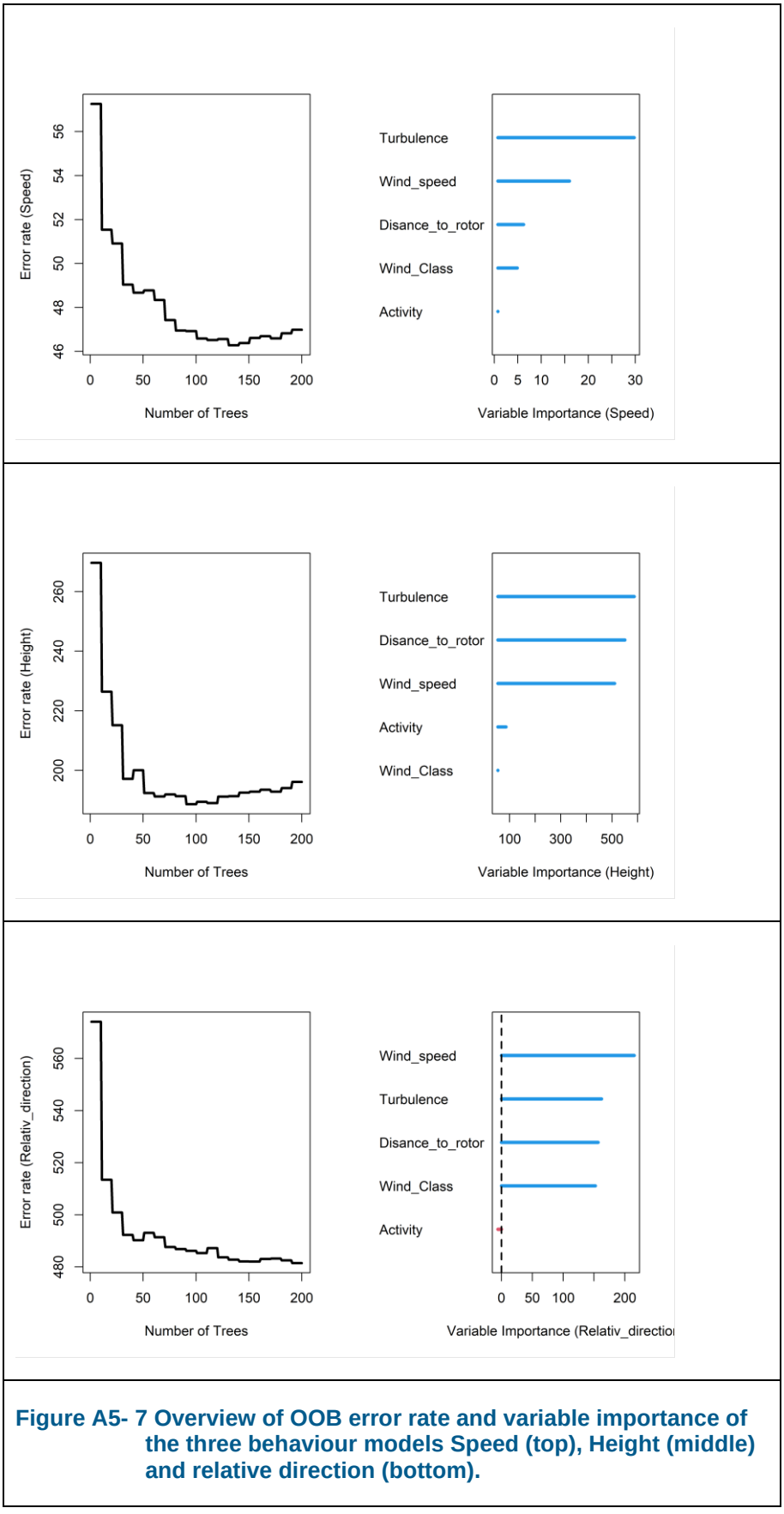

Figure A5- 7 Overview of OOB error rate and variable importance of the three behaviour models Speed (top), Height (middle) and relative direction (bottom).

Herring Gull

```
                        Sample size: 3866
                     Number of trees: 200
          Forest terminal node size: 1
       Average no. of terminal nodes: 2079.995
No. of variables tried at each split: 4
              Total no. of variables: 5
              Total no. of responses: 3
         User has requested response: Height
       Resampling used to grow trees: swor
    Resample size used to grow trees: 2443
                            Analysis: mRF-R
                              Family: regr+
                     Splitting rule: mv.mse *random*
       Number of random split points: 10
                     (OOB) R squared: 0.69799035
   (OOB) Requested performance error: 239.20757751
```

```
                        Sample size: 3866
                     Number of trees: 200
          Forest terminal node size: 1
       Average no. of terminal nodes: 2079.995
No. of variables tried at each split: 4
              Total no. of variables: 5
              Total no. of responses: 3
         User has requested response: Speed
       Resampling used to grow trees: swor
    Resample size used to grow trees: 2443
                            Analysis: mRF-R
                              Family: regr+
                     Splitting rule: mv.mse *random*
       Number of random split points: 10
                     (OOB) R squared: 0.29358039
   (OOB) Requested performance error: 29.97602835
```

```
                        Sample size: 3866
                     Number of trees: 200
          Forest terminal node size: 1
       Average no. of terminal nodes: 2079.995
No. of variables tried at each split: 4
              Total no. of variables: 5
              Total no. of responses: 3
         User has requested response: Relativ_direction
       Resampling used to grow trees: swor
    Resample size used to grow trees: 2443
                            Analysis: mRF-R
                              Family: regr+
                     Splitting rule: mv.mse *random*
       Number of random split points: 10
                     (OOB) R squared: 0.51477339
   (OOB) Requested performance error: 331.1978952
```

Figure A5- 8 Results from multivariate random forest on Herring Gull flight behaviour, Flight height (top), flight speed (middle), relative flight direction (bottom)

Comparison of observed and predicted variables

Overall there was a good correspondence when comparing predicted variables with observed ones, with a correlation between observed and predicted variables on average at 0.98 (Flight height 0.98, Flight speed 0.97, Flight direction 0.98) Figure A5- 9).

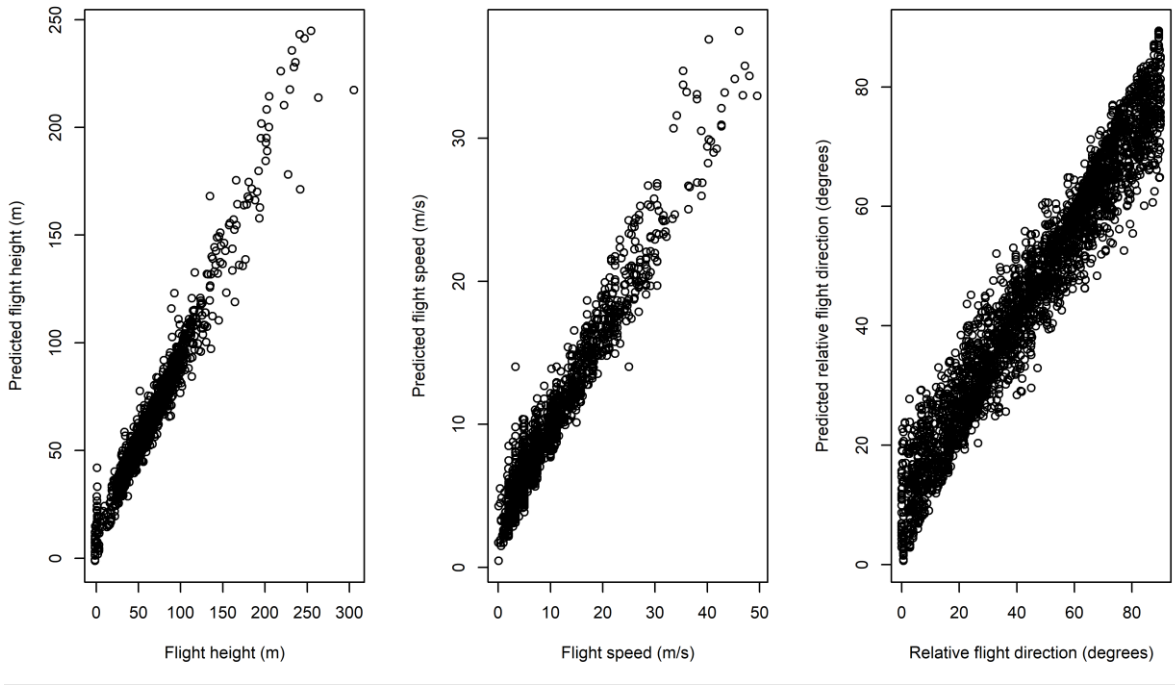

Figure A5- 9 Comparison between observed and predicted variables

Additionally, some autocorrelation was left in the residuals on the flight altitude, which could not be removed.

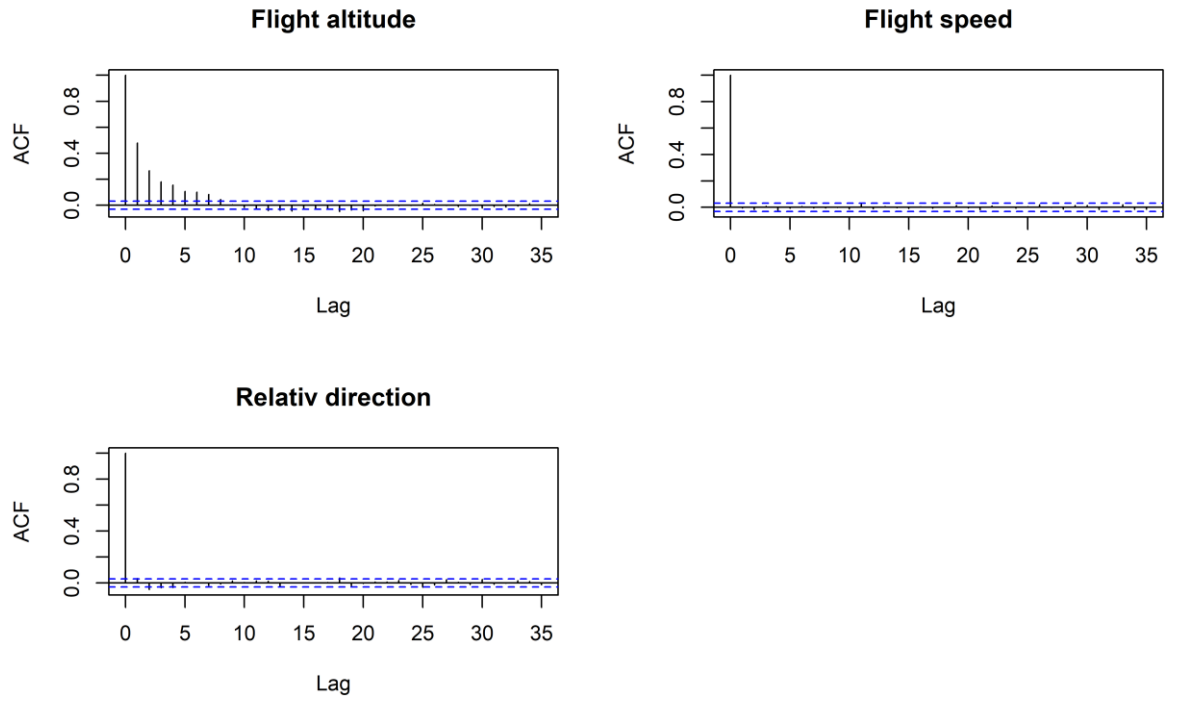

Figure A5- 10 ACF plots of residuals.

From the analysis of importance (Figure A5- 11) it was evident seen that it was not the same variables that drove each behaviour. Flight speed was primarily driven by turbulence, wind speed and distance to rotor, while flight height has determined by turbulence, distance to rotor and wind speed. Most factors determined the relative flight direction, except activity.

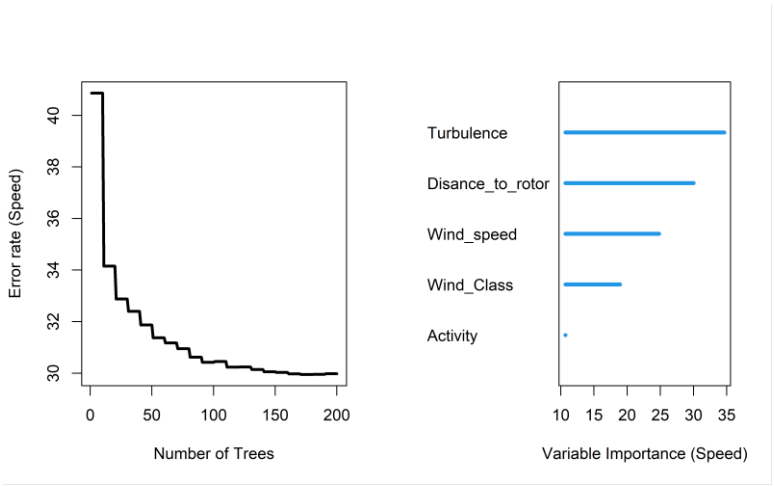

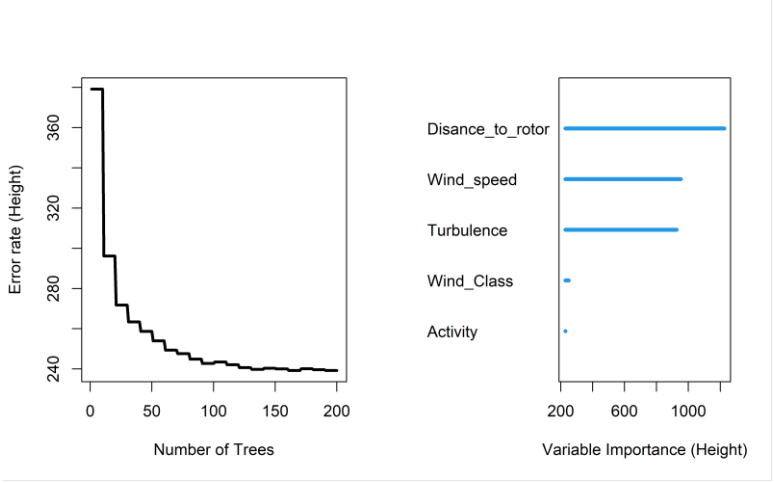

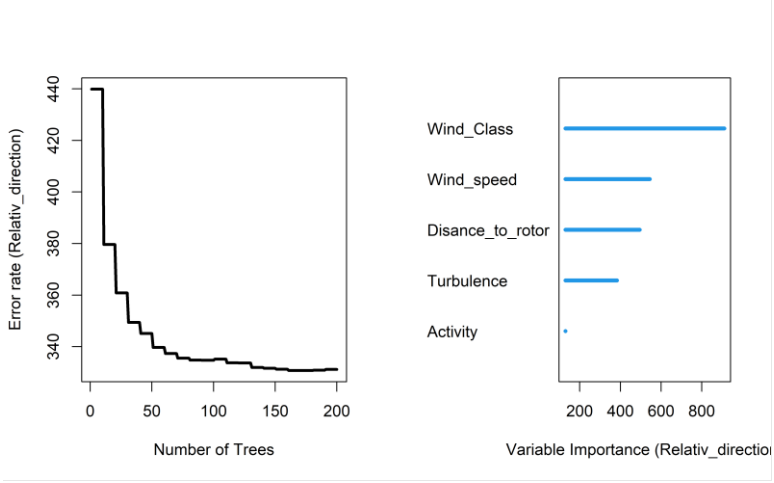

Figure A5- 11 Overview of OOB error rate and variable importance of the three behaviour models Speed (top), Height (middle) and relative direction (bottom).

Great Black-backed Gull

```
                        Sample size: 204
                     Number of trees: 200
           Forest terminal node size: 1
       Average no. of terminal nodes: 121.23
No. of variables tried at each split: 2
              Total no. of variables: 5
              Total no. of responses: 3
        User has requested response: Height
      Resampling used to grow trees: swor
   Resample size used to grow trees: 129
                          Analysis: mRF-R
                            Family: regr+
                    Splitting rule: mv.mse *random*
      Number of random split points: 10
                    (OOB) R squared: 0.55039636
  (OOB) Requested performance error: 404.129811
```

```
                        Sample size: 204
                     Number of trees: 200
           Forest terminal node size: 1
       Average no. of terminal nodes: 121.23
No. of variables tried at each split: 2
              Total no. of variables: 5
              Total no. of responses: 3
        User has requested response: Speed
      Resampling used to grow trees: swor
   Resample size used to grow trees: 129
                          Analysis: mRF-R
                            Family: regr+
                    Splitting rule: mv.mse *random*
      Number of random split points: 10
                    (OOB) R squared: 0.0146026
  (OOB) Requested performance error: 40.59784602
```

```
                        Sample size: 204
                     Number of trees: 200
           Forest terminal node size: 1
       Average no. of terminal nodes: 121.23
No. of variables tried at each split: 2
              Total no. of variables: 5
              Total no. of responses: 3
        User has requested response: Relativ_direction
      Resampling used to grow trees: swor
   Resample size used to grow trees: 129
                          Analysis: mRF-R
                            Family: regr+
                    Splitting rule: mv.mse *random*
      Number of random split points: 10
                    (OOB) R squared: 0.28910655
  (OOB) Requested performance error: 489.38496468
```

Figure A5- 12 Results from multivariate random forest on great black-backed gull flight behaviour, Flight height (top), flight speed (middle), relative flight direction (bottom)

Comparison of observed and predicted variables

On overall there was a good correspondence when comparing predicted variables with observed ones, with a correlation between observed and predicted variables on average at 0.97 (Flight height 0.97, Flight speed 0.97, Flight direction 0.97) (Figure A5- 13).

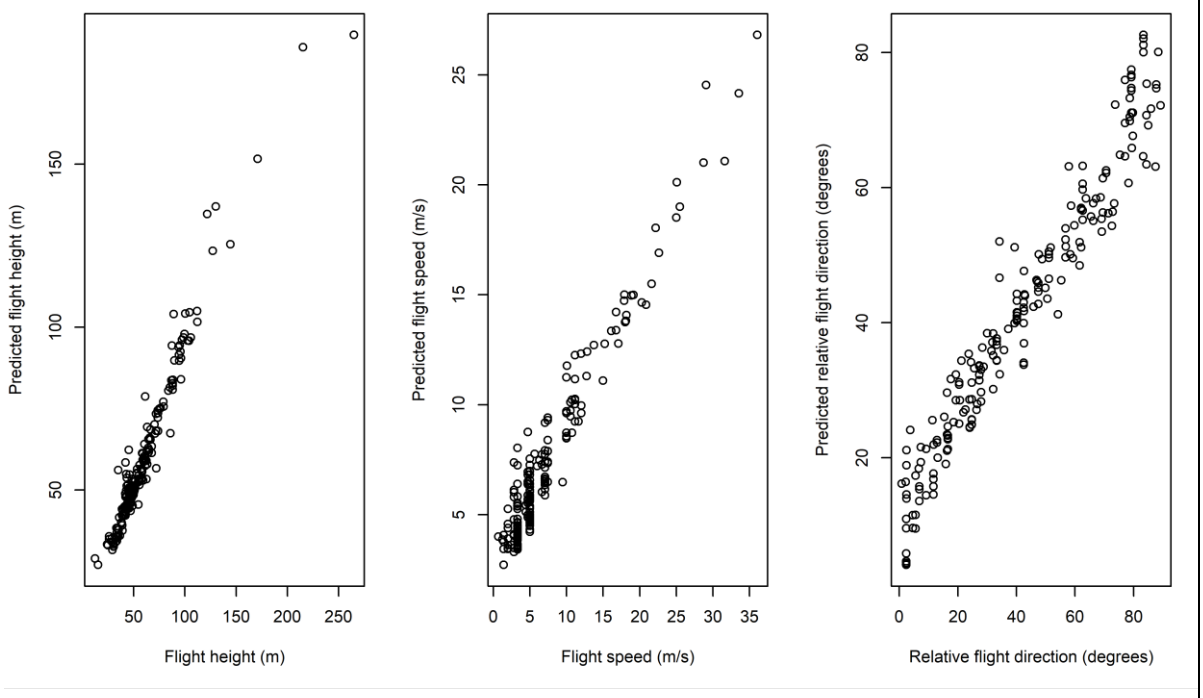

Figure A5- 13 Comparison between observed and predicted variables

Additionally, no significant autocorrelation was evident in the residuals from the model.

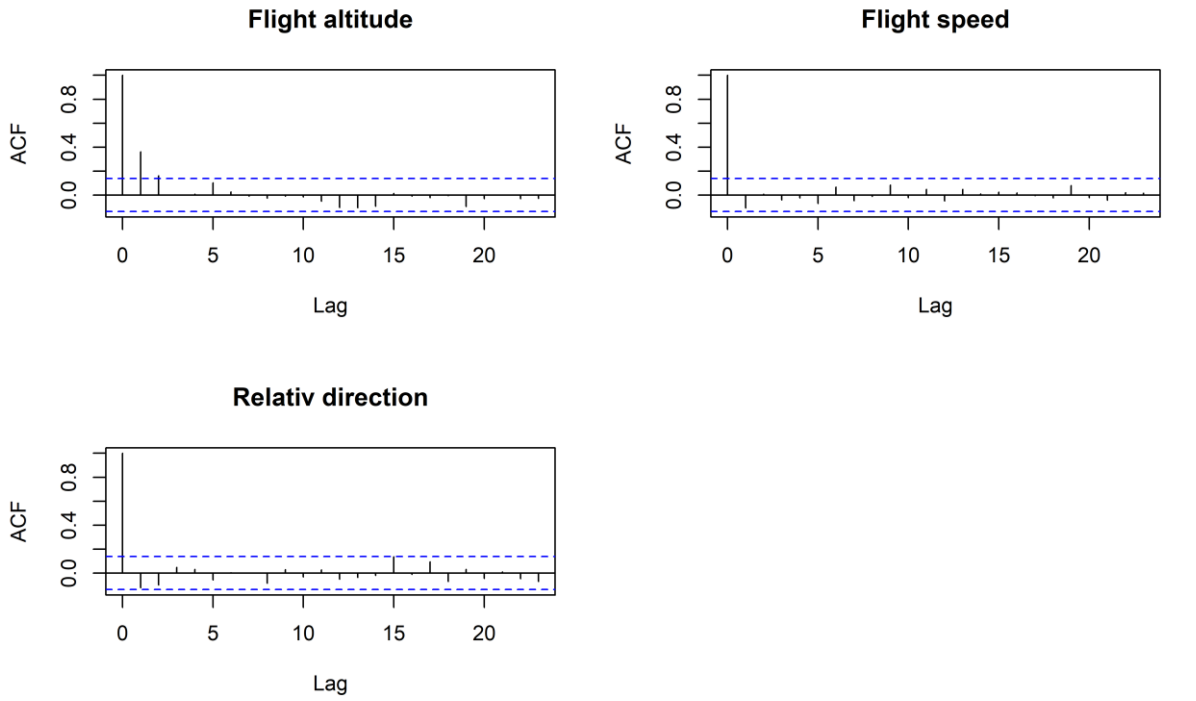

Figure A5- 14 ACF plots of residuals.

From the analysis of importance (Figure A5- 15) it was evident seen that it was not the same variables that drove each behaviour. Flight speed was primarily driven by turbulence and wind class, while flight height has determined by distance to rotor. Most factors determined the relative flight direction.

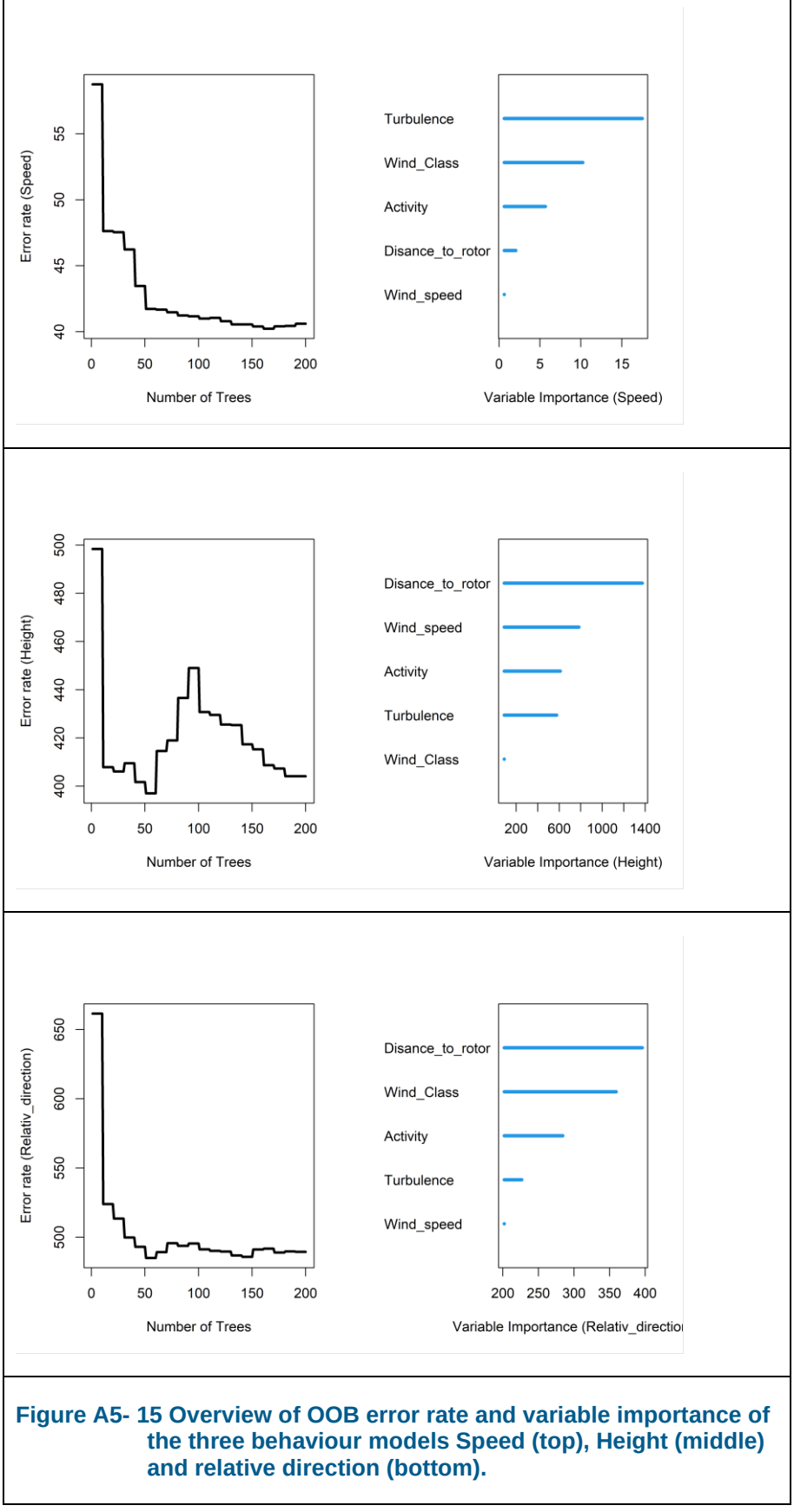

Figure A5- 15 Overview of OOB error rate and variable importance of the three behaviour models Speed (top), Height (middle) and relative direction (bottom).